# Including the Effect of Shielding in Prediction of Weather Window for Offshore Lifting Operations

## Camilla Waldum Olsen

**NTNU  Trondheim**
**Norwegian University of Science and Technology**
*Department of Marine Technology*

# MASTER THESIS IN MARINE TECHNOLOGY

# SPRING 2015

# FOR

# Camilla Waldum Olsen

# Including the effect of shielding in prediction of weather window for offshore lifting operations

The background for this project is offshore lifting operations, where the operational window is given as a limit on the significant wave height Hs. The task is defined in cooperation with DeepOcean. They are currently not implementing the effect of shielding from the ship hull on the lee side of the ship when they determine the maximum Hs acceptable for a certain lifting operation. The objective of this master project is to determine the importance of heading for the actual ability of the vessel to carry out its mission, which is considered as lowering objects through the water surface ("splash zone"). Furthermore, the importance of ship geometry for the shielding effect should be investigated, in order to know whether it should be required to include a new calculation of the shielding effect for each new ship and loading condition.

The following topics should therefore be covered in the master project:

- Perform a literature study to clarify how the operational limit for such lifting operations is currently determined, characteristics of the wave environment, and the theory and limitations of the software to be used in the investigation.

- An important shortcoming in the project thesis was the use of long-crested waves when determining the wave field around the ship. Therefore, the analysis of the shielding should be extended to cover the effect of short-crested waves, and the results with long- and short-crested waves be compared.

- For the vessel investigated in the project thesis, perform an analysis of a lifting operation using Orcaflex; with and without taking the shielding effect into consideration. Different wave conditions should be included in the study.

- To check whether the shielding effect has to be computed for every new hull geometry and loading condition, it is recommended, if time allows, to carry out a parametric study of the influence of various hull geometry parameters (most importantly main dimensional ratios like L/B, B/T, $C_B$ etc.).

- If it is found justifiable (ref the previous bulletpoint), a method to use a general set of wave elevation RAOs, including shielding, in Orcaflex shall be proposed, if time allows.

In the thesis the candidate shall present her personal contribution to the resolution of problem within the scope of the thesis work.

Theories and conclusions shall be based on mathematical derivations and/or logic reasoning identifying the various steps in the deduction.

**NTNU Trondheim**
**Norwegian University of Science and Technology**
*Department of Marine Technology*

The thesis work shall be based on the current state of knowledge in the field of study. The current state of knowledge shall be established through a thorough literature study, the results of this study shall be written into the thesis. The candidate should utilize the existing possibilities for obtaining relevant literature.

The thesis should be organized in a rational manner to give a clear exposition of results, assessments, and conclusions. The text should be brief and to the point, with a clear language. Telegraphic language should be avoided.

The thesis shall contain the following elements: A text defining the scope, preface, list of contents, summary, main body of thesis, conclusions with recommendations for further work, list of symbols and acronyms, reference and (optional) appendices. All figures, tables and equations shall be numerated.

The supervisor may require that the candidate, in an early stage of the work, present a written plan for the completion of the work. The plan should include a budget for the use of computer and laboratory resources that will be charged to the department. Overruns shall be reported to the supervisor.

The original contribution of the candidate and material taken from other sources shall be clearly defined. Work from other sources shall be properly referenced using an acknowledged referencing system.

The thesis shall be submitted electronically (pdf) in DAIM:
- Signed by the candidate
- The text defining the scope (signed by the supervisor) included
- Computer code, input files, videos and other electronic appendages can be uploaded in a zip-file in DAIM. Any electronic appendages shall be listed in the main thesis.

The candidate will receive a printed copy of the thesis.

Supervisor       : Professor Sverre Steen
Start            : 15.01.2015
Deadline         : 10.06.2015


Trondheim, 15.01.2015

Sverre Steen
Supervisor

# Preface

This master thesis has been carried out as a part of the study program Marine Technology at NTNU, during the spring semester of 2015. It is part of the requirements of the degree Master of Science in Marine Technology. The work performed in this thesis is based on results obtained in the project work carried out in the autumn of 2014. The thesis is written in cooperation with DeepOcean.

The main objective has been to investigate how the implementation of shielding affect the operational limit for different structures as they are lifted through the splash zone. Prior to the thesis I was not familiar with the software program Orcaflex. A lot of time has therefore been used to obtain sufficient knowledge to perform dynamic analyzes using this software.

I would particularly like to thank my supervisor at NTNU, Sverre Steen, for guidance and that he has taken the time to answer all my questions during this spring. In addition I would like to thank Martin Johan Nore, which has been my supervisor from DeepOcean. He has been of great help with all software related questions and helped me to obtain the necessary input data and information regarding the analyzes and post-processing. The last person i would like to thank is Peter Christian Sandvik from MARINTEK who has answered all my questions regarding offshore lifting operation.

<div align="center">

Trondheim, 10-06-2015

*Camilla W. Olsen*

―――――――――――――――――――――――

Camilla Waldum Olsen

</div>

# Summary

The offshore industry is constantly seeking to operate in more extreme conditions. DeepOcean is a subsea service company, where offshore lifts is a part of every day operations. To remain competitive, it is important to reduce operational downtime, where time spent waiting on weather is one of the main contributors. The main goal of this thesis is to investigate how shielding effects influence the operational limit for offshore lifting operations at different heading angles. Common practice in the offshore industry is to use long-crested waves when determining the operational limit, and shielding effects are often neglected, which is a conservative approach.

A case study of two different structures, a Manifold and a ROV system, has been conducted. Repeated launch and recovery analyzes has been performed in Orcaflex, a time domain finite element program developed for static and dynamic analysis of offshore systems. Irregular waves are applied using a JONSWAP spectrum with $T_p = 5 - 19s$ and $H_s = 1 - 4m$ for the Manifold and $H_s = 2 - 8m$ for the ROV system. Both long- and short-crested waves, as well as 4 heading angles have been investigated. Shielding effects has been accounted for by the use of Sea State RAOs calculated in WADAM, a hydrodynamic analysis program for calculation of wave-structure interaction. The maximum tension in the lifting wire is considered as the dimensioning parameter. Gumbel extreme value statistics has been used to evaluate the distribution of maximum lifting wire tension, based on 20 simulations per sea state.

The calculated maximum wire tension was found to be highly dependent on whether or not slack would occur during a simulation. A slack wire result in snap loads with unpredictable magnitude. Incorporation of shielding in the simulations resulted in a significant drop in the occurrence of slack, for both structures. Thus, shielding effects is found to reduce the uncertainty related to the maximum tension due to a reduction in snap loads. The operational limit for the Manifold was increased with 0.5-1.0 m on average when shielding was included for most periods and heading angles, for both long- and short crested waves. The results obtained for the ROV was found to be highly unpredictable in magnitude due to slack occurring in the dominating part of the simulations, especially for steep waves. In contrast shielding showed to have a consistent positive effect, for heading angles with low vessel motion in roll.

# Sammendrag

Offshoreindustrien jobber kontinuerlig mot å operere under mer ekstreme forhold. DeepOcean er et subsea service selskap, der offshoreløft dominerer i den daglige operasjonen. For å forbli konkurransedyktige, er det viktig å redusere operasjonell nedetid, hvor en stor bidragsyter er tid som blir bruk til å vente på været. Hovedmålet med denne masteroppgaven er å undersøke hvordan skjerming fra fartøyet påvirker operasjonsgrensen løfteoperasjoner offshore, ved ulike headingvinkler. Vanlig praksis i offshoreindustrien er å bruke langkammede bølger når man skal bestemme operasjonsgrensen, og skjerming er ofte neglisjert, noe som anses å være konservativt.

En casestudie av to ulike strukturer, en manifold og ett ROV-system, har blitt gjennomført. Gjentatte løfteanalyser har blitt gjennomført i OrcaFlex, et tidsdomene FEM-analyseprogram utviklet for statisk og dynamisk analyse av offshore systemer. Irregulære bølger beskrevet av et JONSWAP spektrum med $T_p = 5 - 19s$ og $H_s = 1 - 4m$ for Manifoldet og $H_s = 2 - 8m$ for ROV-system. Både lang- og kortkammede bølger samt fire headingvinkler har blitt undersøkt. Skjerming er inkludert ved bruk av Sea State RAOer beregnet i WADAM, et hydrodynamisk analyseprogram for beregning av bølge-struktur interaksjonsproblemer. Den maksimale kraften i løftevaieren anses som den dimensjonerende parameteren. Gumbel ekstremverdistatistikk er blitt brukt til å vurdere fordelingen av maks kraft i løftevaier, hvor 20 simuleringer per sjøtilstand er brukt som grunnlag.

Beregnet maksimal kraft i vaieren ble funnet til å være svært avhengig av hvorvidt slakk eller ikke ville forekomme i løpet av en simulering. Slakk vaier resulterer i rykklaster med uforutsigbar størrelse. Det er observert en betydelig nedgang i forekomsten av slakk vaier når skjerming tas i betraktning. Dette gjelder for begge strukturene. Dette vil si at skjerming bidrar til å redusere usikkerhetene relatert til maks kraft i vaieren, siden antallet rykklaster reduseres. Den operasjonelle grensen for Manifolden økte med 0.5-1.0 m i gjennomsnitt da skjerming ble inkludert for de fleste perioder og heading vinkler, både for lang- og kortkammede bølger. Resultatene for ROV-systemet var veldig uforutsigbare på grunn av høy forekomst av slakk i de fleste simuleringene, spesielt for bølger med høyt $H_s/T_p$ forhold. I motsetning har skjerming vist å ha en konsekvent positiv effekt, for headingvinkler med lav fartøys bevegelse i rull.

# Contents

# List of Figures

# List of Tables

# Nomenclature

**Abbreviations**

AP      Aft Perpendicular

DNV   Det Norske Veritas

IMR    Installation, Maintenance , Repair

LARS  Launch And Recovery System

Loa     Length over all

Lpp     Length between perpendiculars

RAO    Response Amplitude Operator

ROV    Remotely Operated Vehicle

TMS    Theter Management System

WOW   Waiting on Weather

WROV  Work ROV

**Roman Symbols**

$\ddot{x}$      Acceleration Vector

$\dot{x}$       Velocity Vector

$a_r$      Fluid Particle Acceleration Relative to Earth

$A_w$    Slamming Area

$a_w$      Fluid Particle Acceleration Relative to Body

$B$      System Damping

$B_{wire}$      Wire Damping

$C$      System Stiffness

$C_{a33}$      Vertical Added Mass Coefficient

$C_a$      Added Mass Coefficient

$C_s$      Slamming Coefficient

$C_{wire}$      Wire Stiffness

$D(\theta)$      Directional spectrum

$F$      External load

$F_\omega$      Fluid Force

$F_s$      Slamming Force

$F_{winch}$      Winch Drive Force

$F_{x,Weibull}$      Weibull Cumulative Distribution

$F_x(x;\mu,\beta)$      Gumbel Cumulative Distribution

$F_x^*$      Cumulative Distribution of Sample

$G$      Gumbel Parameter

$g$      Acceleration of gravity

$H_s$      Significant wave height

$L$      Total Length of Winch Wire Path

$L_0$      Unstretched Length of Winch Wire Paid Out

$M$      System Mass

$N$      Number of Samples of a Stochastic Variable

$n$      Spreading Exponent

$q$      Unit Vector

$S(\omega)$      Frequency spectrum

$S_J(\omega)$      JONSWAP wave spectrum

$S_{PM}(\omega)$      Pierson-Moskowitz spectrum

$T$      Wire Tension

$T_p$      Peak period

$T_z$      Zero-up-crossing wave period

$V_n$      Slamming Velocity

$V_r$      Fluid Particle Velocity

$x$      Position Vector

**Greek Symbols**

$\alpha$      Weibull Distribution Parameter

$\beta$      Gumbel Distribution Parameter

$\Delta$      Mass of Displaced Water

$\epsilon$      Wire Strain

$\gamma$      Peak shape parameter

$\mu$      Gumbel Distribution Parameter

$\omega_P$      Spectral peak frequency

$\psi$      Weibull Distribution Parameter

$\rho$      Sea Water Density

$\sigma$        Spectral width parameter

$\theta$        Wave Direction

$\theta_p$       Principal Wave Direction

# Chapter 1

# Introduction

## 1.1 Background and Motivation

DeepOcean offers a wide range of subsea services including installation, maintenance and repair (IMR). To achieve a strong position in the market operational downtime is an important factor. Reducing operational downtime allows DeepOcean to stay competitive and enables them to be more cost efficient in association with marine operations.

One of the main contributions to operational downtime is time spent waiting on weather (WOW). The operational window for lifting operations is restricted by significant wave height $H_s$. This applies to operations with both cranes and remotely operated vehicles (ROVs). To decrease the WOW contribution the effect of shielding has to be investigated. By documenting the effect of shielding on the lee side of a vessel one can implement it into the estimation of operational $H_s$.

Today DeepOcean uses repeated launch/recovery time domain analysis in Orcaflex, and simplified methods provided by DNV (DNV, 2014b) to determine operational $H_s$. None of which the effect of shielding is taken into account.

## 1.2 Objective

The main objective of this master thesis is to investigate how the operational limit for offshore lifts is affected when shielding is taken into account. Time domain analysis in Orcaflex are to be performed for two different structures, at four different heading angles with both long- and short-crested waves. Maximum tension and slack in the lifting wire are to be used as dimensioning criteria for a given sea state. The resulting tension extracted from the simulations are to be evaluated by the use of extreme value statistics.

1

## 1.3 Literature Review

Large quantities of literature discuss problems regarding lifts through the splash zone, especially when it comes to estimation of loads. Bai and Bai (2010) have performed a detailed discussion on different subsea structures, and how they should be analyzed. DNV GL have published the recommended practice "Modeling and Analysis of Marine Operations" which is a detailed discussion on hydrodynamic coefficients, loads, and guidelines for lifting structures through the splash zone. They have also published the Offshore Standard "Lifting Operations" where a detailed description of documentation, loads, and design criteria, to mention a few, is given.

The diffraction-radiation problem is solved by the use of potential theory as discussed by Faltinsen (1990). Although the mathematical background is well established, no relevant literature was found regarding the effect of shielding on the lee side of a ship. Neither general studies on shielding effects, or in relation to marine operations.

## 1.4 Limitations

Due to lack of time, some limitations had to be made with respect to the original problem description.Thus, a parametric study on the influence of different hull geometry parameters has not been performed.

## 1.5 Structure of the Report

The vessel and structures used in the analysis are described in Chapter 2. A short description as well as main dimensions used as basis for the time domain analysis, are presented. The relevant theory of Orcafelx is given in Chapter 3.

In Chapter 4, modeling of the two structures in Orcaflex are described. In addition are the environmental conditions given in this chapter. The use of extreme value statistics is described in Chapter 5. Identified uncertainties are presented and discussed in Chapter 6.

The result obtained from the time-domain analysis are presented and discussed in Chapter 8. Chapter 9 and 10 contains the conclusion and recommendations for further work respectively.

# Chapter 2

# Vessel and Structure Description

## 2.1 Rem Forza

REM Forza is a subsea service vessel chartered by DeepOcean (Figure 2.1). It is designed to perform a variety of offshore operations especially; installation, maintenance and rapair (IMR) on installations below the sea surface. The main dimensions are listed in Table 2.1. The dynamic response of the vessel is described through Response Amplitude Operators (RAOs) in 6 degrees of freedom.



Figure 2.1: Rem Forza (DeepOcean, 2014b)

| Main Characteristics | Value | Unit |
|:---:|:---:|:---:|
| Loa | 108.7 | [m] |
| Lpp | 100 | [m] |
| Breadth | 22.0 | [m] |
| Draught, midship | 5.3 | [m] |

Table 2.1: Main Dimensions REM Forza

## 2.2 Manifold

A manifold is a subsea structure which is permanently installed on the seabed. An example of a Manifold is given in Figure 2.2. It has multiple functions such as, control of well production, distribution of hydraulic control fluid, and provide flow line isolation, just to mention a few. For a manifold can size and weight of the structure vary extremely depending on the purpose for which it will be used. The main characteristics of the manifold considered in this thesis are listed in Table 2.2.
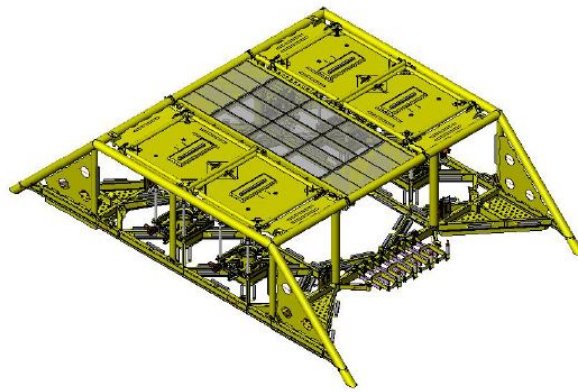


Figure 2.2: Example of Manifold

Table 2.2: Main Dimensions Manifold (DeepOcean, 2014a)

| Main Characteristics | Value | Unit |
|---|---|---|
| Length | 7.5 | [m] |
| Breadth | 7 | [m] |
| Height | 4 | [m] |
| Weight in Air | 50 | [Te] |
| Displacement | 6.4 | [m$^3$] |

Immersion of the manifold is intended to be carried out by a 250Te crane located on the port side of the vessel, 29.5 m from AP (Figure 2.3).
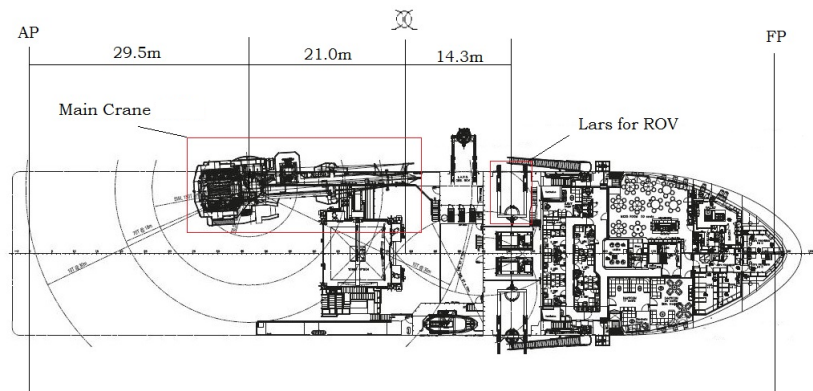


Figure 2.3: Location of Crane and LARS on Main Deck

## 2.3 ROV, TMS and Lifting Frame

The vessel is equipped with two Working-ROV (WROV) of the type Supporter, one on each side of the vessel. The ROVs are linked to the vessel with an umbilical cable which is managed by the tether management system (TMS)(Figure 2.4). The main dimensions of the ROV and TMS are given in Table 2.3.



Figure 2.4: WROV of Type Supporter with TMS

Table 2.3: Main Dimensions ROV and TMS (DeepOcean, 2015)

| Item | Property | Value | Unit |
|------|----------|-------|------|
| Supporter ROV | Length | 2.5 | [m] |
| | Width | 1.70 | [m] |
| | Height | 1.65 | [m] |
| | Mass | 3.05 | [m] |
| | Displacement | 2.98 | [m$^3$] |
| | Weight in Water | 0.0 | [Te] |
| TMS | Diameter | 2.2 | [m] |
| | Height | 2.13 | [m] |
| | Mass | 2.80 | [Te] |
| | Displacement | 0.61 | [m$^3$] |
| | Weight in Water | 2.17 | [Te] |

The ROV is moved on/off deck by a Launch And Recovery System (LARS). The LARS lifts the ROV from inside the hangar, through a hatch on the ship side. The LARS longitudinal position on main deck is given in Figure 2.3. It is located 14.3 m from midships (64.8 m from AP).

# Chapter 3

# Theory of Orcaflex

OrcaFlex is a time domain finite element program, developed by Orcina. It is designed for static and dynamic analysis of a wide range of offshore systems. This includes all types of risers (flexible and rigid), moorings, installation and towed systems. The software is equipped with a graphical interface to assist understanding. The theory in this section is outlined, according to the OrcaFlex User Manual, Orcina (2012).

## 3.1   Analysis

A static analysis is used to determine the conditions of equilibrium of the system under weight, buoyancy, etc, and to decide initial conditions for a dynamic analysis. The static analysis is performed in three iterative stages. For more information see the Orcaflex user manual Section 5.5 (Orcina, 2012). The dynamic analysis is initiated from the equilibrium position calculated by the static analysis, where the models motions are simulated over a time period specified by the user. The dynamic analysis is divided into two main parts, the build-up, and the main simulation part(s). During the build-up stage the waves and model motions are increased gradually from zero (static) to a fully developed condition (dynamic). This gradual increase helps reduce transients when changing from a static position to a dynamic motion. The second part of the dynamic analysis is where the dynamic equation of motion is solved. The main part is usually divided into several user defined sub-stages, dependent on what one wants to simulate. In this thesis are stages used to be able to vary the winches length, payout rate, and payout rate change. This is further discussed in Section 3.6.5.

To solve the dynamic equation of motion (Equation 3.1), Orcaflex uses explicit and implicit integration. From the static equilibrium both methods recalculate the system geometry for every time step. By doing so, Orcaflex accounts for geometric non-linearities.

$$M\ddot{x} = F - B\dot{x} - Cx \tag{3.1}$$

where:

M : System Mass

B : System Damping

C : System Stiffness

F : External Load

$x, \dot{x}, \ddot{x}$ : position, velocity and acceleration vectors respectively

By the use of explicit integration, is the position and orientation of all objects obtained in the static analysis, used at the start of the simulation. Based on the equilibrium obtained in the static analysis, the local equation of motion is solved for the acceleration vector at the first time step. This is done for each free body and line node in the model. The position, velocity, and acceleration at the end of the time step is determined by the use of forward Euler integration. The result is used as the basis for solving the local equation of motion again, and the process is repeated using a constant time step throughout the simulation time. The implicit integration calculates forces, damping, moments etc. in the same way as the explicit integration. The main difference is that the implicit method solves the system equation of motion at the end of the time step, instead of the local equation of motion for each object. Since the position, velocity and acceleration are unknowns a series of iterations are required to get a solution that converges for each time step.

## 3.2 Coordinate Systems

Orcaflex essentially operates with two types of coordinate systems, a global, and a local coordinate system. The global coordinate system is donated GXYZ, where GX, GY, and GZ are the global axes. One local coordinate system is defined for each object included in the model, vessels, 6D buoys, 3D buoys, links, and winches are all defined as objects, further discussed in Section 3.6.

## 3.3 Jonswap Spectrum

Orcaflex offers five different wave frequency spectra to describe irregular waves: JONSWAP, ISSC, Ochi-Hubble, Torsethaugen, and Gaussian swell. In this thesis is the JONSWAP specter is used to describe the sea state.

The JONSWAP spectrum is a five-parameter, one peaked spectrum, based on the Pierson-Moskowitz (PM) spectrum. It is frequently applied for wind seas, and is originally based on measurements performed in the south-east part of the North Sea (Myrhaug, 2007). The JONSWAP spectrum is frequently used to describe sea states which are not fully developed. Based on the PM specter (Equation 3.2) the JONSWAP specter is expressed in Equation 3.3 (DNV, 2010).

$$S_{PM}(\omega) = \frac{5}{16} H_s^2 \omega_p^4 \omega^{-5} exp\left(-\frac{5}{4}\left(\frac{\omega}{\omega_p}\right)^{-4}\right) \tag{3.2}$$

$$S_J(\omega) = A_\gamma S_{PM}(\omega) \gamma^{exp\left(-0.5\left(\frac{\omega-\omega_p}{\sigma\omega_p}\right)^{-4}\right)} \tag{3.3}$$

where:

$S_{PM}(\omega)$ : Pierson-Moskowitz spectrum

$S_J(\omega)$: JONSWAP spectrum

$H_s$ : Significant Wave Height

$\omega_P = \frac{2\pi}{T_p}$ : Spectral Peak frequency

$\gamma$ : Non-dimensional peak shape parameter

$\sigma$: Spectral width parameter

$\quad\sigma = \sigma_a$ for $\omega \leq \omega_p$

$\quad\sigma = \sigma_a$ for $\omega > \omega_p$

$A_\gamma$: $1 - 0.287 ln(\gamma)$

The peak shape parameter is defined in the following way:

$$\gamma = \begin{cases} 5 & \text{if } \frac{T_p}{H_s} \leq 3.6 \\ exp\left(5.75 - 1.15 \cdot \frac{T_p}{H_s}\right) & \text{if } 3.6 < \frac{T_p}{H_s} < 5 \\ 1 & \text{if } \frac{T_p}{H_s} \geq 5 \end{cases} \tag{3.4}$$

## 3.4 Directional Spread Spectrum

Short-crested waves are defined by the product of a frequency spectrum $S(\omega)$ and a directional spreading function $D(\theta)$ (Equation 3.5). The resulting spectrum is thus dependent of both wave direction and frequency.

$$S(\omega, \theta) = S(\omega) \cdot D(\theta) \tag{3.5}$$

The directional spreading specter (Equation 3.6) is defined by the spreading exponent $n$, the wave direction $\theta$, and the principal wave direction $\theta_p$.

$$D(\theta) = \frac{\Gamma\left(1 + n/2\right)}{\sqrt{\pi} \cdot \Gamma\left(1/2 + n/2\right)} cos^n\left(\theta - \theta_p\right) \quad \text{for} \quad \frac{-\pi}{2} \leq \theta - \theta_p \geq \frac{\pi}{2} \tag{3.6}$$

An example of a directional spreading spectrum, is given in Figure 3.1. The principal wave direction is $\theta_p = 0$ and 9 wave directions are taken into account (appears as red dots on the x-axis). The number of wave directions is a user specified number, in this case equal to 9, i.e. the principal wave direction plus 8 more. The principal direction is set by the user, and Orcaflex determines the remaining directions by the use of an Equal Energy Approach. More information about the Equal Energy Approach can be found in Section 5.10.6 of the Orcaflex user manual, (Orcina, 2012).
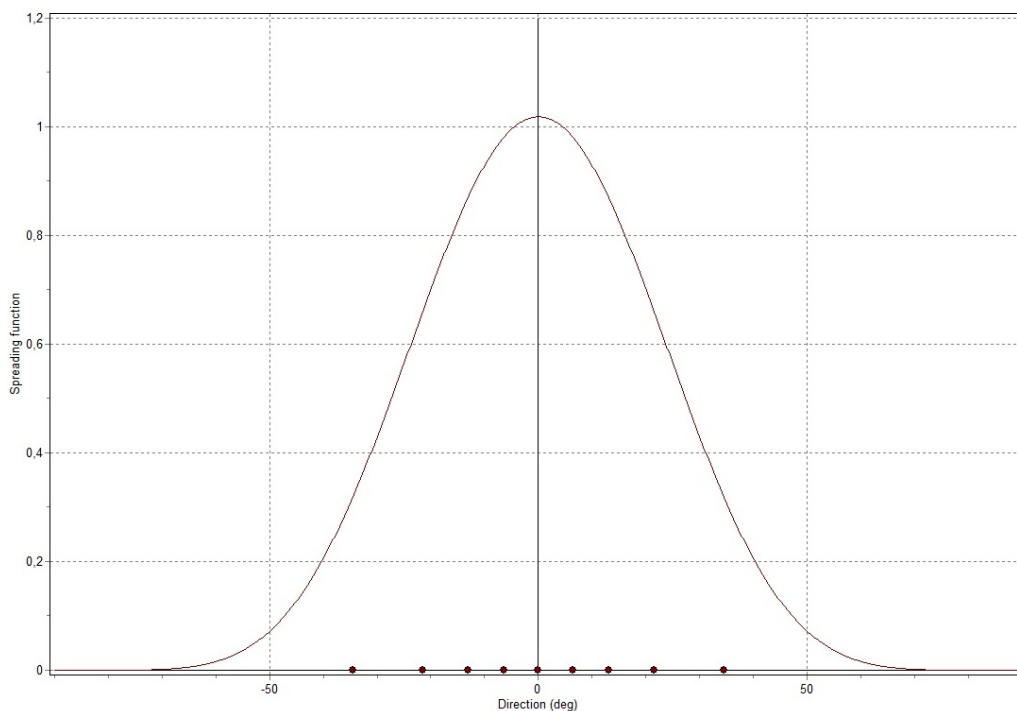


Figure 3.1: Direction Spreading Spectrum from Orcaflex

## 3.5   Sea State RAOs

The effect of shielding and radiation is taken into account via the Sea State RAOs. Without this type of RAOs, objects will experience the undisturbed wave. An example of that is a wave which is not affected by for example a vessel floating on the surface. The sea state RAOs take into account how an object affects the passing waves due to its presence, i.e. the wave radiation and diffraction problem. The sea state RAOs are used to calculate elevation, fluid velocity and acceleration in the disturbed sea. The sea state RAOs contain the following information:

1. Heading

2. Wave Frequency

3. Position

4. Velocity Potential

    (a) Amplification Factor & Phase

5. Velocity Potential Gradient (x-, y-, z-direction)

    (a) Amplification Factor & Phase

The amplification factor and phase shift for the velocity potential components are functions of heading angle, position and wave frequency. The Sea State RAOs are in practice used as scaling factors between the undisturbed incoming wave components and the disturbed wave components (Orcina, 2014). Position refers to a point on the free surface where the velocity potential components are defined. It is recommended to arrange these points as a grid with equal spacing between each point (Figure 3.2). For points on the free surface where the sea stat RAOs are not defined interpolation is used.
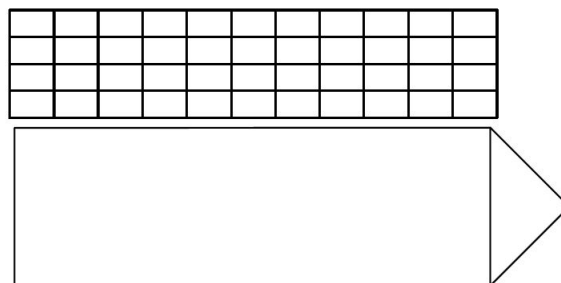


Figure 3.2: Sea State RAO point location example

## 3.6 Objects

### 3.6.1 Vessel

The object type Vessel is frequently used to model ships, platforms, semi-subs or other floating structures. A vessel is specially suitable for floating structures where wave diffraction is of significance, because the vessel motions are determined based on RAOs. It is free to move in six degrees of freedom, three translations (surge, sway, and heave) and three rotations (roll, pitch, and yaw). The vessel motions are divided into two categories: low frequency and wave frequency motions. Both types of motions are usually present, in that case they are modeled separately and the wave frequency motions are superimposed of the low frequency motions. Further information about how Orcaflec treats vessel motions are given in the user manual Section 6.7.1 (Orcina, 2012).

### 3.6.2 6D Buoy

A 6D buoy is a rigid body with 6 degrees of freedom, 3 translations and 3 rotations. Common for both 3D and 6D buoys is that their motions are calculated by Orcaflex, i.e the response is not specified via RAOs as done for vessels. Orcaflex distinguishes between three different types of buoys: spar-, towed fish- and lumped-buoy. Spar- and tow fish-buoys are used to model axi-symmetric geometry whose axis are vertical and horizontal respectively. Lumped buoys are used without reference to a specific geometry (Orcina, 2014). In this thesis only lumped buoys have been used due its flexibility regarding geometry. The following definitions and equations applies to lumped buoys.

Hydrodynamic loads on lumped buoys are calculated by using an extended version of Morison's Equation (3.7). This also applies for loads on 3D buoys.

$$F_w = \left(\Delta a_w + C_a a_r\right) + \frac{1}{2}\rho C_D A V_r |V_r| \tag{3.7}$$

$F_w$ is the fluid force which is defined as the sum of the inertia force and drag force. The inertia force is dependent on the water particle acceleration. $\Delta$ is the mass of displaced water, $a_w$ and $a_r$ are the fluid particle acceleration relative to the body and the earth respectively, and $C_a$ is the added mass coefficient. The drag force is dependent on the fluid particle velocity. The fluid particle velocity $V_r$ is calculated relative to the body, $A$ is the drag area, and $C_d$ is the drag coefficient. The accelerations $a_w$, $a_r$ and velocity $V_r$ are calculated in the buoy center of the wetted volume.

Slamming loads on lumped buoys are calculated according to Equation 3.8. It is applied in the buoy center of wetted volume. Slamming loads can only be applied to 6D buoys in Orcaflex. Notice that a drag formulation is used to calculate slamming loads, instead of rate change in vertical added mass coefficient $C_{a33}$.

$$F_s = \pm \rho C_s A_w |V_n|^2 q \tag{3.8}$$

where $C_s$ is the slamming coefficient, $A_w$ is the slamming area, $V_n$ is the vertical velocity of the buoy relative to the fluid, and q is the unit vector in water surface outward direction. The slamming force is positive for fluid entry and negative for fluid exit.

### 3.6.3  3D Buoy

A 3D buoy is a rigid body which is free to move in 3 degrees of freedom (surge, sway, and heave), and are restrained from rotation. Properties as weight, buoyancy, drag, and added mass can be defined for a 3D bouy. 3D buoys are suitable to use for modeling of small bodies where rotations are negligible. If the properties of the buoy are neglected, a 3D buoy is suitable for modeling nodes in the system.

### 3.6.4  Links

Links are mass-less connections used to connect two other objects together. Two types of links are available tethers which are elastic ties, and springs/dampers (which is a combination of springs and damper units). Tether type links are frequently used to model slings in a lifting operation.

### 3.6.5 Winch

Winches are mass-less objects used to connect two or more objects in the model together. During a static analysis where the initial length of the winch wire is defined, the wire tension T and the winch drive force $F_{winch}$ are both set equal to:

$$T = F_{winch} = C_{wire} \cdot \epsilon \tag{3.9}$$

where:

$C_{wire}$ : Wire Stiffness

$\epsilon$ : Wire strain

$L$ :Total length of the winch wire path

$L_0$ : Unstretched length of winch wire paid out

Simulations of lifting operations are typically divided into stages dependent on the specified winch properties. Three different properties have been used in this thesis:

1. Specified Length : Value which defines the winch wire's unstretched length. Basis for the static analysis of the wire tension.

2. Specified Velocity (Payout Rate): Value that specifies the rate for which the winch wire is paid out (positive) or drawn in (negative).

3. Specified Acceleration (Payout Rate Change): Value which defines the payout rate change during a given stage of the simulation. Used to soften the transition between a stand-still and a moving stage for the wire or conversely .

During the dynamic stage of the simulation, the winch wire tension $T$ is calculated according to Equation 3.10.

$$T = K \cdot \epsilon + B_{wire} \cdot C_{wire} \cdot \frac{d\epsilon}{dt} \tag{3.10}$$

where:

$B_{wire}$ : Wire Damping

$\frac{d\epsilon}{dt}$ : Wire strain rate

Compression is not allowed in the winch wire, if $T$ calculated from Equation 3.10 is negative. Then the wire is considered to have gone slack, and the wire tension $T$ is set equal to zero. Snap loads that occur after the winch wire has gone slack is also covered by Equation 3.10.

# Chapter 4

# Modeling

The applied environmental conditions and the modeling performed in Orcaflex are described in this chapter. In addition, are the limiting criteria and analysis procedure given.

## 4.1 Environmental Conditions

The applied environmental conditions applied in the Orcaflex analysis are described in this section. In addition is the procurement of the sea state RAOs described.

### 4.1.1 Wave Directions

Analysis are performed for 4 different wave directions\heading angles: 180° (head sea),150°, 120° and 90° (beam sea). The definition of wave directions are shown in Figure 4.1

Leeward Side

0

180

90
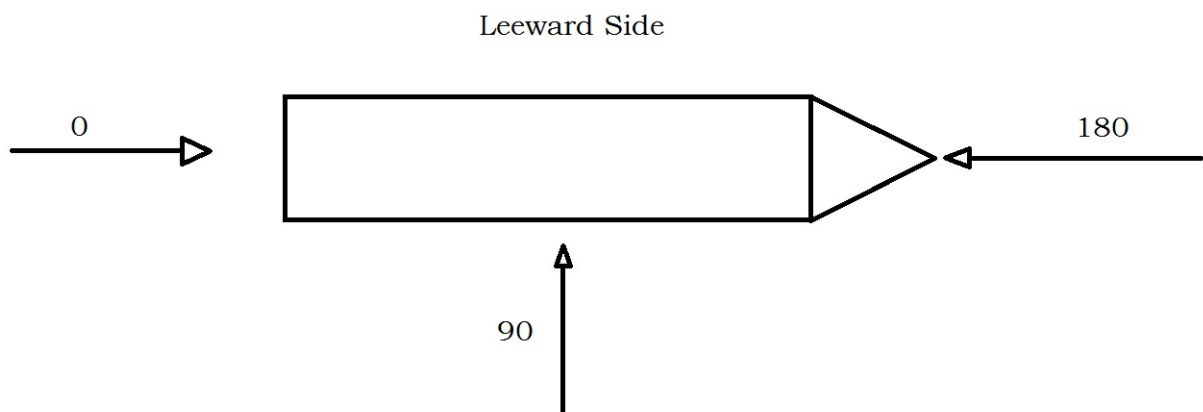
Figure 4.1: Definition of Wave Directions

### 4.1.2 Design Wave

Irregular waves described by the JONSWAP spectra are used in the analysis, previously discussed in Section 3.3. For a analysis where the wave period is varied the range of zero-up-crossing periods $T_z$ for a given significant weave height $H_s$ given by Equation 4.1 should be taken into account (DNV, 2014b).

$$8.9 \cdot \sqrt{\frac{H_s}{g}} \leq T_z \leq 13 \tag{4.1}$$

Where the breaking wave limit is given by the lower limit of $T_z$ given above. For a JONSWAP spectrum the relationship between $Tz$ and $Tp$ is given by:

$$\frac{T_Z}{T_P} = 0.6673 + 0.05037\gamma + 0.00623\gamma^2 + 0.0003341\gamma^4 \tag{4.2}$$

Inserting the average values $\gamma = 3.3$, $\sigma_a = 0.07$, and $\sigma_b = 0.09$ the relation between $T_p$ and $T_z$ is given in Equation (DNV, 2010).

$$T_P = 1.2859 T_Z \tag{4.3}$$

Combining Equation 4.2 and 4.3 and solving for $H_s$ gives:

$$H_s = g \cdot \left( \frac{T_p}{1.2859 \cdot 8.9} \right)^2 \tag{4.4}$$

Which defines the wave breaking limit given in Figure 4.2.
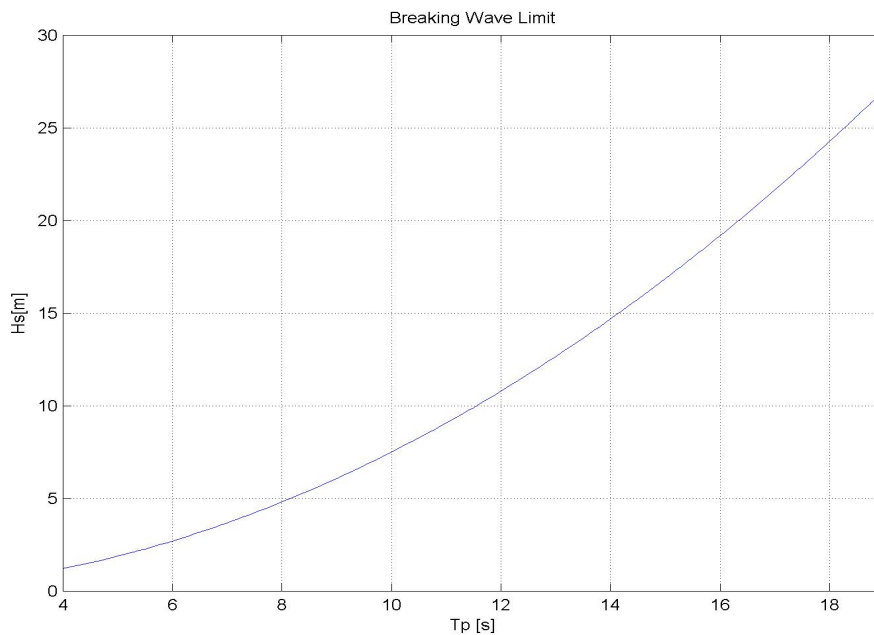


Figure 4.2: Breaking Wave Limit

The breaking wave limit defines the distinction between physically possible and impossible waves, it represents the maximum operational limit possible for all combinations of $H_s$ and $T_p$. In addition, it has been used to limit the number of simulations needed. It is possible to run analyzes for physically impossible combinations of $H_s$ and $T_p$ without getting inaccurate results. Thus, for $T_p = 6$ where the limiting $H_s$ is 2.7m analysis has only been carried out for $H_s$ up to maximum 3.0 m.

### 4.1.3 Directional Spreading Function

As described in Section 3.4 are short-crested waves implemented by the use of a spreading function. No data about the wave spreading was available, the following wave spreading parameters for the JONSWAP spectrum were assumed (Sandvik, 2015):

- Number of wave directions: 9

- Spreading exponent n is equal to $H_s$

The spreading function for all investigated heading angles are given in Appendix A.

### 4.1.4 Wave Period and Hs Combinations

The combination of $H_s - T_p$ applied in the dynamic analysis of the Manifold, varies with both heading and sea-state (long- and short-crested waves and Shielding/No Shielding). A base case with $H_s = 2m$ and $T_p = [5 - 19s]$ were applied for all cases. Which periods that should be analyzed at higher/lower $H_s$ was decided based on the base case results. Thus, if the capacity was exceeded for a given period at $H_s = 2m$ it would not be included in a simulation with $H_s = 2.5$ and so on. The combinations of $H_s$ and $T_p$ taken into account for all heading angles and sea states is given in Appendix B where the occurrence of slack is registered.

The combinations of $H_s - T_p$ applied in the dynamic analysis of the ROV system are given in Table 4.1. The same range of periods are applied for all heading angles and sea-states.

Table 4.1: Environmental Input Variables used in Dynamic Analysis for ROV System

| Hs | 2 | 2.5 | 3 | 3.5 | 4 | 4.5 | 5 | 5.5 | 6 | 6.5 | 7 | 7.5 | 8 |
|----|----|-----|----|-----|----|-----|----|-----|----|-----|----|-----|----|
| Tp | 5-12s | 6-12s | 6-13s | 7-13s | 7-12s | 8-13s | 8-19s | 9-19s | 9-19s | 9-19s | 10-19s | 10-19s | 10-19s |

### 4.1.5 Shielding Effects

Shielding effects in Orcaflex are included via a set of Sea State RAOs as described in Section 3.5. To obtain these RAOs, some alterations to the WADAM model developed in the project (performed this past fall) had to be made (Olsen, 2014). WADAM is part of the Sesam software package developed by DNV , and is short for "Wave Analysis by Diffraction and Morisons Theory". It is designed to calculate wave-structure interaction of fixed and floating structures. The graphical interface HydroD has been used to run WADAM.

A large part of the project assignment was to build a hull model for the vessel, the same model has been used here. A new set of "offbody points" surrounding the vessel on both sides were applied. A total of 350 points equally distributed on each side were used (Figure 4.3). An increment of 5 and 2.5m were used in x- and y-direction respectively. Offbody point are points on the sea surface for which WADAM calculates fluid kinematics. More information about WADAM could be found in the Project Thesis "Analysis of Wave Damping due to Wave Ship Interaction", given in Appendix C.1 together with the used WADAM model.
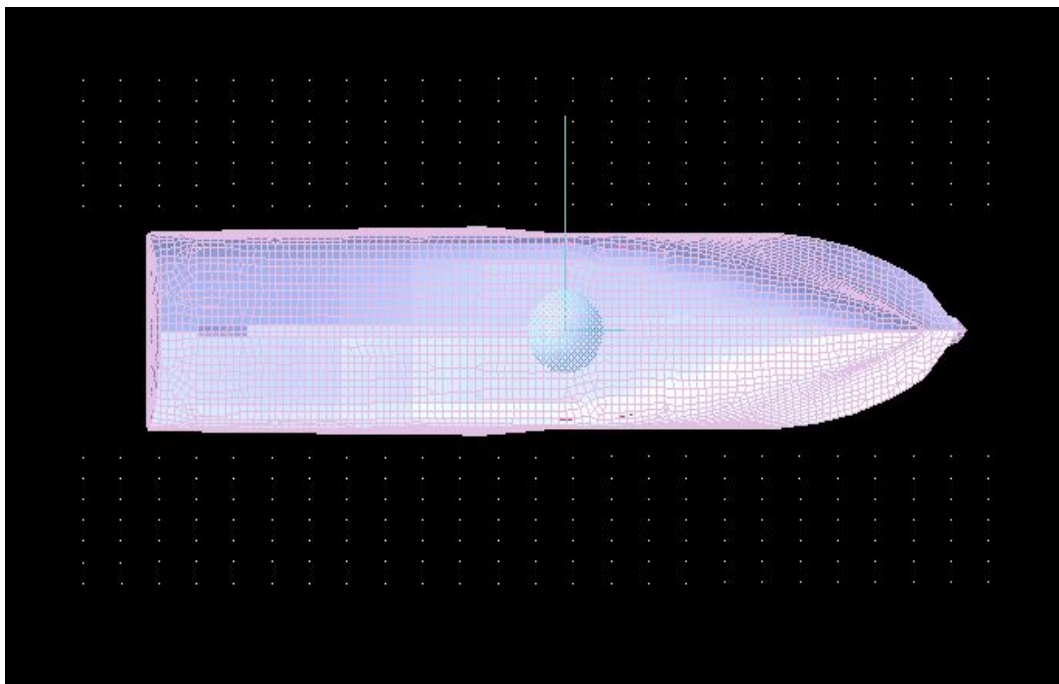


Figure 4.3: Hull Model with Offbody Points

The sea state RAO's were calculated in WADAM, and exported as a wamit.out file before they could be imported to Orcaflex. The resulting Sea State RAOs are given in Appendix C.2.

## 4.2   Orcaflex

The following section describes the modeling of the vessel, Manifold and ROV in Orcaflex. All input data is provided by DeepOcean, unless otherwise noted. The entire model in Orcaflex is built by the use of objects, previously described in Section 3.6.

### 4.2.1   Vessel

A model of REM Forza already developed by DeepOcean has been used in the analysis. All hydro-dynamic and structural properties for the vessel are stored here. The vessels motions are described by RAO's. The vessel is visualized by a simple box shaped geometry in Orcaflex (Figure 4.4). The vessels local origin is located 50.5 m from AP , midships, on the waterline in x-, y- and z-direction respectively.

(a) Wire Frame Model
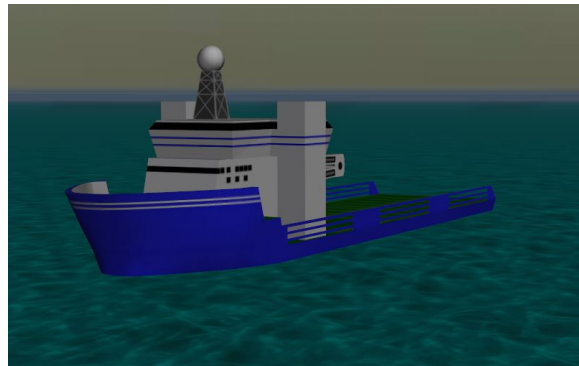
(b) Shaded Graphics Model

Figure 4.4: Model of Vessel used in Orcaflex

The only alteration made to the vessel model is the implementation of sea state RAO's (see Section 4.1.5), which was not part of the original model.

### 4.2.2 Manifold

The manifold model built in Orcaflex is shown i Figure 4.5 and 4.6 below. Which type of objects that have been used is shown, all 6D buoys have been marked with assigned properties.
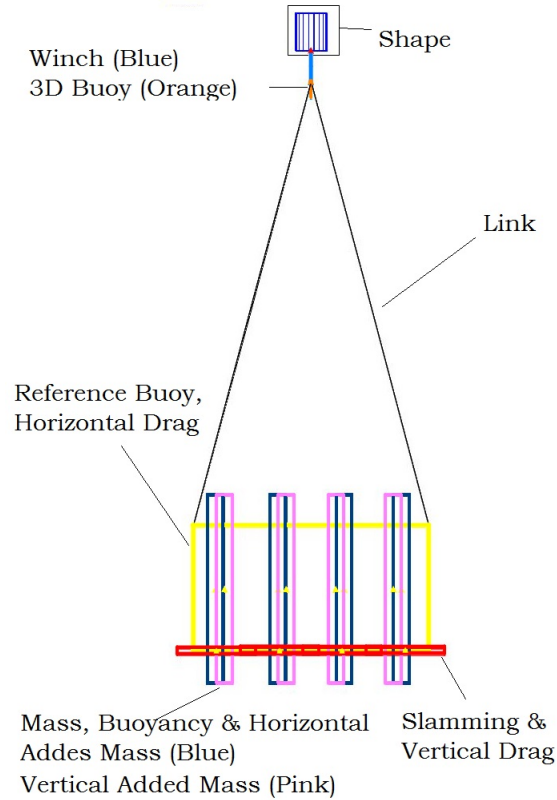


Figure 4.5: Orcaflex Model of Manifold: Side View
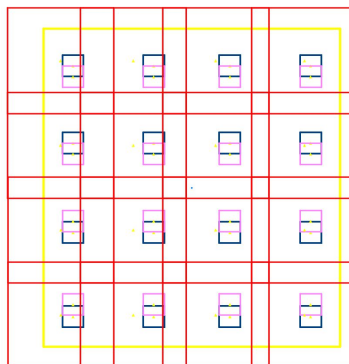


Figure 4.6: Orcaflex Model of Manifold: Top View

**Added Mass, Mass, and Buoyancy**

Mass, buoyancy, and horizontal added mass (A11 and A22) are modeled with 16 slender elements with height 6m, evenly distributed over the surface of the structure. Applied properties are given in Table 4.2 and 4.3. Both mass and buoyancy are evenly distributed along the element. Thus, buoyancy and horizontal added mass will not reach full potential before the structure is fully submerged.

Table 4.2: Mass and Volume Properties

| Property | Unit | Value |
|----------|------|-------|
| Mass (1 of 16) | Te | 3.13 |
| Volume (1 of 16) | m³ | 0.4 |

Table 4.3: Mass Moment of Inertia and Horizontal Added Mass Properties Manifold

| Property | Direction | |
|----------|-----------|---|
| | X | Y |
| Mass Moment of Inertia [Te.m²] | 3 | 3 |
| Added Mass Coefficient | 16.9 | 18.4 |

The vertical added mass (A33) is modeled by the use of 16 separate slender 6D buoys with height 10m. All which are evenly distributed over the surface of the structure. The properties assigned to each buoy are given in Table 4.4. Using slender elements will prevent a sudden change in added mass which can cause a force impulse to occur (slamming). This is done to avoid a double slamming effect, since slamming is separately accounted for. The vertical added mass will not reach its full potential until the structure has descended to a depth corresponding to approximately half the breadth of the structure. Thus, longer elements has been used to model A33 compared to A11 and A22.

Table 4.4: Mass Moment of Inertia and Vertical Added Mass Properties for Manifold

| | |
|----------|------|
| Mass Moment of Inertia [Te.m²] | 3 |
| Added Mass [Te] | 24.5 |
| Added Mass Coefficient | 1 |

**Drag and Slamming**

Horizontal drag in both directions are modeled with one 6D buoy. The same buoy is also used as a reference frame for the entire Manifold, its center is positioned in (x,y,z)=(-21.0,17.5,10.9) relative

to the vessel origin. The Manifolds projected area in x- and y-direction is used as the drag area. The assigned properties are given in Table 4.5.

Table 4.5: Horizontal Drag Properties of Manifold

|                  | Unit | Direction | |
|------------------|------|-----|-----|
|                  |      | X   | Y   |
| Drag Area        | m²   | 30  | 28  |
| Drag Coefficeint | -    | 2.5 | 2.5 |

Vertical drag and slamming on the structure is modeled with 6D buoys representing the bottom surface of the manifold. Orcaflex applies the slamming loads in the buoy center of wetted volume, 16 buoys has therefore been used to distribute the load. The water entry slamming coefficient is set equal to 5 according to DNV (2014b). All applied properties are given in Table 4.6.

Table 4.6: Slamming and Vertical Drag Properties Manifold

| Property                    | Unit | Value |
|-----------------------------|------|-------|
| Slamming Area (1 of 16)     | m²   | 3.28  |
| Slamming Coefficient (Entry)| -    | 5.0   |
| Drag Area (1 of 16)         | m²   | 3.28  |
| Drag Coefficient            | -    | 7.00  |

**Crane and Rigging**

The Manifold is connected to the vessel via 3 objects. Four links one in each corner of the structure is used to model slings that keep the structure stable. All links are 15.0m long and a stiffness equal to 145,0E3 kN is applied. Each link is connected to a 3D buoy which represents a 10 Te lump weight. A winch which represents the crane and crane wire is used to connect the lump weight to the vessel. The winch is used to control lowering of the manifold, this is done in stages dependent on the winch properties (Table 4.7). Since the winch is connected to the vessel it also assures that the manifold moved with the vessel motion. The winch wire stiffness is set to 600.0E3 kN. The "shape" seen in Figure 4.5 is used only to get e better visual of the crane movement, it has no properties that affect the simulation.

Table 4.7: Simulation Stages and Winch Modes for Manifold

| Stage   | Duration [s] | Time at Stage End [s] | Mode                         | Value |
|---------|--------------|-----------------------|------------------------------|-------|
| Statics | -            | -                     | Specified Length             | 1     |
| 0       | 8            | 0                     | Specified Payout Rate Change | 0.3   |
| 1       | 80           | 80                    | Specified Payout Rate        | 0.3   |

### 4.2.3 ROV

The finished model of the entire ROV system is shown in Figure 4.7. ROV and TMS is modeled by the use of 6D buoys only, and a winch is used to model the LARS system. The assigned properties for 6D buoys are shown in the figure below.
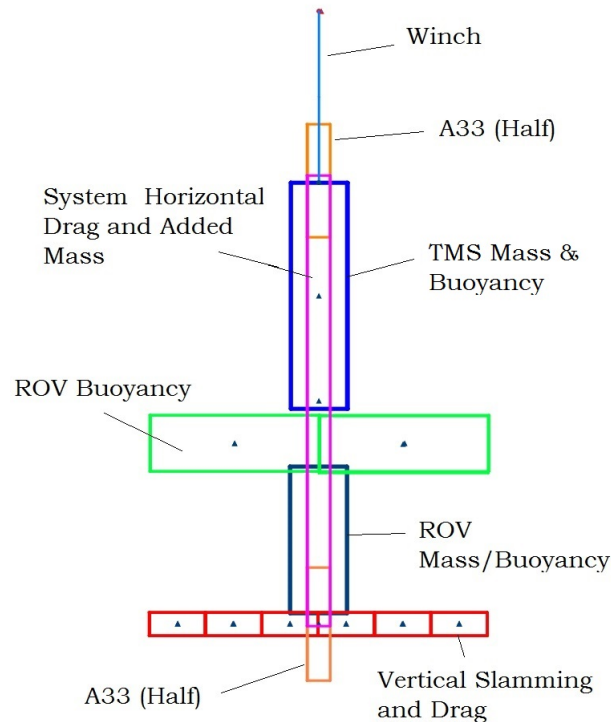


Figure 4.7: Orcaflex Model of ROV

**Mass, and Buoyancy**

Mass and buoyancy are modeled separately for the ROV and TMS. One 6D bouy is used for the TMS, which is assigned both mass and volume properties. A total of five 6D buoys has been used for the ROV. On the real ROV is the upper part dominated by buoyancy-elements, while the lower part consists of pipes, rods, electronics and more. Thus, most of the ROVs volume is located in the upper part. Four 6D buoys assigned volume properties representing the upper part and one with both mass and volume properties representing the lower part has therefor been used. The latter is also used as a reference frame for the rest of the ROV system, its center was placed in (x,y,z)=(7.5,15.8,3.6) relative to the vessel origin. The properties assigned to each buoy are given in Table 4.8 and 4.9, the same name convention ass used in Figure 4.7 applies. Orcaflex does not allow mass less objects to have volume properties. Thus, a negligible mass has been assigned to the ROV Buoyancy elements.

Table 4.8: Mass and Buoyancy Properties ROV

|                        | Mass [Te] | Volume [m³] |
|------------------------|-----------|-------------|
| TMS Mass & Buoyancy    | 2.8       | 0.61        |
| ROV Buoyancy (1 of 4)  | 0.0001    | 0.5         |
| ROV Mass/Buoyancy      | 3.05      | 0.98        |

Table 4.9: Mass Moment of Inertia ROV

|                     | Moment of Inertia [Te.m²] | | |
|---------------------|-----|-----|-----|
|                     | X   | Y   | Z   |
| ROV Mass/Buoyancy   | 4.5 | 5   | 4.5 |
| TMS Mass & Buoyancy | 3   | 3   | 3   |

**Added Mass and Horizontal Drag**

Horizontal added mass (A11 and A22) and drag are modeled with one slender element for both ROV and TMS together. Since it is stretched in the vertical direction forces will be scaled relative to the wetted part of the system.

Vertical added mass (A33) is modeled with two separate slender elements, one at the top and one at the bottom of the structure. Each representing half of the vertical added mass for the entire system (ROV and TMS). The same reasoning ass for the Manifold also applies here, slender elements vertically distributed will prevent a sudden change in added mass which can cause force impulses to occur. The applied properties are listed in Table 4.10.

Table 4.10: Added Mass and Horizontal Drag Properties

|                        | Unit | Direction | | |
|------------------------|------|------|------|------|
|                        |      | X    | Y    | Z    |
| Added Mass             | Te   | 3.68 | 3.68 | 1.84 |
| Added Mass Coefficient | -    | 2.87 | 3.45 | 2.5  |
| Drag Area              | m²   | 5.15 | 6.47 | -    |
| Drag Coefficeint       | -    | 2    | 2    | -    |

**Vertical Drag and Slamming**

Vertical drag and slamming is modeled with 6D buoys representing the bottom surface of the ROV. 18 buoys with equal properties have been used, to distribute the slamming force evenly on the bottom surface. The properties assigned to each buoy are listed in Table 4.11.

Table 4.11: Drag and Slamming Buoy Properties ROV System

| Property | Unit | Value |
|---|---|---|
| Slamming Area | m² | 0.25 |
| Slamming Coefficient (Entry) | - | 5.0 |
| Slamming Coefficient (Exit) | - | 2.0 |
| Drag Area | m² | 0.25 |
| Drag Coefficient | - | 2.50 |

**LARS**

The launch and recovery system (LARS) is modeled by the use of a simple winch, which connects the ROV with TMS to the vessel. It is defined to move with the vessels motions. A 30.0E3 kN stiffness has been set for the winch wire. The launch and recovery process is controlled by the winch, a total of 8 stages has been used to define the main simulation time. In addition is a static stage and a build up stage used. All stages with accompanying winch modes are given in Table 4.12.

Table 4.12: Simulation Stages and Winch Modes for ROV System

| Stage | Duration [s] | Time at Stage End [s] | Mode | Value | |
|---|---|---|---|---|---|
| Statics | | | Specified Length | 17.3 m | |
| 0 | 8 | 0 | Specified Payout Rate | 0 | |
| 1 | 4 | 4 | Specified Payout Rate Change | 1 | |
| 2 | 12,5 | 16.5 | Specified Payout Rate | 1 | LAUNCH |
| 3 | 4 | 20.5 | Specified Payout Rate Change | -1 | |
| 4 | 4 | 24.5 | Specified Payout Rate | 0 | Stand Still |
| 5 | 4 | 28.5 | Specified Payout Rate Change | -1 | |
| 6 | 12 | 40.5 | Specified Payout Rate | -1 | |
| 7 | 4 | 44.5 | Specified Payout Rate Change | 1 | RECOVERY |
| 8 | 8 | 52.5 | Specified Payout | 0 | |

## 4.3 Limiting Criteria

The limiting criteria used for the winch wire tension for the Maniflod and ROV system are given in this section.

### 4.3.1 Manifold

Two limiting criteria has been used:

1. The maximum dynamic amplification factor should not exceed DAF=2

2. Slack should not occur in more than 10% of the simulations for each sea state.

In practice are both thees conditions related to the occurrence of slack winch wire. Slack winch wire occur if the hydrodynamic forces exceeds the static weight of the structure, which may cause snap loads to occur (DNV, 2014b). In that case will the dynamic amplification factor (DAF) exceed 2 (Equation 4.5). The relationship between slack and snap loads are further discussed in Chapter 7.

$$DAF = \frac{F_{tot}}{F_{static}} = \frac{F_{hyd} + F_{static}}{F_{static}} = \underbrace{\frac{F_{snap} + F_{static}}{F_{static}}}_{\text{If Snap Loads Occur}} \tag{4.5}$$

Inserting the relevant values the following max tension is obtained:

$$F_{capasity} = DAF \cdot F_{static} = 2 \cdot 9.81 \cdot \left( \underbrace{50\,Te}_{\text{Manifold}} + \underbrace{10\,Te}_{\text{Lump Weight}} \right) = 1177.2\,kN \tag{4.6}$$

Thus, if the obtained max tension in a simulation exceeded 1177.2 kN it is most likely caused by a slack with following snap load. The second condition stating that slack should not occur in more than 10% of the simulations is used since the magnitude of the snap loads are dependent on the slack duration and are therefore highly unpredictable. For a set of 20 simulation, the combination of $H_s$ and $T_p$ is only accepted if slack has not occurred more than twice. Two observations of slack within one set of simulations (20 simulations)is from now referred to as the "slack limit".

### 4.3.2 ROV

The wire capacity for the LARS umbilical is 490kN. A safety factor of $\gamma_{sf} = 3.0$ (DNV, 2014a) is used to obtain the winch wire capacity used as the limiting criteria for the ROV: 490kN/3.0=163kN.

## 4.4 Analysis Procedure

Lifting through the splash zone is analyzed for both the structures in the time domain. The analysis for the manifold is stopped when the structure has passed the critical wave zone and the wire tension starts to level out. The stages which defines the simulation for the Manifold are previously given in Table 4.7. Both launch and recovery are simulated for the ROV . Thus, the simulation is stopped when the ROV is back at the initial position before launch. The stages which defines the ROV simulation are previously given in Table 4.12.

The function "Batch processing" has been used in Orcaflex which allows the user to set up a list of simulations that are to be conducted. The sea state for each simulation is pre-defined in a Orcaflex data file (.yml format). A Excel spreadsheet developed by Orcina has been used to generate thees files (spreadsheet is given in Appendix C.3). Each data file contain a reference to the relevant simulation file containing the Orcaflex model. As well as significant wave height, peak period, heading angle, seed number,and peak shape parameter. For short-crested waves are also the number of wave directions, and spreading exponent defined in the data file. Four different simulation files have been used, two for each structure, these are given in Appendix C.3. Seed numbers has been used to create 20 different realizations of each sea state, the number of seeds are further discussed in Chapter 6.

The maximum and minimum dynamic wire tension are extracted from the simulations for each of the 20 realizations of a given sea state. The maximum and minimum tension are assumed to follow a Gumbel extreme value distribution and is further plotted in a Gumbel probability paper. The statistical evaluation and underlying assumptions are further discussed in Chapter 5.

# Chapter 5

# Extreme Value Statistics

The process of choosing a statistical model for the wire tension is described in this chapter. In addition the construction and evaluation of a probability paper are described.

## 5.1  Choosing a Probabilistic Model

To perform a statistical evaluation of a physical phenomenon, some assumptions most be made about the process. A realization of a general stochastic process is given i Figure 5.1. $X(t)$ represents the wave elevation in this case. Every instance of the wave height is assumed to be Gaussian distributed (indicated with X). In addition, all individual maximum (indicated with O) are assumed to be statistically independent, and identically Rayleigh distributed (Myrhaug, 2014).
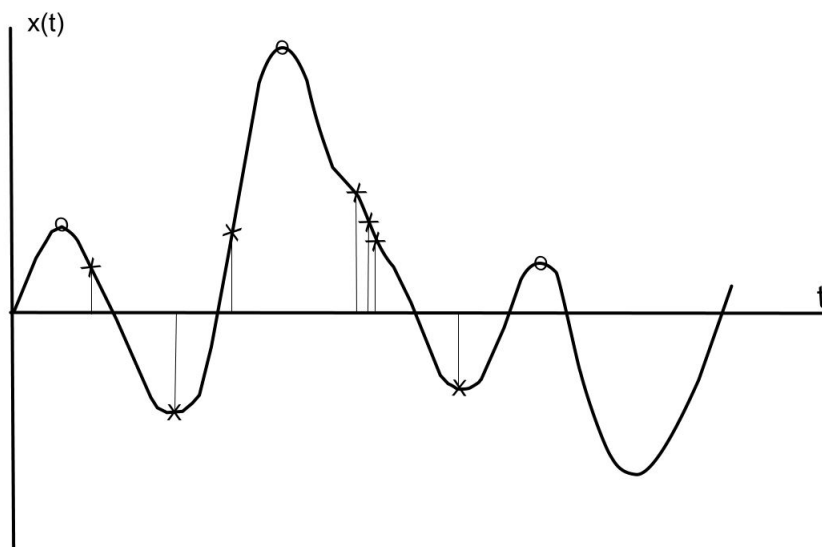


Figure 5.1: General Stochastic Process

The quantity of interest in this thesis, is the wire tension, which is assumed to be non-linearly dependent on the wave height. The distribution of max tension in the wire can therefore be found through a transformation of the Rayleigh distribution, using a nonlinear polynomial function. That will result in a Weibull distribution of individual maxima for the wire tension (Equation 5.1). The Weibull distribution has proven to be an appropriate model to describe maximum and is frequently used to model similar physical phenomenons in the offshore industry ((Leira, 2014a) and (Leira, 2014b)).

$$F_{x,Weibull} = 1 - exp\left(-\left(\frac{x}{\alpha}\right)^{\psi}\right) \tag{5.1}$$

where $x$ is a stochastic variable, and $\alpha$ and $\psi$ are the distribution parameters.

## 5.2   Extreme Value Distribution

The distribution of the largest\smallest among $N$ outcomes of a stochastic variable is called the extreme value distribution. The available extreme value distributions are classified based on tail behavior of initial distribution. Three types of extreme value distributions are available (Leira, 2014b)

- Type 1: Exponential distributions, which results in a Gumbel extreme value distribution.
- Type 2: Distributions with finite moments, which results in a Frechet extreme value distribution
- Type 3: Bounded distributions, which results in a Weibull extreme value distribution

The individual maxima of the wire tension is assumed to be Weibull distributed which is a exponential distribution (Equation 5.1). The largest among $N$ maximum of the wire tension is therefore assumed to be Gumbel distributed. The same distribution is also applied to the minimum tension.

The Gumbel cumulative distribution function (CDF) is given as:

$$F_x\left(x;\mu,\beta\right) = exp\left(-exp\left[\frac{x-\mu}{\beta}\right]\right) \tag{5.2}$$

where $\mu$ and $\beta$ are distribution parameters. Figure 5.2 shows the shape of a typical Gumble CDF.
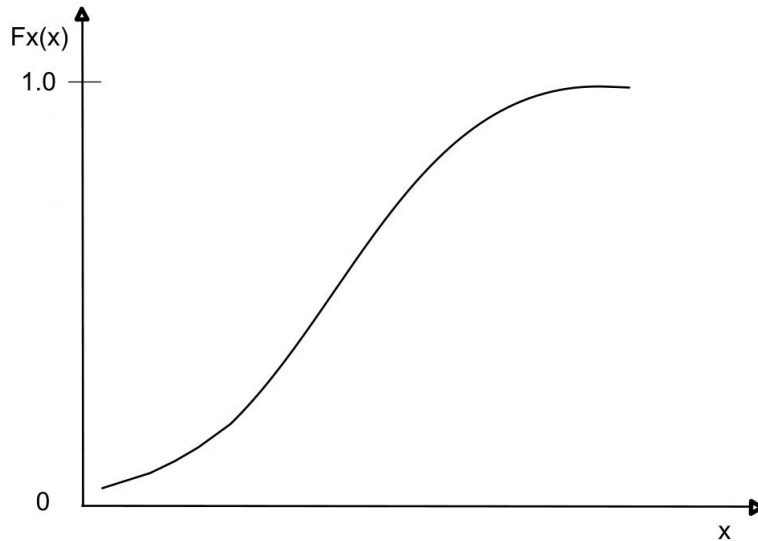
Figure 5.2: Gumbel Cumulative Distribution Function

## 5.3   Probability Paper

The principal behind a probability paper is to apply a linear transformation on the x- and y-axis in Figure 5.2. If the proposed model is correct, the cumulative distribution function becomes a straight line, when plotted in the paper. Construction of a Gumbel probability paper starts with substituting the Gumbel parameter G (Equation 5.3) into the expression for the Gumbel CDF (Equation 5.2). The steps are shown in Equation 5.3 to 5.6.

Gumbel parameter:

$$G = -\frac{x - \mu}{\beta} \tag{5.3}$$

Substitution of G into Equation 5.2:

$$F_x = exp\left(-exp\left(G\right)\right) \tag{5.4}$$

The probability of non-exceedance for the given sample is taken as:

$$F^* = \frac{N - i + 1}{N} \tag{5.5}$$

For a sorted sample of $x$ is i equal to 1 for the larges value, equal to 2 for the second largest value

31

and so on. $N$ is the total number of values in the samples. The next step is to substitute $F_x^* = F_x$ into Equation 5.4 and solve for G:

$$G = -ln\left(-ln\left(F_x^*(x)\right)\right) \tag{5.6}$$

The right-hand part of Equation 5.6 is the transformation on the y-axis. When a Gumbel distribution is used, it is not necessary to perform a transformation on the x-axis. The procedure of construction a probability paper is illustrated in Table 5.1.

Table 5.1: Procedure for Construction of a Probability Paper

| Stochastic Sample | Sorted Sample | i=1,2,...N | Probability on Non-Exceedance F*=((N-i+1)/N) | Gumbel Parameter G= -ln(-ln(F*)) |
|---|---|---|---|---|
| 100 | 200 | 1 | 1 | NaN |
| 85 | 160 | 2 | 0,8 | 1,499939987 |
| 200 | 110 | 3 | 0,6 | 0,671726992 |
| 110 | 100 | 4 | 0,4 | 0,087421572 |
| 160 | 85 | 5 | 0,2 | -0,475884995 |
| N=5 | x-axis Values | | | y-axis Values |

The x- and y-axis values indicated by the table are plotted against each other.

Figure 5.3 shows the relation between $F_x^*$ and G.
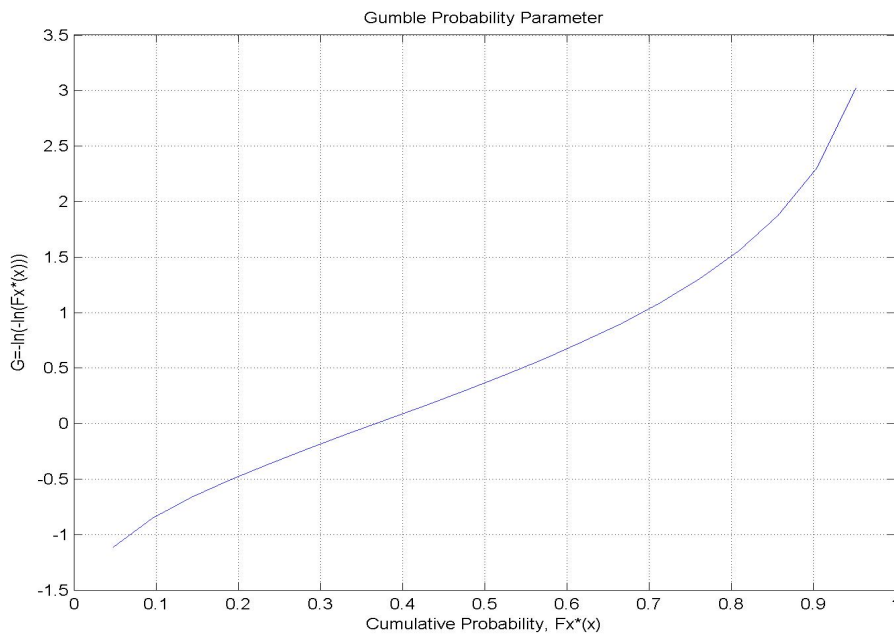


Figure 5.3: Gumbel Probability Parameter

## 5.4   Statistical Analysis of Wire Tension

The first step in evaluation of the maximum wire tension, is to calculate the values used in the probability paper for each sea state. These are further plotted together with the capacity as seen in Figure 5.4. Each line in the graph represents one sea state. A 90% probability of no-exceedance is used in this thesis, which corresponds to G=2.25. Using the figure as an example, one can see that for Tp2 the tension which corresponds to G=2.25 is larger than the capacity. Therefore, the given sea state is not accepted. For Tp1 one can se the opposite result, where the tension which corresponds to G=2.25 lies below the capacity. Thus, it follows that the sea state is accepted.
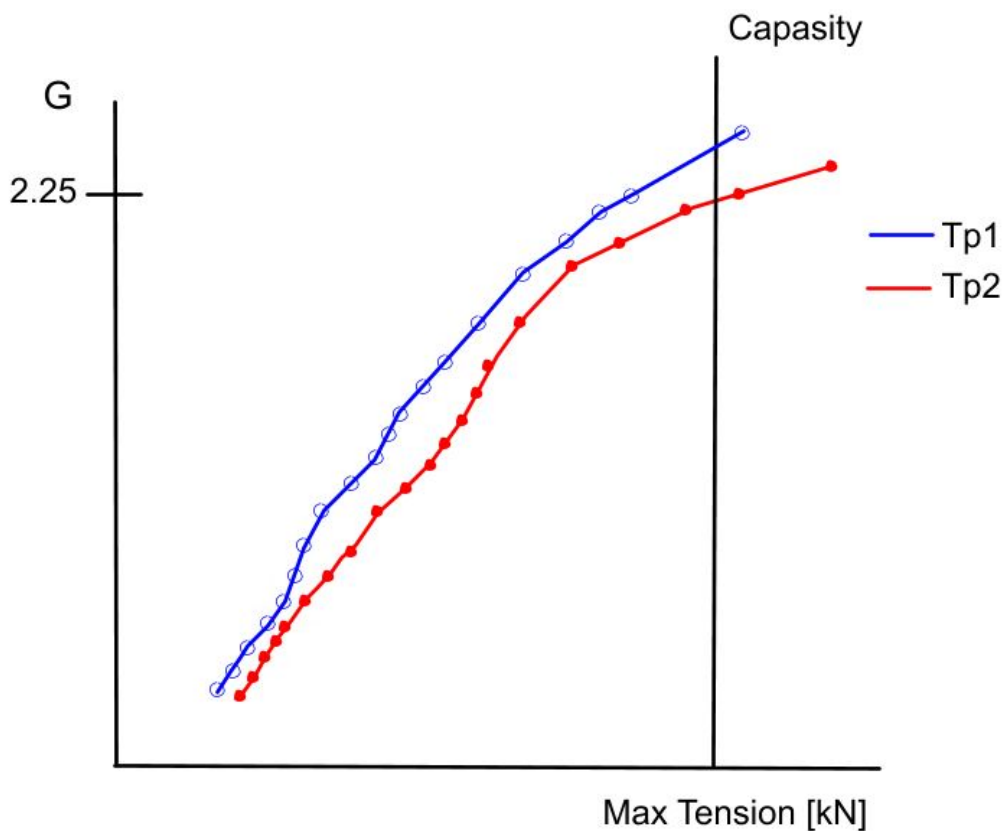


Figure 5.4: Example on the use of Probability Paper

The evaluation procedure for the probability papers described above, is used for all sea states to decide the operational limit for both structures evaluated in this thesis. The capacity used for the structures are previously given in Section 4.3

# Chapter 6

# Uncertainties and Error Estimation

This chapter contains a sensitivity study, assessing the number of seeds needed for each sea state in the time-domain simulations. It also contains a presentation of the uncertainties and limitations related to Orcaflex and an evaluation of the results. In addition, the uncertainty is related to the 90% tension fractile assessed in this chapter.

## 6.1 Uncertainties and Limitations

For operations restricted by weather conditions, there will be uncertainties related to the weather forecast. This can be accounted for by lowering the design limit, which is restricted by $H_s$ in this case. This can bee done by multiplying the design limit with a location specific $\alpha$-factor (DNV, 2011). This has not been accounted for in this thesis, and the operational limits presented in Chapter 8 are therefore equivalent to the design limit for the operations.

The parameter variation of $H_s$ is performed in increments of 0.5 m, which may cause significant drops in the operational limit for adjacent periods. The limiting $H_s$ may for all periods be up to 0.4m higher than what is indicated. A smaller increment in $H_s$ could have been used, but it would have increased the simulation time significantly. It is important to keep this in mind during the evaluation of the results.

The models of the Manifold and the ROV system used in Orcaflex are simplified, and there lies uncertainties in the estimation of the hydrodynamic coefficients. Hence the simulations have inherent uncertainties with respect to the actual lift.

It is impossible to predict the exact wave which would be present when the structure is lowered through the splash zone. Thus, different seed numbers have been used to assure that different realizations of the waves occur. When one is working with stochastic variables such as irregular waves the computed wire tension will vary, even when all other conditions related to the simulation are the same. The uncertainty related to the computed tension is further discussed in Section 6.3.

Both wind and current are environmental conditions that are present during marine operations. Neither has been taken into account in the simulation to reduce the complexity of the problem.

Only the wire tension has been used as the limiting criteria for both structures. When the vessel motions are large will the structures experience pendulum motions. The magnitude of these motions has not been investigated in this thesis.

## 6.2   Seed Sensitivity Analysis

During a real lifting operation the wire tension will vary each time the structure is lowered through the splash zone. This is accounted for in the simulations by the use of seed numbers, each representing a unique realization of the wave. The number of seeds needed to get a confident statistical basis for assessing the max wire tension, has been evaluated through a seed sensitivity analysis. The ROV system has been used as a base case, with $H_s = 2.5m$ and $T_p = 7s$. The following variation in number of seeds has been used:

Table 6.1: Number of Seeds used in Seed Sensitivity Analysis

|                  | Case 1 | Case 2 | Case 3 | Case 4 | Case 5 | Sum of All Cases |
|------------------|--------|--------|--------|--------|--------|------------------|
| Number of Seeds  | 20     | 40     | 60     | 80     | 100    | 300              |

Five different sets of simulation has been conducted, and the max wire tension extracted from each run was plotted in a Gumbel probability paper (Figure 6.1). A combination of all five cases is representative for a set of 300 simulations, which is also indicated in the figure.
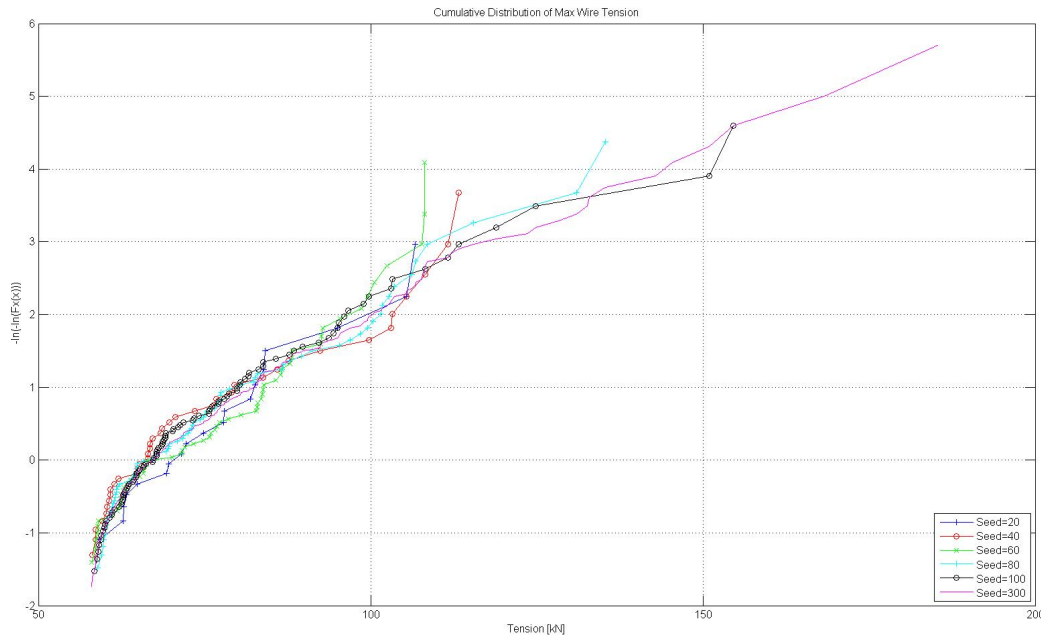
Figure 6.1: Seed Sensitivity

The maximum wire tension is observed to follow the same trend line for all cases. The difference in the tension is seen to lie between 5-20kN for all values of the Gumbel parameter $G < 3$. Therefore, it appears that 20 seeds should be sufficient to get a estimate of the 90% fractile in this case. Another argument of using few seeds is that the simulation time is kept to a minimum since it increases linearly with the number of seeds.

## 6.3   Uncertainty Analysis

The extracted maximum wire tension from one simulation is just one example of what the real tension could be. The variation in seed number results in a different maximum tension for each simulation. To know how far the calculated value may be from the unknown true value, an uncertainty analysis has to be performed. The goal of a uncertainty analysis is to provide a measure of how reliable the calculated values are. The total error related to a set of values may be divided into bias- and precision-error. Where bias error are errors which can not be uncovered through repetition, in contrast precision error may be found by repeated simulations since this type of error appears as "scatter" in the results (Steen, 2014). When a sample is available, one can calculate the precision error. The procedure is described in the next section.

37

### 6.3.1 Procedure for Calculation of Precision Error

The following steps used to calculate the precision error is a rendering of the procedure described in Steen (2014) (section 12.2.2).

When the number of samples of a stochastic variable goes to infinity it is common to assume that the given values are Gaussian distributed, according to:

$$f(X) = \frac{1}{\sigma\sqrt{2\pi}} e^{-\frac{(X-\mu)^2}{2\sigma^2}} \tag{6.1}$$

where $\mu$ is the mean value and $\sigma$ is the standard deviation.

The mean value $\overline{X}$ for a sample of size N is calculated as:

$$\overline{X} = \frac{1}{N}\sum_{j=1}^{N} X_j \tag{6.2}$$

further is the standard deviation of the sample is given as:

$$S_X = \sqrt{\frac{1}{N-1}\sum_{j=1}^{N}\left(X_j - \overline{X}\right)^2} \tag{6.3}$$

The standard deviation of the mean $\overline{X}$ is given as:

$$S_{\overline{X}} = \frac{S_X}{\sqrt{N}} \tag{6.4}$$

For the Gaussian distribution is the confidence interval $\gamma$ of the sample given as:

$$Prob\left(X_j - t\sigma \le \mu \le X_j + t\sigma\right) = \gamma \tag{6.5}$$

The standard deviation of the Gaussian distribution $\sigma$ is unknown for a finite sample. Because $\sigma$ is unknown is also $t$ unknown. By substituting $\sigma = S_X$ and rearranging Equation 6.5 one gets:

$$Prob\left(-t \le \frac{X_j - \mu}{S_X} \le t\right) = \gamma \tag{6.6}$$

The random variable $\frac{X_j - \mu}{S_X}$ is Student's $t$ distributed with N-1 degrees of freedom. $t$ for a given confidence interval is decided by the use of the function TINV$(1 - \gamma; N - 1)$ in Excel (Figure 6.2).

When $N \to \infty$, will $t$ converge towards the value for a Gaussian distribution.
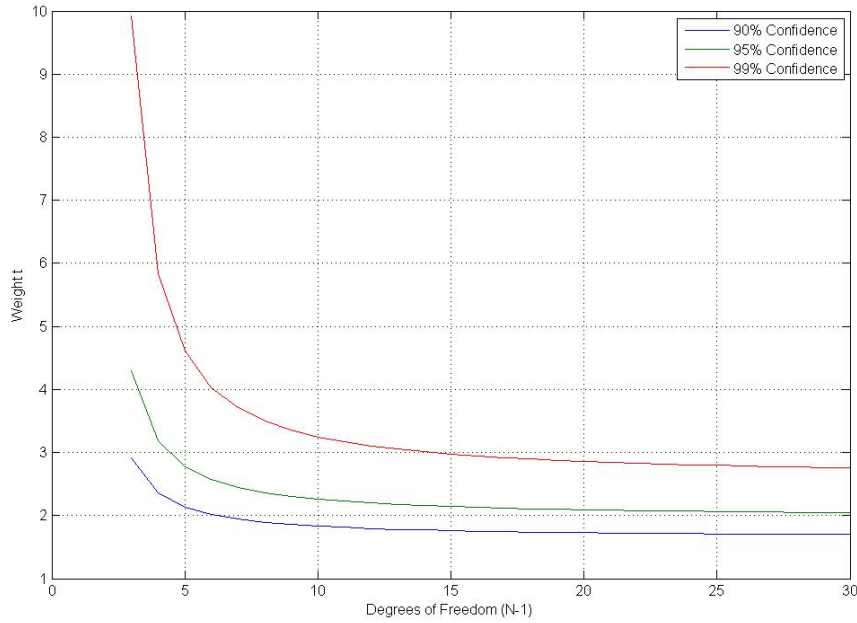


Figure 6.2: Weight of t for Different Confidence Interval using a Stundet's t Distribution, adapted from Steen (2014)

### 6.3.2 Calculated Precision Error

The precision error has been calculated for both the structures. The relevant values in this case are the tension corresponding to a 90% fractile. 15 sets of 20 simulations has been conducted to obtain a sufficient amount of samples to perform the uncertainty analysis. The applied environmental parameters are given in Table 6.2. All simulations has been performed with long-creasted waves, without shielding and at head sea.

Table 6.2: Environmental Conditions used during Calculation of Precision Error

|          | Tp | Hs1 | Hs2 |
|----------|----|-----|-----|
| Manifold | 7  | 1   | 2   |
| ROV      | 9  | 4   | 6   |

The results from the uncertainty analysis for the Manifold are given in Table 6.3, and for the ROV in Table 6.4. It is observed that the uncertainty of a single sample increases drastically when the significant wave height increases, which could be caused by the increasing risk of snap loads due to higher vessel response and increased particle velocity (see. Section 7.3 and 7.4)

Table 6.3: Precision Error for Manifold

|  | Hs=1 | Hs=2 | Unit |
|---|---|---|---|
| Mean $\overline{X}$ | 718.28 | 1080.86 | [kN] |
| Standard Deviation | 16.67 | 110.67 | [kN] |
| N | 15 | 15 | - |
| t | 1.76 | 1.76 | - |
| Precision Limit Sample $P_X$ | 29.36 | 194.93 | [kN] |
| Precision Limit Mean $P_{\overline{X}}$ | 7.58 | 50.33 | [kN] |
| Single Test Uncertainty | **4.09 %** | **18.03 %** | - |
| Mean Uncertainty | **1.06 %** | **4.66 %** | - |

Table 6.4: Precision Error for ROV

|  | Launch | | Recovery | | Unit |
|---|---|---|---|---|---|
|  | Hs=4 | Hs=6 | Hs=4 | Hs=6 |  |
| Mean $\overline{X}$ | 74.91 | 90.58 | 104.15 | 148.80 | [kN] |
| Standard Deviation | 5.09 | 10.80 | 16.63 | 33.57 | [kN] |
| N | 15 | 15 | 15 | 15 | - |
| t | 1.76 | 1.76 | 1.76 | 1.76 | - |
| Precision Limit Sample $P_X$ | 8.97 | 19.03 | 29.30 | 59.13 | [kN] |
| Precision Limit Mean $P_{\overline{X}}$ | 2.32 | 4.91 | 7.56 | 15.27 | [kN] |
| Single Test Uncertainty | **11.97 %** | **21.01 %** | **28.13 %** | **39.74 %** | - |
| Mean Uncertainty | **3.09 %** | **5.42 %** | **7.26 %** | **10.26 %** | - |

# Chapter 7

# Lifting Through the Splash Zone

How structures are affected when they are lowered though the splash zone is a complex hydrody-namic problem consisting of various physical phenomenons acting together. The following section describes some physical phenomenons which are expected to occur, and how they may affect the lifted structure.

## 7.1 Lifting Operations

Performing thorough investigations to determine design loads for lifting operations helps reduce the risk related to waiting on weather, and increases the safety of the operation. A subsea lift can be divided into four main phases (DNV, 2014b):

- Lifting off deck and in clearance of the vessel
- Lowering through the splash zone
- Lowering down to seabed
- Positioning and landing

Although all phases should be evaluated, lowering through the splash zone is often considered as the most critical phase of the lift in terms of design loads. Crane lifts are divided into two categories dependent on the weight-displacement ratio between the lifted structure and the vessel. A lift is categorized as light, if the weight of the structure is less than 1-2% of the vessel displacement. The weight of the structure does not affect the motion characteristics of the vessel (at the crane tip). The other category is heavy lift which covers lift of structures that weigh more than 1-2% of the vessels displacement. The motion characteristic at the crane tip can no longer be considered

as unaffected by the structure, and coupled dynamics between the structure and vessel must be considered (DNV, 2014b). The crane lift considered in this thesis falls under the category light lift.

## 7.2   Shielding and Radiation Effects

Shielding and radiation effects are important when a structure is deployed on the leeward side of a vessel. Shielding addresses how the vessels presence affect the incoming waves. Waves passing "through" the vessel will experience the hull as a wall partially blocking their path, causing the displacement, velocity, and acceleration of the waves to decrease. This effect reduce short waves more than long wave components, since the vessel will follow the motion of the waves at higher periods. Shielding is particularly important in terms of slamming loads, due to the reduction in relative velocity between the structure and sea surface (see Section 7.3).

The incoming waves causes the vessel to move in 6 degrees of freedom (DOF). Waves generated by the vessel due to its motions is categorized as radiation effects. Radiation effects can be measured by forcing the vessel to oscillate in all 6 DOF without incident waves. Radiation effects are maximized near the natural heave and pitch periods of the vessel (Sandvik, 2015). The relevant Response Amplitude Operators are given in Section 7.5. Radiation effects can both be considered as positive and negative. Positive if the radiated waves are not in phase with the incoming waves, i.e. causing cancellation to occur. Negative if they are in phase and thus amplify the incoming waves.

The shielding effect will dominate in most cases, and both effects weaken towards longer waves. These effects are accounted for by including Sea-State RAO's in the time domain analysis previously discussed in Section 4.1.5.

## 7.3   Slamming

Slamming is a nonlinear phenomenon which refers to structure-liquid impacts. It appears as impulse loads with high pressure peaks. The severity of slamming increases as the local relative velocity (and acceleration) between structure and fluid increases, and as the impact angle $\beta$ decreases (Figure 7.1). Slamming is highly sensitive to how the structure impacts with the water. Several

other physical phenomenons, like air-cavity entrapment, and vortex shedding can happen dependent on how the structure hits the waves (Faltinsen, 1990).
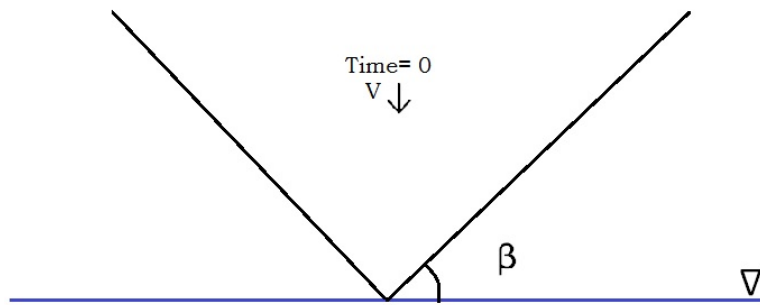


Figure 7.1: Impact Angle for Slamming

In this thesis slamming is especially critical for the manifold, since it has a large horizontal bottom-surface ($\beta = 0$). A time series of the wire tension and slamming load for the manifold is shown in Figure 7.2. When the structure-fluid impact happens will the impulse load that occur act in the opposite direction with respect to the structures direction of movement. This opposite force causes the structures vertical velocity to suddenly drop. The slamming load does not affect the winch pay-out rate (constant) which results in a sudden drop in tension, with a following peak load, as seen on the figure below. Worst case scenario is that the wire goes to slack, which can cause snap loads to happen (see Section 7.4).
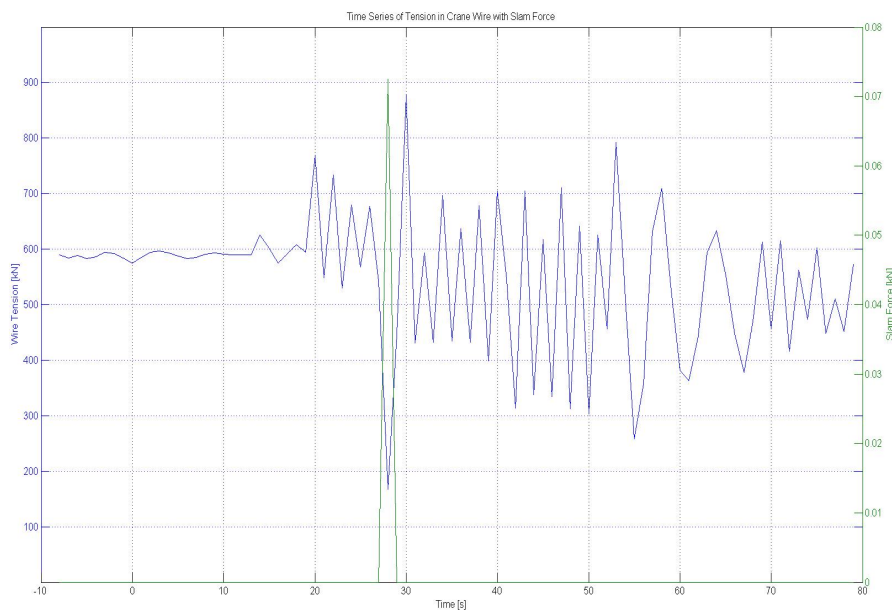


Figure 7.2: Time Series Showing Max wire Tension and Slamming Loads

The magnitude of slamming loads is very difficult to predict, due to large nonlinearities. Thus, it is difficult to predict whether or not there will be slack with subsequent snap load in the water entry/exit phase of the lift. Since slamming loads are dependent on the relative vertical velocity between structure and fluid, it is reasonable to assume that the risk of occurrence increases with the vessel motions.

## 7.4 Slack and Snap Loads in Wire

A slack occur if the hydrodynamic force acting on the structure exceed the combined static weight of the lifted structure with rigging. The number of observed slack in the wire is therefore expected to increase with decreasing weight of the structure. It is recommended to avoid slack as far as possible. A slack wire alone is not dangerous, it is the following snap load that is critical for the capacity. The severity of the snap load increases with the slack duration, and is therefore highly unpredictable. In addition it is possible that the wire can experience oscillation-like behavior causing it to go directly in slack again after a snap load (Sandvik, 2015). This behavior is shown in Figure 7.3.
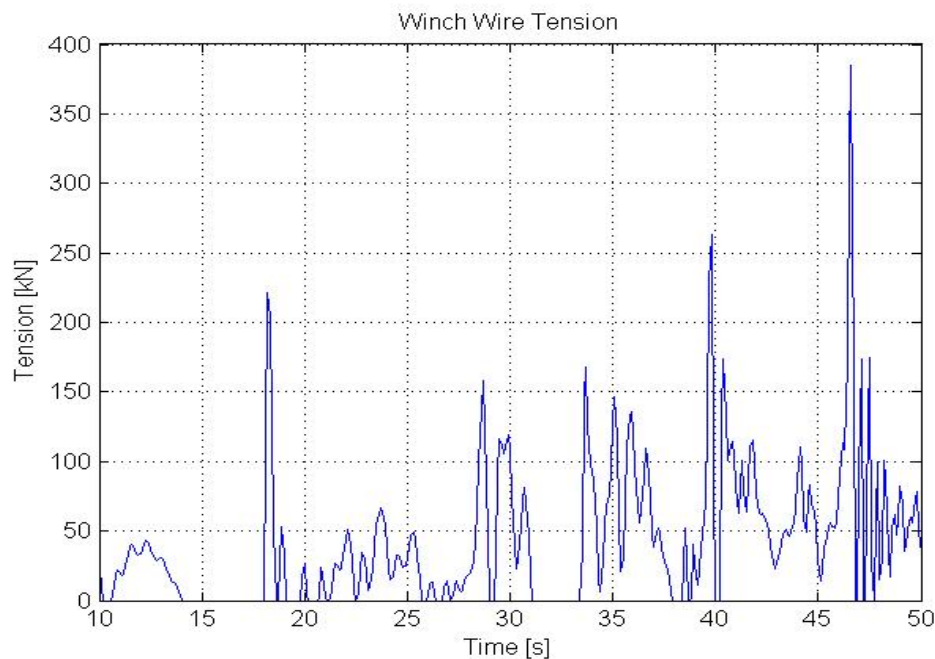


Figure 7.3: Time Series Showing Max wire Tension with hight occurance of Slack

## 7.5 Vessel Motions

The vessel will move in 6 DOF when exposed to incoming waves, these motions are described through the vessels Response Amplitude Operators (RAO). The RAOs indicates the vessel response as a function of both period and heading angle. In this thesis the vertical displacements, velocities and accelerations are considered critical parameters. The DOF surge, pitch and yaw are not included since they are motions in the horizontal plane. The RAOs for the vertical DOFs heave, roll and pitch are given in Figure 7.4-7.6 below for the relevant heading angles investigated in this thesis.
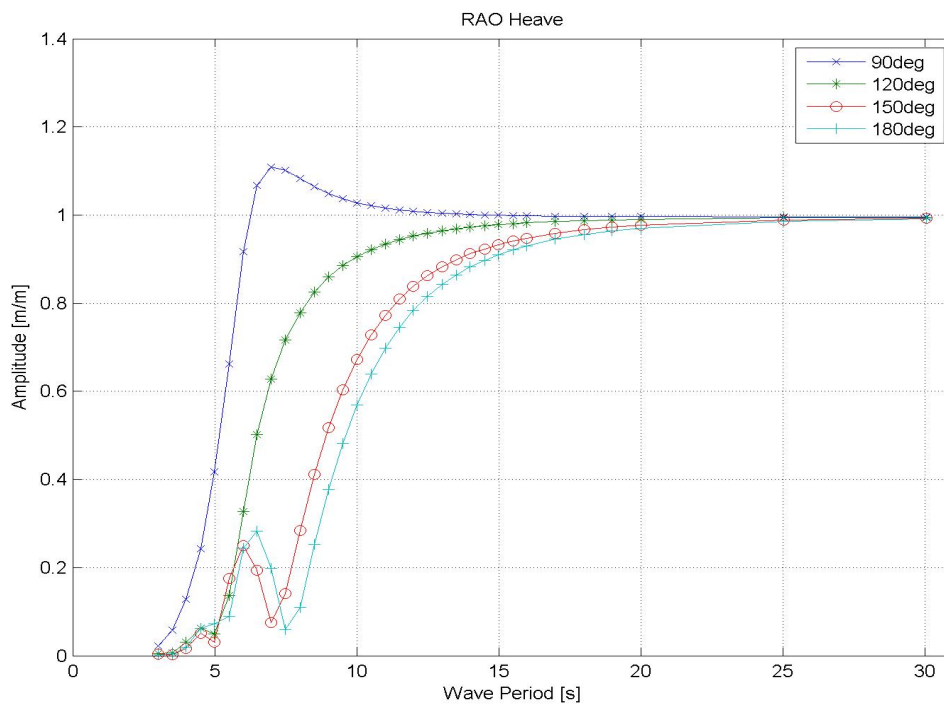


Figure 7.4: RAO Heave
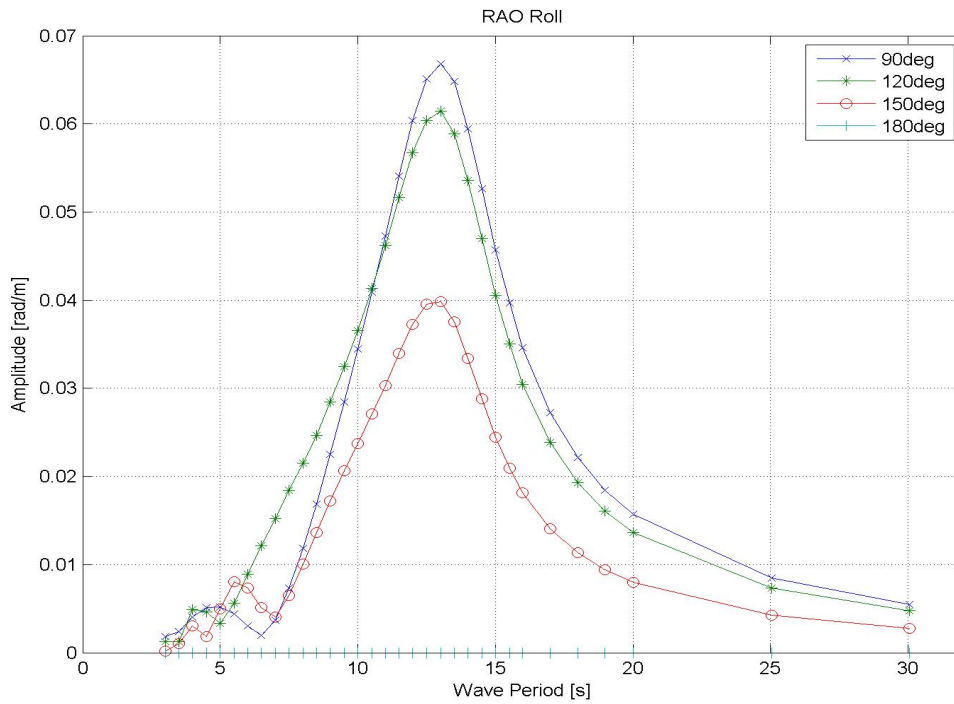
Figure 7.5: RAO Roll
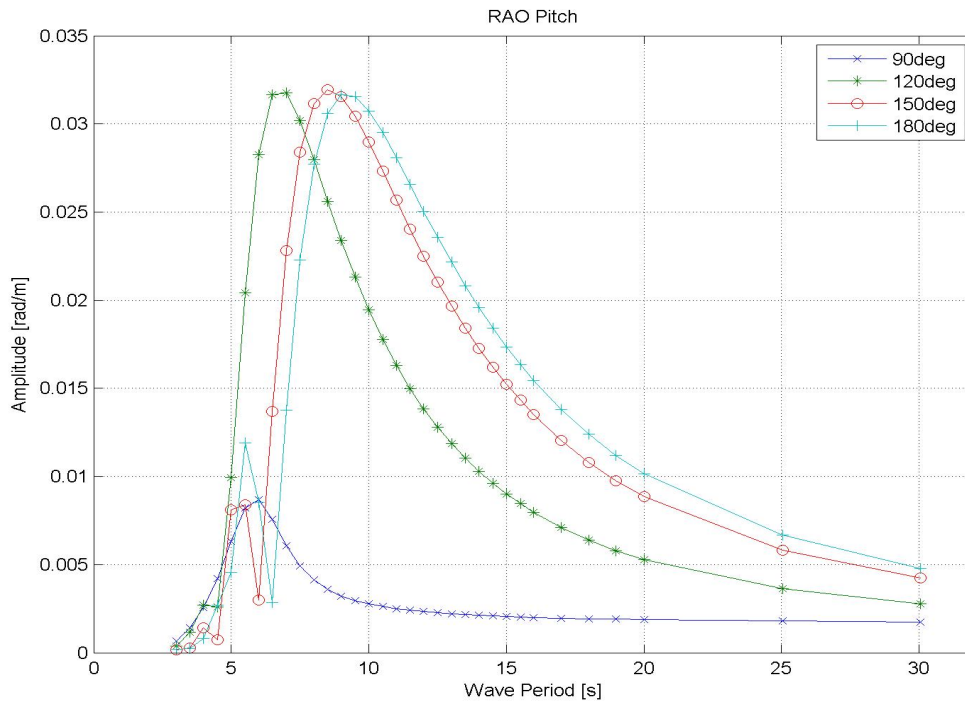


Figure 7.6: RAO Pitch

The vertical motions of the lifted structure are assumed to be equal to the vessel motions due to the light lift condition (Section 7.1). The RAOs can therefore be used to partially describe the difference in operational limit for different periods and headings, especially for long-crested waves.

This becomes more difficult for short-crested waves, due to the directional spreading. For periods where the vessel responses are large the risk of slamming loads will increase, due to larger vertical velocities in the lifted structure. In areas where the responses are small, or where cancellation effects occur, shielding effects are maximized.

## 7.6 Differences Between Long- and Short-Crested Waves

A study on how the directional spreading function $D(\theta)$ affects the vertical velocity of the crane tip, and the fluid particles, has been performed for three combinations of $H_s - T_p$ (Table 7.1). This is done to investigate the physical changes that occurs when short-crested waves are used instead of long-crested waves. As discussed in Section 4.1.3 is the spreading exponent $n$ set equal to $H_s$.

Table 7.1: Cases used in Directional Spreading

|        | Case 1 | Case 2 | Case 3 |
|--------|--------|--------|--------|
| $T_p$  | 7      | 10     | 13     |
| $H_s$  | 2      | 4      | 6      |

A one hour long simulation for each case and heading is used to obtain the results presented in this section. The effect is demonstrated by counting the number of times during a simulation the vertical velocity exceeds a certain limit. A limit equal to 0.5m/s and 1.5 m/s is set for the crane velocity and particle velocity respectively. Note that these velocities are not critical limits, they are just used to investigate the difference between long- and short-crested waves. Shielding is not taken into account in this investigation, this is done to isolate the effect of spreading without the influence from other physical phenomenons.

Table 7.2 to 7.5 shows the observed number of exceedances for each velocity, case, and heading.

Table 7.2: Number Exceedances of Vertical Crane and Fluid Particle Velocity at 90deg heading

|                                 |               | Case 1 | Case 2 | Case 3 |
|---------------------------------|---------------|--------|--------|--------|
| Crane Vertical Velocity         | Long-Crested  | 295    | 771    | 892    |
|                                 | Short-Crested | 101    | 649    | 799    |
| Vertical Fluid Particle Velocity | Long-Crested | 15     | 85     | 112    |
|                                 | Short-Crested | 12     | 79     | 132    |

At 90° heading there is a significant decrease in high vertical velocity in the crane, the fluid particles does also experience some decrease in number of peaks. With the reduction in the velocity there is

less risk of high slamming loads to occur at water entry/exit (Section 7.3). It is therefore expected that a directional spreading function will cause the risk of slamming to decrease for 90° heading. That is beneficial in terms of tension in the wire.

Table 7.3: Number Exceedances of Vertical Crane and Fluid Particle Velocity at 120deg heading

|  |  | Case 1 | Case 2 | Case 3 |
|---|---|---|---|---|
| Crane Vertical Velocity | Long-Crested | 158 | 755 | 890 |
|  | Short-Crested | 77 | 644 | 851 |
| Vertical Fluid Particle Velocity | Long-Crested | 17 | 65 | 106 |
|  | Short-Crested | 19 | 73 | 108 |

Also for 120° heading, the directional function decreases the number of times the crane velocity exceeds the limit. The fluid particle velocity experience more peaks above $1.5m/s$ with directional spreading. Compared to beam sea (90° heading) one can see that the changes are not as significant and therefore expect that the effect not will be as beneficial at 120° heading.

Table 7.4: Number Exceedances of Vertical Crane and Fluid Particle Velocity at 150deg heading

|  |  | Case 1 | Case 2 | Case 3 |
|---|---|---|---|---|
| Crane Vertical Velocity | Long-Crested | 0 | 325 | 554 |
|  | Short-Crested | 22 | 513 | 729 |
| Vertical Fluid Particle Velocity | Long-Crested | 17 | 78 | 108 |
|  | Short-Crested | 17 | 74 | 118 |

The effect is reversed at 150° heading, from the table above one can see that there are fewer peaks above the limit in the crane velocity for long-crested waves compared to short-crested waves. Looking at the spreading function in Appendix A one can see that directional spreading at this heading results in waves propagating from the leeward side. From this one can see that the structure is directly exposed to the waves, and will not have the benefit of shielding from the vessel for all passing waves.

Table 7.5: Number Exceedances of Vertical Crane and Fluid Particle Velocity at 180deg heading

|  |  | Case 1 | Case 2 | Case 3 |
|---|---|---|---|---|
| Crane Vertical Velocity | Long-Crested | 0 | 324 | 725 |
|  | Short-Crested | 1 | 486 | 808 |
| Vertical Fluid Particle Velocity | Long-Crested | 22 | 71 | 123 |
|  | Short-Crested | 15 | 84 | 109 |

Considering head sea Table 7.5 shows that the directional function causes more peak velocities in the crane, especially for Case 2 and 3. When the direction of the incoming waves deviates from

head sea, the vessel will experience roll motion, which causes higher velocities in the lifted structure. Only small variations in the particle velocity is observed.

Comparing the different heading angles, it is seen that the vertical crane tip velocity decreases with the reducing roll motion of the vessel. The crane velocity is observed to be highest for all cases at 90° and 120° heading for both long- and short-crested waves. The lowest occurrence of high velocity is observed at 150° heading. Thus, the risk of slamming loads should be considerably lower compared to the other heading angles.

## 7.7 Combined Effects

As discussed in Section 7.2-7.6 there are many different factors that influence the wire tension, and with it the operational limit, during a lifting operation. How these interact and affect each other is therefore difficult to predict.

The calculated wire tension is primary dependent on a favorable combination of low vertical particle and structure velocity, at the moment of water-entry/exit. Measures that provides a reduction in fluid particle velocity may result in higher structure velocity or conversely. The goal is to find an ideal heading and location of the lifted structure, where the effect of shielding is utilized while the vertical velocity of the structure is minimized.

Evaluation of the results are based on the assumptions and reasoning done in this chapter.

# Chapter 8

# Results

This chapter contains the limiting $H_s - Tp$ values for the Manifold as well as a selection of computed DAF resulting from the launch-recovery analysis of the ROV. The results are evaluated based on the investigation of physical phenomenons discussed in Chapter 7.

## 8.1 Manifold

The limiting operational $H_s$ for the Manifold is based on a 90% fractile estimated from Gumble probability paper. A 90% fractile corresponds to the Gumbel parameter G=2.25 according to Figure 5.3. The entire collection of Gumbel probability papers for all sea states are given in Appendix D (Electronic), an excerpt is given in Appendix . As discussed in Section 4.3.1, the occurrence of slack in the crane wire is only permitted in up to 10% of the simulations. A complete overview is given in Appendix B.

### 8.1.1 Heading=90°

In this section the resulting operational limit for 90° heading for long- and short-crested waves are presented, as well as a general comment.

**Long-Crested Waves**

The resulting operational $H_s$ for 90° heading for long-crested waves, with and without shielding, is given in Figure 8.1. By incorporation of shielding in the simulation, one can see that it has a

positive effect on the operational $H_s$ for most periods. For $T_p \geq 18s$ the lines coincide, and the vessels presence does no longer effect the incoming waves. The implementation of shielding increases the operational $H_s$ with 0.5-1.0m for most $T_p < 18s$. There is observed no gain in the use of shielding for $T_p = 5s$, 7s, and 12s.
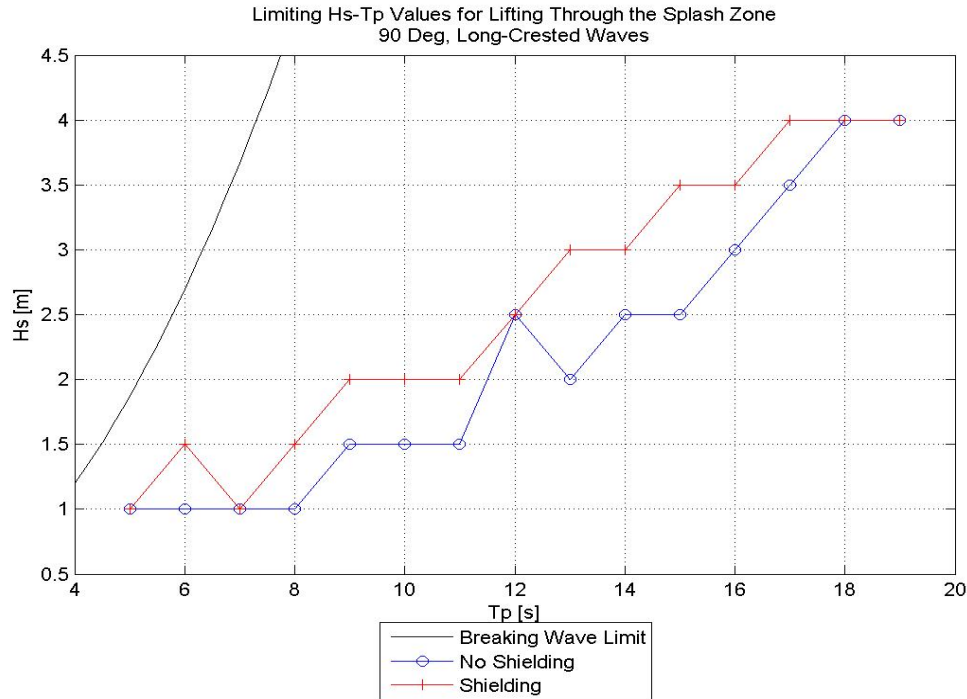


Figure 8.1: Limiting Hs-Tp Values Manifold, 90°, Long-Crested Waves

By further investigating, the Gumbel probability paper (Figure D.2 and occurrence of slack (Table B.1) for $T_p = 5s$, it is observed that the operational limit when shielding is included is only restrained from exceeding $H_s = 1$ by the occurrence of slack in the crane wire. Without shielding, slack is observed in 10 of 20 simulations. The number of observed slack is reduced to 3 when shielding is included. The reduction is significant but since the limiting number of slack is 2 (10%) the reduction does not improve the limiting $H_s$ in this case. This is also the case for $T_p = 12s$ where the number of observed slacks is reduced from 10 to 6 when shielding is included.

The vessels heave motion is at max for $T_p = 7s$, causing large vertical motions. The effect of shielding is visible when comparing the probability papers (Figure D.1 and D.2)for $H_s = 1.5m$, where the 90% fractile is reduced with almost 200kN, but no reduction in slack is observed. Since the slack limit is exceeded in both cases, with and without shielding this restricts the $H_s$ from exceeding 1m. The drop in operational $H_s$ without shielding at $T_p = 13s$ is caused by a high occurrence of slack causing peak loads in the crane wire (Table B.1). The natural roll period of the vessel is 13s. Thus, it is expected that the relative velocity between the structure and sea surface increases, and give rise

to slamming loads with following slack at water entry. The operational limit with shielding does not experience a drop at 13s, despite the fact that the rotations are large.Therefore, it is reason to assume that the particle velocity is adequately reduced to avoid large slamming loads.

**Short-Crested Waves**

The limiting operational $H_s$ for 90° for short-crested waves, with and without shielding, is given in Figure 8.2. The implementation of shielding increases the operational $H_s$ with 0.5-1.0m for all spectral peak periods $T_p$ <18s. Including shielding does not show any effect for larger periods.
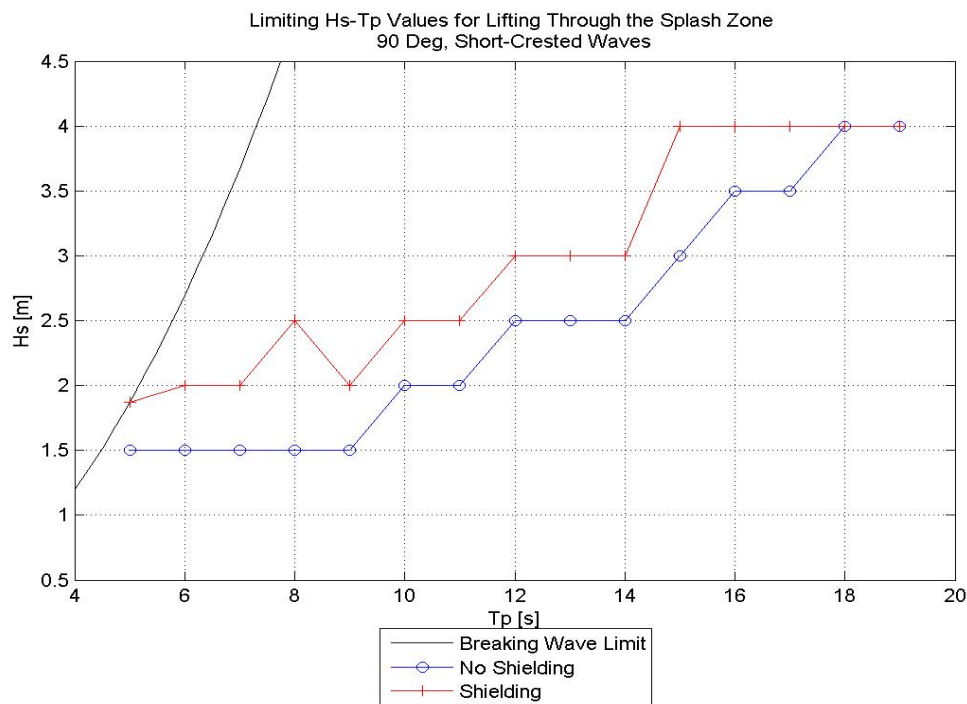


Figure 8.2: Limiting Hs-Tp Values Manifold, 90°, Short-Crested Waves

From the RAOs given in Section 7.5, one can see that for $T_p$ >15s the response in roll experience quick decay, and that the heave response is dominating. The vessel will follow the vertical motion of the wave, and only experience small rotations. The operational limit without shielding at these periods is restricted by the slack limit.

Pay special attention to the operational $H_s$ for $T_p$ =5s when shielding is included, where the operational limit is equal to the breaking wave limit. In practice, this means that launch of the Manifold is safe for all $H_s$ when $T_p$ =5s. The drop in $H_s$ at $T_p$ =9s is caused by a higher occurrence of slack than for surrounding periods causing a higher density of snap loads to occur in the wire.

**General**

Comparing Figure 8.1 and 8.2, one can see that by evaluating short-crested instead of long-crested waves has a positive effect on the operational limit as expected. The operational limit is increased with 0.5-1.0m for most periods both with and without shielding. The directional spreading in wave propagation direction affect both the vessel response and shielding capabilities. Since the transition from long- to short-crested waves seem to have the same positive impact, both with and without shielding, it is reason to believe that it is the vessel response that change and not the shielding capabilities. In Table 8.1 and 8.2, the relative change in operational $H_s$ are given for long- and short-crested waves. One can see that the relative gain of including shielding in general, is larger for short-crested waves. From the vessel RAO's (Section 7.5) one can see a decrease in both heave and roll response when the wave propagation direction deviates from beam sea. As mentioned in Section 7.6 it follows that the relative vertical velocity between the structure and sea surface is expected to decrease, and thus also the risk of slamming loads on the structure.

Table 8.1: Effect of Shielding on Long-Crested Waves in Percent at 90° Heading

| Tp [s] | 5 | 6 | 7 | 8 | 9 | 10 | 11 | 12 | 13 | 14 | 15 | 16 | 17 | 18 | 19 |
|--------|-----|------|-----|------|------|------|------|-----|------|------|------|------|------|-----|-----|
| Change [%] | 0,0 | 50,0 | 0,0 | 50,0 | 33,3 | 33,3 | 33,3 | 0,0 | 50,0 | 20,0 | 40,0 | 16,7 | 14,3 | 0,0 | 0,0 |

Table 8.2: Effect of Shielding on Short-Crested Waves in Percent at 90° Heading

| Tp [s] | 5 | 6 | 7 | 8 | 9 | 10 | 11 | 12 | 13 | 14 | 15 | 16 | 17 | 18 | 19 |
|--------|------|------|------|------|------|------|------|------|------|------|------|------|------|-----|-----|
| Change [%] | 24,8 | 33,3 | 33,3 | 66,7 | 33,3 | 25,0 | 25,0 | 20,0 | 20,0 | 20,0 | 33,3 | 14,3 | 14,3 | 0,0 | 0,0 |

## 8.1.2   Heading=120°

In this section are the resulting operational limit for 120° heading for long- and short-crested waves presented, as well as a general comment.

**Long-Crested Waves**

The resulting operational $H_s$ for 120° heading , for long-crested waves with and without shielding, is given in Figure 8.3. The shielding effect is observed to have a positive impact for all $T_p$ <15s, where the operational limit is increased by 0.5-1m. For periods longer than 15s there is no increase in operational $H_s$ when shielding is taken into account.
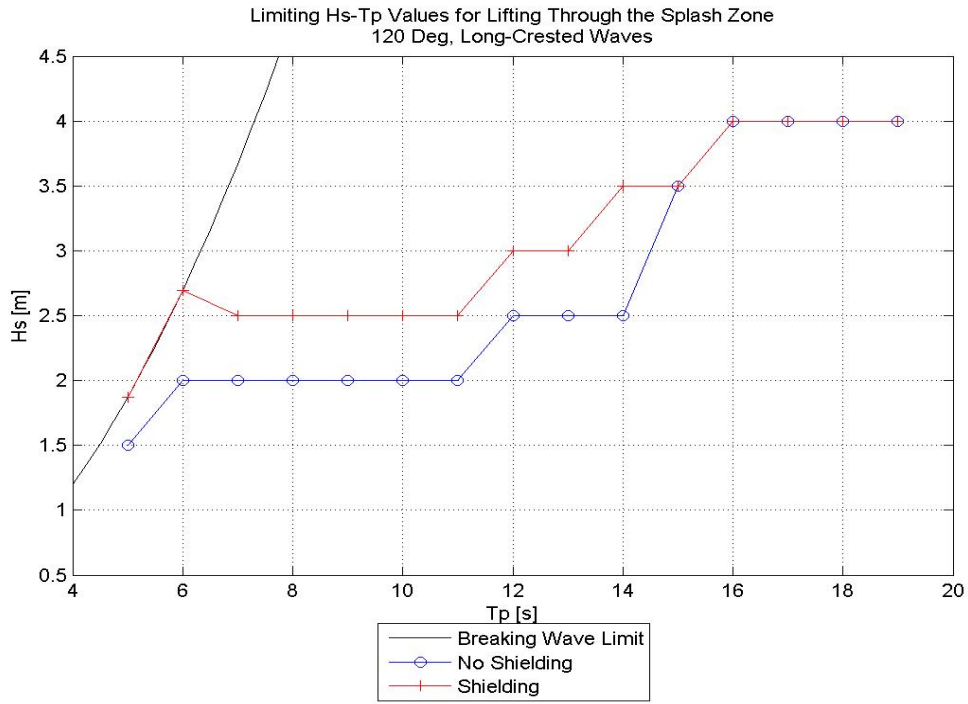
Figure 8.3: Limiting Hs-Tp Values Manifold 120deg Long-Crested Waves

Both for $T_p$ = 5s and 6s is the operational limit equal to the breaking wave limit when shielding is taken into account. Launch of the structure is thus safe for all $H_s$ at these periods. Studying the probability papers in Appendix D (Figure D.4 to D.6) for $H_s = [2-3]$ one can see that the max wire tension for $T_p$ =5s and 6s lies in the lower range compared to the other periods analyzed. This suggests that the effect of shielding is significant for $T_p$ = 5s and 6s. This is caused by small vessel responses in this area, which maximizes the effect of shielding, and minimizes radiation effects. The vessel motions increase rapidly for periods greater than 5s, especially in heave and pitch. In addition, the radiation effects are maximized near the natural pitch period ($T$ =7s), as discussed in Section 7.2. This combination may cause the slight drop in the operational limit observed for $T_p \geq$ 7s when shielding is included.

**Short-Crested Waves**

The limiting operational $H_s$ at 120° heading for short-crested waves with and without shielding, is given in Figure 8.4. Also, the operational $H_s$ increases when shielding is taken into account for most peak periods $T_p <$ 15s.
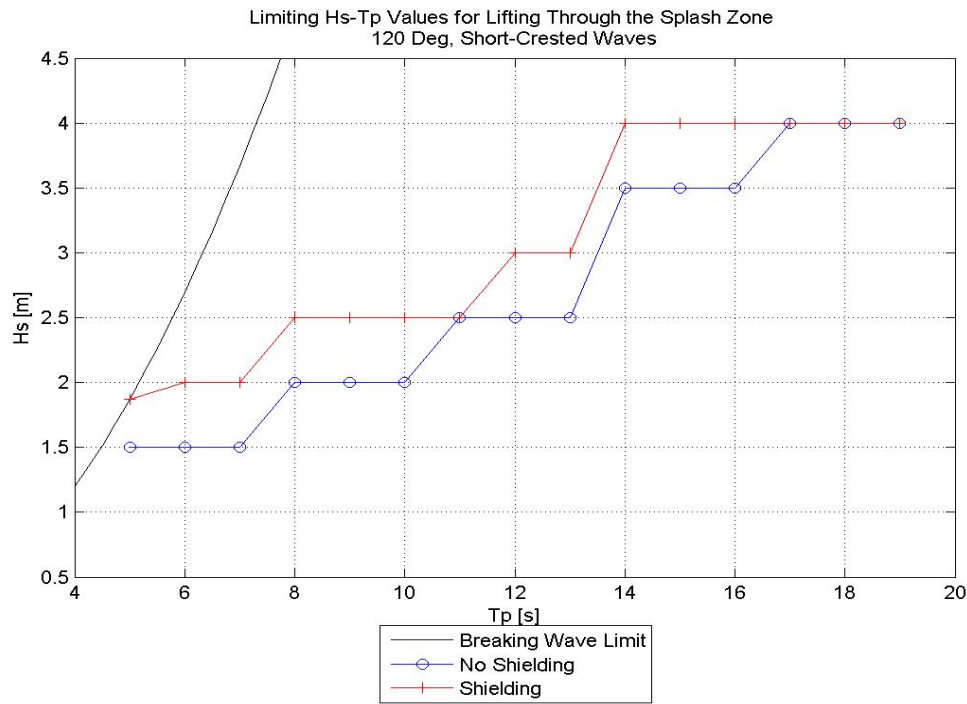
Figure 8.4: Limiting Hs-Tp Values Manifold 120deg Short-Crested Waves

At long wave periods, shielding effects are expected to decrease. The operational limit, with and without shielding, should coincide at this point (here at 17s). From Figure 8.4 one can see that the curves also coincide at $T_p$ =11s. Assuming that the difference in $H_s$ should be 0.5m as the general trend suggests, then the question is why this is not the case. The max wire tension at 90% fractile for $T_p$ =11s is given in Table 8.3 evaluated at $H_s$ =3m (0.5m above the operational limit). This is done to see why the limit could not be equal to 3.0m. From the table, one can see that the max wire tension is reduced with 13%, when shielding is included. The effect does have a positive influence. The reduction is just not large enough to affect the operational $H_s$.

Table 8.3: Effect of Shielding at 120° heading for $T_p$ =11s

|  |  | Max Wire Tension [kN] |  |  |
| --- | --- | --- | --- | --- |
| $H_s$ [m] | $T_p$ [s] | No Shielding | Shielding | Decrease |
| 3 | 11 | 1494 | 1300 | 13% |

**General**

Comparing Figure 8.3 and 8.4, it appears that the use of short-crested waves has a negative effect on the operational limit for spectral peak periods less than 8s both with and without shielding. This despite the fact that the vertical crane velocity is expected to be reduced with short-crested

waves. Some reduction in the particle velocity is shown in Table 7.3, which indicates that radiation causes some cancellation effects. With shielding there is no difference between long- and short-crested waves for 8s$\geq T_p \leq$13s. Without shielding one can see that the operational limit takes turn on being highest for long- and short-crested waves.

Table 8.4 and 8.5 shows the relative change in operational $H_s$, when the effect of shielding is taken into account for long- and short-crested waves respectively.

Table 8.4: Effect of Shielding on Long-Crested Waves in Percent at 120° Heading

| Tp [s] | 5 | 6 | 7 | 8 | 9 | 10 | 11 | 12 | 13 | 14 | 15 | 16 | 17 | 18 | 19 |
|---|---|---|---|---|---|---|---|---|---|---|---|---|---|---|---|
| Change [%] | 24,8 | 34,8 | 25,0 | 25,0 | 25,0 | 25,0 | 25,0 | 20,0 | 20,0 | 40,0 | 0,0 | 0,0 | 0,0 | 0,0 | 0,0 |

Table 8.5: Effect of Shielding on Short-Crested Waves in Percent at 120° Heading

| Tp [s] | 5 | 6 | 7 | 8 | 9 | 10 | 11 | 12 | 13 | 14 | 15 | 16 | 17 | 18 | 19 |
|---|---|---|---|---|---|---|---|---|---|---|---|---|---|---|---|
| Change [%] | 24,8 | 33,3 | 33,3 | 25,0 | 25,0 | 25,0 | 0,0 | 20,0 | 20,0 | 14,3 | 14,3 | 14,3 | 0,0 | 0,0 | 0,0 |

### 8.1.3 Heading=150°

In this section, the resulting operational limit for 150° heading for long- and short-crested waves are presented as well as a general comment.

**Long-Crested Waves**

The resulting operational $H_s$ for 150° heading , for long-crested waves with and without shielding, is given in Figure 8.5. The shielding effect is observed to have positive impact for all $T_p$ <12s. For periods greater than 12s is the operational limit in both cases equal to 4m, i.e. the larges $H_s$ tested for this structure.
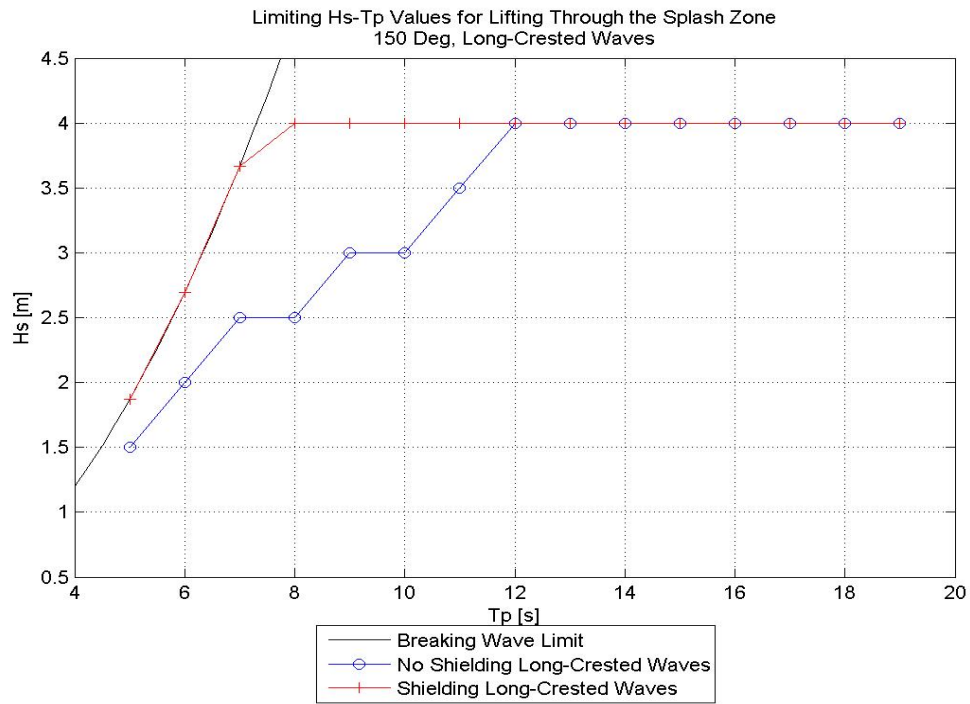
Figure 8.5: Limiting Hs-Tp Values Manifold 150deg Long-Crested Waves

The operational limit is either equal to the breaking wave limit ($T_p \leq 7$s) or the max tested $H_s$ when shielding is included. From this it follows that launch of the structure is considered safe for all physically possible waves, if $H_s$ is less than or equal to 4m. A gradual increase in operational $H_s$ is observed when shielding is not included. The RAO's given in Section 7.5 shows small response in heave and roll at this heading. This is beneficial when considering both shielding and radiation as discussed in Section 7.2.

**Short-Crested Waves**

The limiting operational $H_s$ at 150° heading for short-crested waves, with and without shielding, is given in Figure 8.6. Shielding is observed to improve the operational limit with 0.5-1.5m for all spectral peak periods less than 14s. For periods greater than 14s, the limits coincide for the two cases.
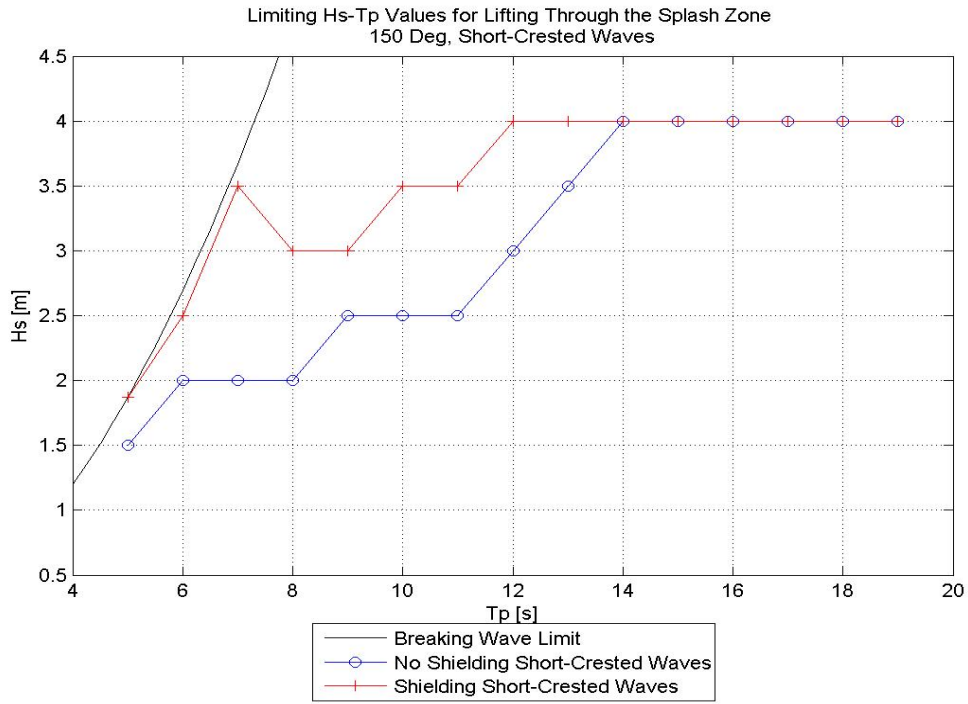
Figure 8.6: Limiting Hs-Tp Values Manifold 150deg Short-Crested Waves

The limiting $H_s$ is observed to increase rapidly for $T_p = [5-7s]$ when shielding is included. Around the natural pitch period 8.5s, a drop is observed. The combination of high pitch and increasing crane velocity leads, to higher incidence of peak loads causing the operational limit to drop. In addition, the operational limit gradually increases with $T_p$ when shielding is not included.

**General**

Comparing Figure 8.5 and 8.6, it is clear that the directional function has a negative effect on the operational limit as expected (see Section 7.6). The operational limit without shielding decreases with 0.5-1.0m for all periods in the range $T_p = [7-13s]$ when directional spreading is taken into account. With shielding one can see that the directional spreading has the highest impact on periods in the range $T_p = [8-11s]$.

Table 8.6 and 8.7 shows the relative change in operational $H_s$ when the effect of shielding is taken into account for long- and short-crested waves respectively.

Table 8.6: Effect of Shielding on Long-Crested Waves in Percent at 150° Heading

| Tp [s] | 5 | 6 | 7 | 8 | 9 | 10 | 11 | 12 | 13 | 14 | 15 | 16 | 17 | 18 | 19 |
|---|---|---|---|---|---|---|---|---|---|---|---|---|---|---|---|
| Change [%] | 24,8 | 34,8 | 46,8 | 60,0 | 33,3 | 33,3 | 14,3 | 0,0 | 0,0 | 0,0 | 0,0 | 0,0 | 0,0 | 0,0 | 0,0 |

Table 8.7: Effect of Shielding on Short-Crested Waves in Percent at 150° Heading

| Tp [s] | 5 | 6 | 7 | 8 | 9 | 10 | 11 | 12 | 13 | 14 | 15 | 16 | 17 | 18 | 19 |
|---|---|---|---|---|---|---|---|---|---|---|---|---|---|---|---|
| Change [%] | 24,8 | 25,0 | 75,0 | 50,0 | 20,0 | 40,0 | 40,0 | 33,3 | 14,3 | 0,0 | 0,0 | 0,0 | 0,0 | 0,0 | 0,0 |

### 8.1.4 Heading=180°

In this section, the resulting operational limit for 180° heading for long- and short-crested waves are presented as well as a general comment. The vessel is not expected to provide any shielding at head sea, it is therefore reasonable to assume that any differences in the operational limit is caused by radiation effects.

**Long-Crested Waves**

The resulting operational $H_s$ for 180° heading , for long-crested waves with and without shielding is given in Figure 8.7. It is evident that for most $T_p$ >8s there are no increase in the operational limit when shielding is included. The operational limit is shown to gain 0.5m and 1m for $T_p$ =6s and 7s respectively.
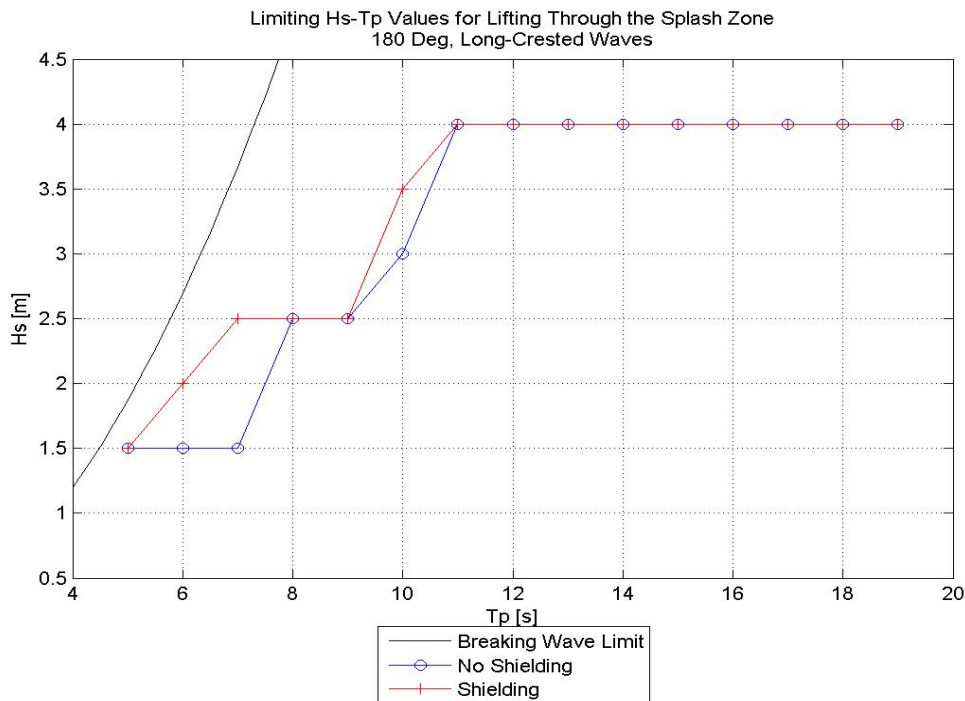


Figure 8.7: Limiting Hs-Tp Values Manifold 180deg Long-Crested Waves

The vessel responses are in general small for periods in the range 5-8s compared to higher periods, but local max/min is observed both in heave and pitch in this region. Since the operational limit is seen to bee higher when shielding is included, it is reasonable to assume that it is caused by cancellation effects that occurs between both the incoming waves and the waves generated by the vessel.

**Short-Crested Waves**

The limiting operational $H_s$ at 180° heading for short-crested waves, with and without shielding, is given in Figure 8.8. Shielding is observed to improve the operational limit with up to 1.0m for most spectral peak periods less than 14s. For periods greater than 14s the limits coincide for the two cases.
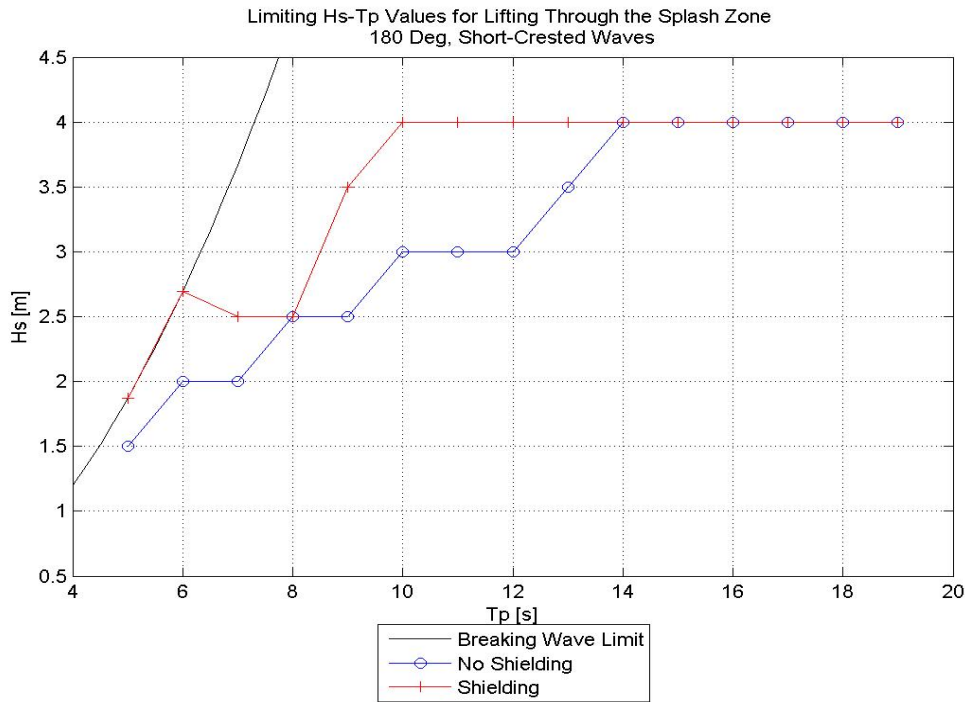


Figure 8.8: Limiting Hs-Tp Values Manifold 180deg Short-Crested Waves

For $T_p$ =8s there is no difference between shielding and no shielding. The positive effect shielding has at this period is visible on the probability papers (Figure D.7 and D.8) and in the overview of slack in Table B.8. It is observed that for $H_s$ =3m the 90% fractile is reduced with about 200kN and slack is reduced from 5 to 0 when shielding is taken into account. The reduction is significant, but not adequate, to increase the operational limit from 2.5m to 3.0m when shielding is included.

**General**

Comparing the use of long- versus short-crested waves, it appears that short-crested waves increases the operational limit for most periods when shielding is included. Without shielding the effect of short-crested waves are observed to have a positive impact in the lover range of periods ($T_p$ =5-8s) and a negative impact for higher periods($T_p$ =11-13s). From Table 8.8 and 8.9 one can see that by evaluation of short- instead of long-crested waves, shielding effects have an impact on a larger range of periods.

Table 8.8: Effect of Shielding on Long-Crested Waves in Percent at 180° Heading

| Tp [s] | 5 | 6 | 7 | 8 | 9 | 10 | 11 | 12 | 13 | 14 | 15 | 16 | 17 | 18 | 19 |
|---|---|---|---|---|---|---|---|---|---|---|---|---|---|---|---|
| Change [%] | 0,0 | 33,3 | 66,7 | 0,0 | 0,0 | 16,7 | 0,0 | 0,0 | 0,0 | 0,0 | 0,0 | 0,0 | 0,0 | 0,0 | 0,0 |

Table 8.9: Effect of Shielding on Short-Crested Waves in Percent at 180° Heading

| Tp [s] | 5 | 6 | 7 | 8 | 9 | 10 | 11 | 12 | 13 | 14 | 15 | 16 | 17 | 18 | 19 |
|---|---|---|---|---|---|---|---|---|---|---|---|---|---|---|---|
| Change [%] | 24,8 | 34,8 | 25,0 | 0,0 | 40,0 | 33,3 | 33,3 | 33,3 | 14,3 | 0,0 | 0,0 | 0,0 | 0,0 | 0,0 | 0,0 |

## 8.1.5   Effect of Heading

With long-crested waves in considering, it is observed that the operational limit is highest at 150° heading for all periods. But when short-crested waves are taken into account does a 180° heading provide a higher operational limit for some periods. In both these cases, the roll and heave motion of the vessel is in general lower compared to 120° and 90 ° heading. With the reduced motion, especially in roll, the risk of slamming is significantly reduced.

## 8.2 ROV

The wire tension results for the ROV were initially processed in the same way as for the Manifold. A set of $H_s - T_p$ graphs (Appendix E)were developed based on the Gumbel probability papers given in Appendix C.4. It proved to be only small differences in the operational limit, for the various heading angles, and also when shielding effects where taken into account. Most likely caused by the high limiting capacity. Thus, for presentation of the results for the ROV a different approach were chosen.

The "worst" operational limit was found for 90° heading, without shielding with long-crested waves, extracts given in Table 8.10. This was used as a base case for the comparison of the ROV results. The maximum tension corresponding to a 90% fractile were extracted for all tested sea states for the given combinations of $H_s$ and $T_p$. The corresponding DAF (Equation 4.5) was calculated and used as basis of comparison to investigate the effect of shielding.

Table 8.10: Hs-Tp Combinations, used in evaluation of ROV Results

| Tp | 5 | 7 | 9 | 11 | 13 | 15 |
|----|-----|-----|-----|-----|-----|-----|
| Hs | 2.0 | 3.0 | 4.0 | 5.0 | 5.0 | 8.0 |

The resulting DAF at launch and recovery for each heading and sea state, are presented in this section. Conditional formatting has been used to show the percent change in DAF between the no shielding and shielding cases. The applied colors are given in Table 8.11, where negative change indicates reduction in DAF and positive change is equivalent to increase, when shielding is taken into account.

Table 8.11: Color Scale Indicating Percent Change in DAF for ROV

| Change>0% | -0,1%> Change >-15% | -15,1%> Change >-35% | -35,1%>Change |
|-----------|---------------------|----------------------|---------------|

The static weight used in calculation of DAF is calculated based on the ROV+TMS mass given in Table 2.3 :

$$F_{static} = Mg = \left( \underbrace{3.05 Te}_{ROV} + \underbrace{2.80 Te}_{TMS} \right) \cdot 9.81 m/s^2 = 57.4 kN \tag{8.1}$$

A DAF=2.79 corresponds to a wire tension equal to the capacity of the LARS system, and should therefore not be exceeded.

### 8.2.1 Heading=90°

The resulting DAF for launch and recovery at 90° heading for all sea states are given in Table 8.12 and 8.13 respectively.

|         | Long-Crested Waves | | Short-Crested Waves | |
|---------|--------------|-----------|--------------|-----------|
| Tp [s]  | No Shielding | Shielding | No Shielding | Shielding |
| 5       | 1,49         | 1,24      | 1,32         | 1,17      |
| 7       | 2,08         | 1,55      | 1,50         | 1,15      |
| 9       | 2,19         | 2,54      | 2,19         | 1,70      |
| 11      | 2,03         | 2,32      | 2,06         | 1,88      |
| 13      | 2,19         | 2,14      | 1,35         | 1,19      |
| 15      | 2,28         | 2,61      | 3,00         | 1,93      |

Table 8.12: Dynamic Amplification Factor,Heading=90°, Launch

|         | Long-Crested Waves | | Short-Crested Waves | |
|---------|--------------|-----------|--------------|-----------|
| Tp [s]  | No Shielding | Shielding | No Shielding | Shielding |
| 5       | 1,89         | 1,45      | 1,80         | 1,26      |
| 7       | 2,11         | 1,55      | 1,76         | 1,50      |
| 9       | 2,69         | 1,72      | 2,21         | 1,53      |
| 11      | 2,10         | 2,41      | 1,99         | 1,79      |
| 13      | 2,11         | 1,85      | 1,74         | 1,68      |
| 15      | 2,63         | 1,84      | 2,68         | 2,08      |

Table 8.13: Dynamic Amplification Factor,Heading=90°, Recovery

During launch it is observed that shielding has negative, or small impact, on the wire tension for larger periods when long-crested waves are considered. At lower periods where shielding effects are expected to be maximized, a decrease in DAF is observed. For short-crested waves is the effect solely positive for all periods, most likely caused by the reduction in roll motion that occurs when the wave propagation direction deviates from beam sea.

Some of the same tendencies are also observed during recovery. The effect of shielding is most pronounced for shorter periods, and tend to decay when the peak period increases.

Comparing launch and recovery, it is seen that the wire tension during recovery is in general higher, and so is the reduction in DAF when shielding is taken into account. The launch phase of the lift is highly dominated of slack especially for $H_s \geq 4m$, the calculated snap loads are highly unpredictable. Hence, the calculated tension is subject to inherent uncertainty.

## 8.2.2 Heading=120°

The resulting DAF for launch and recovery at 120° heading for all sea states are given in Table 8.14 and 8.15 respectively.

| Tp [s] | Long-Crested Waves | | Short-Crested Waves | |
|---|---|---|---|---|
| | No Shielding | Shielding | No Shielding | Shielding |
| 5 | 1,57 | 1,16 | 1,41 | 1,26 |
| 7 | 1,24 | 1,20 | 1,50 | 1,23 |
| 9 | 1,70 | 1,32 | 1,48 | 1,97 |
| 11 | 2,20 | 2,23 | 1,82 | 1,45 |
| 13 | 1,68 | 1,30 | 1,27 | 1,18 |
| 15 | 2,31 | 2,07 | 2,00 | 1,85 |

Table 8.14: Dynamic Amplification Factor,Heading=120°, Launch

| Tp [s] | Long-Crested Waves | | Short-Crested Waves | |
|---|---|---|---|---|
| | No Shielding | Shielding | No Shielding | Shielding |
| 5 | 1,97 | 1,28 | 1,62 | 1,28 |
| 7 | 1,80 | 1,49 | 1,80 | 1,49 |
| 9 | 1,77 | 1,64 | 1,71 | 1,56 |
| 11 | 1,76 | 1,50 | 2,02 | 1,76 |
| 13 | 1,91 | 1,81 | 1,64 | 1,58 |
| 15 | 2,29 | 2,21 | 1,90 | 1,71 |

Table 8.15: Dynamic Amplification Factor,Heading=120°, Recovery

During launch it is observed that shielding effect have a positive impact for both long- and short-crested waves for most periods. A negative effect is shown in two cases, for long-crested waves when $T_p$ =11s, and for short-crested waves when $T_p = 9s$. Comparing long- and short-crested waves when shielding is included, one can see that for periods less than 9s does long-crested waves result in the lowest tensions. For higher periods is this reversed, i.e. short-crested waves gives the best results.

During recovery the DAF reduces for all periods, when shielding is taken into account for both long- and short-crested waves. There is also a significant reduction in slack wire compared to during launch. In addition, the effect of shielding is seen to decrease with increasing periods, which agrees with the expected behavior.

### 8.2.3 Heading=150°

The resulting DAF for launch and recovery at 150° heading for all sea states are given in Table 8.16 and 8.17 respectively.

| Tp [s] | Long-Crested Waves | | Short-Crested Waves | |
|---|---|---|---|---|
| | No Shielding | Shielding | No Shielding | Shielding |
| 5 | 1,37 | 1,20 | 1,40 | 1,31 |
| 7 | 1,40 | 1,19 | 1,56 | 1,18 |
| 9 | 1,36 | 1,18 | 1,31 | 1,15 |
| 11 | 1,52 | 1,23 | 1,28 | 1,18 |
| 13 | 1,23 | 1,18 | 1,21 | 1,14 |
| 15 | 1,25 | 1,12 | 1,46 | 1,15 |

Table 8.16: Dynamic Amplification Factor,Heading=90°, Launch

| Tp [s] | Long-Crested Waves | | Short-Crested Waves | |
|---|---|---|---|---|
| | No Shielding | Shielding | No Shielding | Shielding |
| 5 | 1,58 | 1,34 | 1,58 | 1,35 |
| 7 | 1,90 | 1,39 | 1,64 | 1,50 |
| 9 | 1,67 | 1,38 | 1,82 | 1,58 |
| 11 | 1,93 | 1,62 | 1,68 | 1,48 |
| 13 | 1,64 | 1,40 | 1,66 | 1,56 |
| 15 | 1,81 | 1,55 | 1,82 | 1,65 |

Table 8.17: Dynamic Amplification Factor,Heading=150°, Recovery

The obtained DAF is observed to decrease when shielding is included, both during launch and recovery, which indicates that the relative velocity between the ROV and the sea surface decreases, and with it the risk of slamming. During launch, the reduction in DAF is observed to switch between being largest for long- and short-crested waves. During recovery is the highest reduction observed for long-crested waves.

Studying Table F.17-F.24 in Appendix F it is clear that the occurrence of slack wire is significantly reduced when shielding is included in the simulations. That means that the risk of snap loads is equally reduced, and also the uncertainty related to the calculated tension.

### 8.2.4 Heading=180°

The resulting DAF for launch and recovery at 180° heading for all sea states are given in Table 8.18 and 8.19 respectively.

| Tp [s] | Long-Crested Waves | | Short-Crested Waves | |
|---|---|---|---|---|
| | No Shielding | Shielding | No Shielding | Shielding |
| 5 | 1,35 | 1,34 | 1,42 | 1,30 |
| 7 | 1,44 | 1,46 | 1,50 | 1,24 |
| 9 | 1,31 | 1,41 | 1,20 | 1,30 |
| 11 | 1,45 | 1,23 | 1,31 | 1,27 |
| 13 | 1,17 | 1,18 | 1,21 | 1,20 |
| 15 | 1,23 | 1,23 | 1,38 | 1,28 |

Table 8.18: Dynamic Amplification Factor,Heading=180°, Launch

| Tp [s] | Long-Crested Waves | | Short-Crested Waves | |
|---|---|---|---|---|
| | No Shielding | Shielding | No Shielding | Shielding |
| 5 | 1,62 | 1,80 | 1,54 | 1,57 |
| 7 | 1,66 | 1,70 | 1,88 | 1,44 |
| 9 | 1,63 | 1,56 | 1,68 | 1,61 |
| 11 | 1,54 | 1,62 | 1,61 | 1,55 |
| 13 | 1,56 | 1,40 | 1,48 | 1,46 |
| 15 | 1,61 | 1,55 | 1,73 | 1,57 |

Table 8.19: Dynamic Amplification Factor,Heading=180°, Recovery

At this heading there are not expected to bee any large effect of shielding, especially for long-crested waves. Thus, the observed changes are assumed to be caused by radiation effects. For long-crested waves one can see that there are some change in DAF between the No shielding and shielding case, both for launch and recovery. But the change is not solely positive, for some periods the DAF does increase when shielding is taken into account. Which can be caused by an amplification of the waves due to the radiated waves from the vessel.

For short-crested waves, the DAF is in general higher compared to long-crested waves for most periods before shielding is taken into account. By taking shielding into account, a reduction in DAF is observed for most periods, both during launch and recovery.

### 8.2.5 General Comment

The results given above shows that the maximum wire tension tends to be unpredictable for the ROV-system, especially at 90° where the roll motion is large. The calculated tension is dominated of snap loads due to high occurrence of slack wire, especially during launch. Due to the unpredictable magnitude of the snap loads, a positive effect of shielding is not always present. Results from snap load calculations are subject to a great deal of uncertainty, and should as such be treated with caution. The occurrence of slack in the winch wire for all heading angles and sea states are given in Appendix F.

The implementation of shielding is seen to reduce the occurrence of slack, and with it the uncertainty related to the calculated tension. In general, the effect of shielding is observed to decrease the DAF for most periods $T_p \leq 9s$ for all heading angles and sea states. At higher periods, the effect of shielding is more unpredictable, especially at 90° heading.

A 150° heading is seen to be most beneficial for the ROV-system. Shielding is found to eliminate the occurrence of slack, for many combinations of $H_s$ and $T_p$, which results in a smaller calculated DAF, compared to the other heading angles, both during launch and recovery, and for long-and short-crested waves.

# Chapter 9

# Conclusion

The main goal of this thesis was to investigate how shielding effects influence the operational limit during offshore lifting operations for different headings. Repeated launch and recovery simulations have been conducted in Orcaflex for one Manifold and one ROV model to obtain samples of the dynamic wire tension, which has been used to determine the operational limit.

It can be concluded, for both structures, that the wave steepness is of great significance for the computed dynamic wire tension. Thus, high dynamic wire tension occur when the ratio between wave height and wave length is large. With increasing steepness, larger relative velocity between the lifted structure and the waves follow, which increases the risk of slamming with following slack. Incorporation of shielding in the simulations has resulted in a significant reduction in the occurrence of slack winch wire for all headings. This suggests that the relative velocity between the lifted structure and the waves experience significant reduction, when shielding is taken into account. With reduction in slack follows reduction in snap loads, which are highly unpredictable. It is reasonable to conclude that the uncertainty related to the calculated tension is reduced when shielding is included. In addition, the magnitude of the dynamic wire tension observed is to decrease in most cases.

Considering the Manifold it has been shown that the operational limit on average increases with between 0.5 m and 1.0 m for most periods when shielding is taken into account, for both long- and short-crested waves. The occurrence of slack decreases significantly when the wave propagation direction deviates from beam sea. The optimal heading for lowering the Manifold through the splash-zone, is found to be 150°. The uncertainty related to the calculated dynamic tension is found to increase with increasing $H_s$ and should be treated with caution.

Considering the ROV, the dynamic wire tension is found to bee highly unpredictable, due to high occurrence of slack in the wire, especially during launch. The use of 20 seeds per sea state does not seem to be sufficient to obtain an accurate distribution of the maximum dynamic wire tension. The calculated DAF is associated with high uncertainty and should therefore be treated with caution. On the other hand, shielding is found to reduce the occurrence of slack for most sea states. When reduction in slack occurs, the uncertainty related to the calculated tension is reduced. The optimal heading for lowering the ROV-system through the splash-zone was found to be 150°. The dynamic amplification factor at this heading was reduced for all investigated sea states, when shielding was included in the simulations.

# Chapter 10

# Recommendations for Further Work

An extensive amount of time were used to build the hull geometry for the given vessel. Considering the time spent on modeling, it would be highly beneficial to investigate if a simplified model of the hull could be used to obtain the same sea stat RAOs.

The study in this thesis is based on one hull, and one loading condition only. It would be of interest to perform a parametric study on how a vessels shielding capabilities are influenced when important main dimensional ratios like L\B, B\T, $C_B$ are varied. This can bee used to check whether shielding effects has to be computed for every new hull geometry, or if a general set of sea state RAOs, with accompanying scaling rules, could be developed.

The resulting tension obtained for the ROV system proved to be highly unpredictable compared to the Manifold, due to high occurrence of snap loads. The method used in this case may therefore not be suitable for structures where the hydrodynamic forces easily provokes slack in the wire (light weight structures). It should therefore be evaluated if another method is more appropriate or if more seeds should be used when structures of relatively light weight are to be evaluated.

A smaller increment in $H_s$ should be used when performing similar studies, to possibly avoid drastic changes in the operational limit between two adjacent periods.

# Bibliography

Bai, Y. and Bai, Q. (2010). In *Subsea Engineering Handbook*. Gulf Professional Publishing, Boston.

DeepOcean (2014a). Dynamic Analysis Petrobras - Manifold Installation.

DeepOcean (2014b). Rem forza specification sheet. *DeepOcean, Haugesund,Norway*.

DeepOcean (2015). Design Calculations ROV Supporter on Volstad Surveyor.

DNV (2010). Recommended practice DNV-RP-C205— Environmental Conditions and Environmental Loads. *DNV, Høvik,Norway*.

DNV (2011). Offshore Standard DNV-OS-H101 Marine Operations General. *DNV, Oslo, Norway*.

DNV (2014a). Offshore Standard DNV-OS-H205— Lifting Operations. *DNV, Høvik,Norway*.

DNV (2014b). Recommended practice DNV-RP-H103 Modelling and Analysis of Marine Operations. *DNV, Oslo, Norway*, pages 31,69–70,137.

Faltinsen, O. (1990). *Sea loads on ship and offshore structures.* Cambridge University Press.

Leira, B. (2014a). Correspondance with Bernt Leira from Institute of Marine Technology at NTNU, date:21.05.2015.

Leira, B. (2014b). *Stochastic Theory of Sealoads, Probabilistic Modeling and Estimtion.* Kompendieforlaget.

Myrhaug, D. (2007). Marin Dynamikk, Uregelmessig sjø.

Myrhaug, D. (2014). Stochastic Theory of Sealoads, Statistics of Narrow Band Processes and Equivalent Linearization.

Olsen, C. W. (2014). Analysis of Wave Damping due to Wave Ship Interaction, Project Thesis.

Orcina (2012). OrcaFlex User Manual Version 9.6a.

Orcina (2014). OrcaFlex User Manual Online. from `http://www.orcina.com/` `SoftwareProducts/OrcaFlex/Documentation/Help/`.

Sandvik, P. (2015). Correspondance with Peter Sandvik from MARINTEK.

Steen, S. (2014). *Experimental Methods in Marine Hydrodynamics.* Kompendieforlaget.

# Appendix A

# Spreading Functions

This appendix contains the applied directional spreading functions, for all four heading angles.
The given spreading functions are given for different values of n. An increment of 1 is applied.
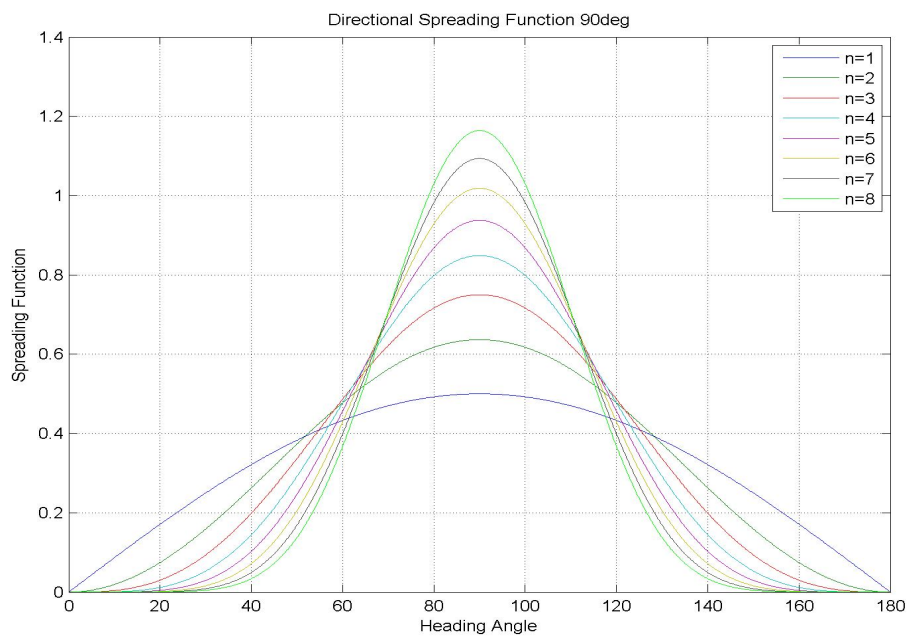


Figure A.1: Spreading Function at 90° Heading
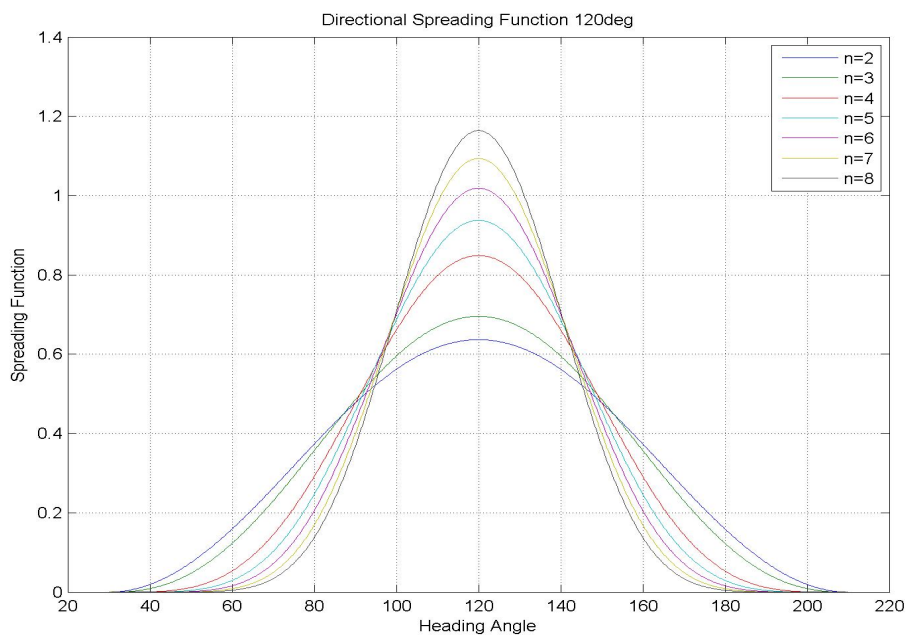
Figure A.2: Spreading Function at 120° Heading
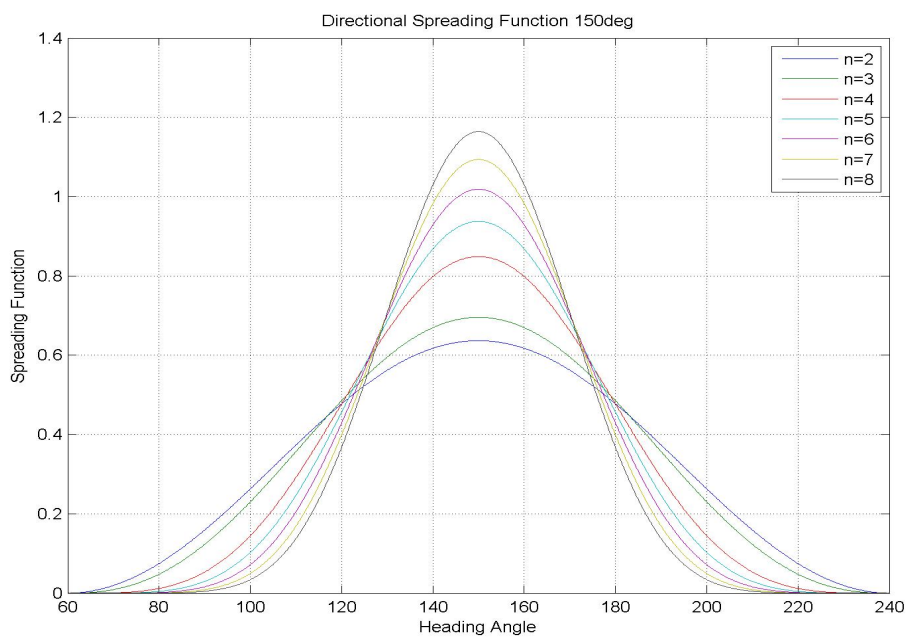


Figure A.3: Spreading Function at 150° Heading
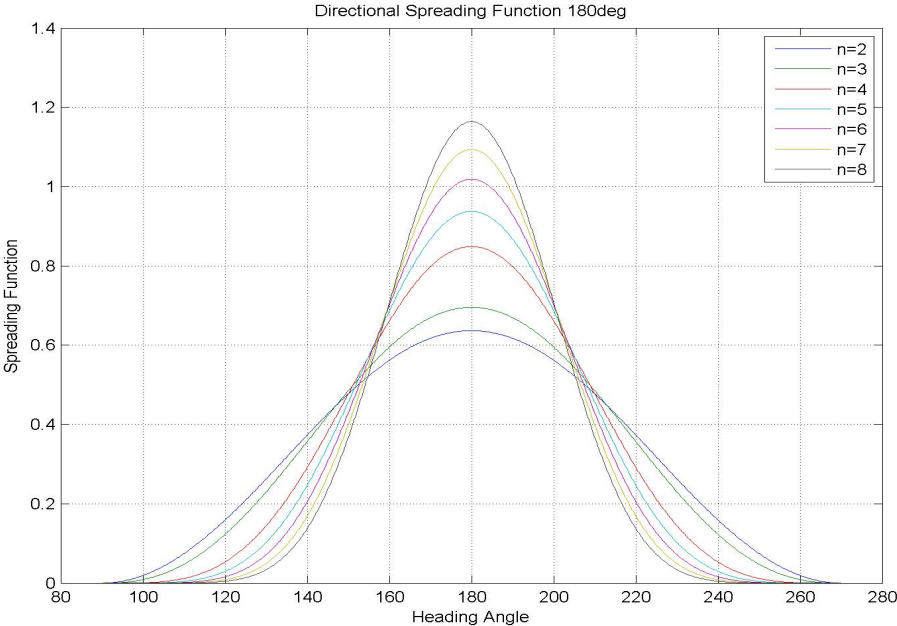
Figure A.4: Spreading Function at 180° Heading

# Appendix B

# Registered Slack for Manifold

The following tables indicate which combinations of $H_s$ and $T_p$ that have been investigated for the Manifold, as well as the occurrence of slack in each set of simulations. When the limit of slack has been exceeded (2 slack per set of simulations) bold font has been used.

Table B.1: Occurrence of Slack , Manifold at 90°, Long-Crested Waves

| | Long-Crested Waves | | | | | | | | | | | | | |
|---|---|---|---|---|---|---|---|---|---|---|---|---|---|---|
| | No Shielding | | | | | | | Shielding | | | | | | |
| Tp [s]/Hs[m] | 1.0 | 1.5 | 2.0 | 2.5 | 3.0 | 3.5 | 4.0 | 1.0 | 1.5 | 2.0 | 2.5 | 3.0 | 3.5 | 4.0 |
| 5 | 0 | **10** | **16** | | | | | 0 | **3** | **9** | | | | |
| 6 | 0 | **5** | **16** | | | | | 0 | 2 | **10** | | | | |
| 7 | 0 | **3** | **13** | | | | | 0 | **3** | **14** | | | | |
| 8 | 0 | **3** | **14** | | | | | 0 | 0 | **9** | | | | |
| 9 | | 1 | **7** | | | | | | 0 | 2 | **10** | | | |
| 10 | | 1 | **6** | | | | | | | 0 | **11** | | | |
| 11 | | 0 | **4** | | | | | | | 0 | **4** | | | |
| 12 | | | 1 | 1 | **10** | | | | | 0 | 1 | **6** | | |
| 13 | | | 0 | **5** | **4** | **7** | | | | 0 | 0 | 2 | **6** | |
| 14 | | | 0 | 0 | **3** | **6** | | | | 0 | 0 | 0 | **4** | **7** |
| 15 | | | 0 | 0 | 1 | **3** | | | | 0 | 0 | 1 | 1 | **5** |
| 16 | | | 0 | | 0 | **3** | **7** | | | 0 | | | 0 | 2 |
| 17 | | | 0 | | 0 | 0 | 2 | | | 0 | | | 1 | 2 |
| 18 | | | 0 | | 0 | 1 | 0 | | | 0 | | | 0 | 0 |
| 19 | | | 0 | | 0 | 0 | 0 | | | 0 | | | 0 | 1 |

Table B.2: Occurrence of Slack , Manifold at 90°, Short-Crested Waves

| Tp [s]/Hs[m] | Short-Crested Waves | | | | | | | | | | |
|---|---|---|---|---|---|---|---|---|---|---|---|
| | No Shielding | | | | | | Shielding | | | | |
| | 1.5 | 2.0 | 2.5 | 3.0 | 3.5 | 4.0 | 2.0 | 2.5 | 3.0 | 3.5 | 4.0 |
| 5 | 0 | **7** | | | | | 0 | | | | |
| 6 | 0 | 1 | | | | | 0 | **9** | | | |
| 7 | 0 | **6** | | | | | 0 | **9** | **12** | | |
| 8 | 0 | **4** | | | | | 0 | 0 | **5** | | |
| 9 | 0 | 2 | | | | | 0 | **5** | **10** | | |
| 10 | 0 | 0 | **5** | | | | 0 | 1 | **6** | | |
| 11 | 0 | 0 | **3** | | | | 0 | 1 | 2 | | |
| 12 | | 1 | 0 | | | | 0 | 0 | 0 | **3** | |
| 13 | | 0 | 0 | **4** | | | 0 | 0 | 0 | 2 | |
| 14 | | 0 | 0 | 2 | **4** | | 0 | | 0 | 2 | 2 |
| 15 | | 0 | 0 | 0 | **3** | | 0 | | 0 | 0 | 1 |
| 16 | | 0 | | 0 | 1 | 2 | 0 | | | 2 | 1 |
| 17 | | 0 | | 0 | 0 | 2 | 0 | | | 0 | 0 |
| 18 | | 0 | | 0 | 0 | 0 | 0 | | | 0 | 0 |
| 19 | | 0 | | 0 | 0 | 0 | 0 | | | 0 | 1 |

Table B.3: Occurrence of Slack , Manifold at 120°, Long-Crested Waves

| Tp[s]/Hs[m] | Long-Crested Waves | | | | | | | | | | | |
|---|---|---|---|---|---|---|---|---|---|---|---|---|
| | No Shielding | | | | | | Shielding | | | | | |
| | 1.5 | 2.0 | 2.5 | 3.0 | 3.5 | 4.0 | 1.5 | 2.0 | 2.5 | 3.0 | 3.5 | 4.0 |
| 5 | 0 | 1 | | | | | | 0 | | | | |
| 6 | 0 | 0 | **9** | | | | | 0 | 0 | 0 | | |
| 7 | 0 | 0 | **7** | | | | | 0 | 0 | **8** | | |
| 8 | 0 | 0 | **6** | | | | | 0 | 0 | **5** | | |
| 9 | 0 | 1 | **6** | | | | | 0 | 0 | **7** | | |
| 10 | 0 | 1 | 2 | | | | | 0 | 0 | **8** | | |
| 11 | | 0 | **3** | | | | | 0 | 1 | **3** | | |
| 12 | | 0 | 0 | 2 | | | | 0 | 0 | 0 | **5** | |
| 13 | | 0 | 0 | 0 | | | | 0 | 0 | 0 | **3** | |
| 14 | | 0 | 0 | 2 | **4** | | | 0 | | 0 | 0 | 0 |
| 15 | | 0 | 0 | 1 | 0 | | | 0 | | 0 | 0 | **6** |
| 16 | | 0 | | 0 | 0 | 0 | | 0 | | | 0 | 0 |
| 17 | | 0 | | 0 | 0 | 0 | | 0 | | | 0 | 0 |
| 18 | | 0 | | 0 | 0 | 0 | | 0 | | | 0 | 0 |
| 19 | | 0 | | 0 | 0 | 0 | | 0 | | | 0 | 1 |

Table B.4: Occurrence of Slack , Manifold at 120°, Short-Crested Waves

| Tp[s]/Hs[m] | Short-Crested Waves | | | | | | | | | | | |
| --- | --- | --- | --- | --- | --- | --- | --- | --- | --- | --- | --- | --- |
| | No Shielding | | | | | | Shielding | | | | | |
| | 1.5 | 2.0 | 2.5 | 3.0 | 3.5 | 4.0 | 1.5 | 2.0 | 2.5 | 3.0 | 3.5 | 4.0 |
| 5 | 0 | 1 | | | | | | 0 | | | | |
| 6 | 0 | **4** | | | | | | 0 | 3 | | | |
| 7 | 0 | **3** | | | | | | 0 | **3** | **6** | | |
| 8 | 0 | 2 | **5** | | | | | 0 | 2 | **7** | | |
| 9 | | 1 | **3** | | | | | 0 | 0 | **7** | | |
| 10 | | 0 | 4 | | | | | 0 | 0 | 2 | | |
| 11 | | 0 | 2 | **5** | | | | 0 | 0 | 2 | | |
| 12 | | 0 | 0 | 2 | | | | 0 | | 0 | 1 | **9** |
| 13 | | 0 | 0 | 0 | | | | 0 | | 0 | **3** | **6** |
| 14 | | 0 | 0 | 0 | 0 | 2 | | 0 | | 0 | 0 | 1 |
| 15 | | 0 | 0 | 0 | 0 | 3 | | 0 | | 0 | 1 | 0 |
| 16 | | 0 | | | 0 | 3 | | 0 | | | 0 | 0 |
| 17 | | 0 | | | 0 | 0 | | 0 | | | 0 | 0 |
| 18 | | 0 | | | 0 | 0 | | 0 | | | 0 | 0 |
| 19 | | 0 | | | 0 | 0 | | 0 | | | 0 | 0 |

Table B.5: Occurrence of Slack , Manifold at 150°, Long-Crested Waves

| Tp[s]/Hs[m] | Long-Crested Waves | | | | | | | | | | |
| --- | --- | --- | --- | --- | --- | --- | --- | --- | --- | --- | --- |
| | No Shielding | | | | | | Shielding | | | | |
| | 1.5 | 2.0 | 2.5 | 3.0 | 3.5 | 4.0 | 2.0 | 2.5 | 3.0 | 3.5 | 4.0 |
| 5 | 1 | 2 | | | | | 0 | | | | |
| 6 | 0 | 0 | | | | | 0 | | | | |
| 7 | 0 | 0 | 0 | | | | 0 | 0 | 0 | | |
| 8 | | 0 | 0 | 1 | | | 0 | 0 | 0 | | 0 |
| 9 | | 0 | 0 | 0 | | | 0 | 0 | 0 | | 0 |
| 10 | | 0 | 0 | 0 | 2 | 2 | 0 | 0 | 0 | | 0 |
| 11 | | 0 | 0 | 0 | 0 | 2 | 0 | 0 | 0 | | 0 |
| 12 | | 0 | 0 | 0 | 0 | 0 | 0 | 0 | 0 | | 0 |
| 13 | | 0 | 0 | 0 | 0 | 0 | 0 | 0 | 0 | | 0 |
| 14 | | 0 | 0 | 0 | 0 | 0 | 0 | 0 | 0 | | 0 |
| 15 | | 0 | 0 | 0 | 0 | 0 | 0 | 0 | 0 | | 0 |
| 16 | | 0 | | | | 0 | 0 | 0 | 0 | | |
| 17 | | 0 | | | | 0 | 0 | 0 | 0 | | |
| 18 | | 0 | | | | 0 | 0 | 0 | 0 | | |
| 19 | | 0 | | | | 0 | 0 | 0 | 0 | | |

Table B.6: Occurrence of Slack , Manifold at 150°, Short-Crested Waves

| Tp[s]/Hs[m] | No Shielding | | | | | | Shielding | | | | |
|---|---|---|---|---|---|---|---|---|---|---|---|
| | 1.5 | 2.0 | 2.5 | 3.0 | 3.5 | 4.0 | 2.0 | 2.5 | 3.0 | 3.5 | 4.0 |
| 5 | 0 | 1 | | | | | 0 | | | | |
| 6 | 0 | 0 | **6** | | | | 0 | | | | |
| 7 | 0 | 0 | 2 | | | | 0 | 0 | 0 | 0 | |
| 8 | | 0 | **5** | **10** | | | 0 | 0 | 0 | 2 | |
| 9 | | 0 | 0 | **5** | | | 0 | 0 | 2 | **3** | |
| 10 | | 0 | 0 | 1 | | | 0 | | 0 | 2 | 2 |
| 11 | | 0 | 0 | 1 | 2 | **4** | 0 | | 0 | 0 | **3** |
| 12 | | 0 | 0 | 0 | 2 | **6** | 0 | | 0 | 0 | 1 |
| 13 | | 0 | | 0 | 2 | **4** | 0 | | 0 | 0 | 0 |
| 14 | | 0 | | 0 | 0 | 1 | 0 | | 0 | 0 | 0 |
| 15 | | 0 | | 0 | 0 | 0 | 0 | | 0 | 0 | 0 |
| 16 | | 0 | | 0 | | 0 | 0 | | | 0 | 0 |
| 17 | | 0 | | 0 | | 0 | 0 | | | 0 | 0 |
| 18 | | 0 | | 0 | | 0 | 0 | | | 0 | 0 |
| 19 | | 0 | | 0 | | 0 | 0 | | | 0 | |

Table B.7: Occurrence of Slack , Manifold at 180°, Long-Crested Waves

| Tp[s]/Hs[m] | No Shielding | | | | | | Shielding | | | | | |
|---|---|---|---|---|---|---|---|---|---|---|---|---|
| | 1.5 | 2.0 | 2.5 | 3.0 | 3.5 | 4.0 | 1.5 | 2.0 | 2.5 | 3.0 | 3.5 | 4.0 |
| 5 | 0 | **4** | | | | | 0 | 2 | | | | |
| 6 | 0 | **3** | | | | | 0 | 1 | **3** | | | |
| 7 | 0 | 2 | | | | | | 0 | 1 | **3** | | |
| 8 | | 0 | 2 | **3** | | | | 0 | 0 | **3** | | |
| 9 | | 0 | 0 | 2 | | | | 0 | 0 | 2 | | |
| 10 | | 0 | 0 | 0 | 2 | **6** | | 0 | 0 | 1 | 0 | 2 |
| 11 | | 0 | 0 | 0 | 0 | 0 | | 0 | | 0 | 0 | 0 |
| 12 | | 0 | 0 | 0 | 0 | 0 | | 0 | | 0 | 0 | 0 |
| 13 | | 0 | 0 | 0 | 0 | 0 | | 0 | | 0 | 0 | 0 |
| 14 | | 0 | 0 | 0 | 0 | 0 | | 0 | | 0 | 0 | 0 |
| 15 | | 0 | 0 | 0 | 0 | 0 | | 0 | | 0 | 0 | 0 |
| 16 | | 0 | | | | 0 | | 0 | | | | 0 |
| 17 | | 0 | | | | 0 | | 0 | | | | 0 |
| 18 | | 0 | | | | 0 | | 0 | | | | 0 |
| 19 | | 0 | | | | 0 | | 0 | | | | 0 |

Table B.8: Occurrence of Slack , Manifold at 180°, Short-Crested Waves

| Tp[s]/Hs[m] | Short-Crested Waves | | | | | | | | | | |
|---|---|---|---|---|---|---|---|---|---|---|---|
| | No Shielding | | | | | | Shielding | | | | |
| | 1.5 | 2.0 | 2.5 | 3.0 | 3.5 | 4.0 | 2.0 | 2.5 | 3.0 | 3.5 | 4.0 |
| 5 | 0 | 1 | | | | | 0 | | | | |
| 6 | 0 | 0 | **5** | **9** | | | 0 | | | | |
| 7 | 0 | 0 | 1 | **4** | | | 0 | 0 | 1 | | |
| 8 | | 0 | 1 | **5** | | | 0 | 0 | 0 | 2 | |
| 9 | | 0 | 0 | 1 | **7** | **11** | 0 | 0 | 0 | 0 | |
| 10 | | 0 | 0 | 0 | **3** | **7** | 0 | 0 | 1 | 0 | 0 |
| 11 | | 0 | 0 | 0 | 1 | **3** | 0 | 0 | 1 | 0 | 0 |
| 12 | | 0 | 0 | 0 | 2 | 2 | 0 | | 0 | 0 | 0 |
| 13 | | 0 | 0 | 0 | 0 | 0 | 0 | | 0 | 0 | 0 |
| 14 | | 0 | 0 | 0 | 0 | 0 | 0 | | 0 | 0 | 0 |
| 15 | | 0 | 0 | 0 | 0 | 0 | 0 | | 0 | 0 | 0 |
| 16 | | 0 | | | | 0 | 0 | | | | 0 |
| 17 | | 0 | | | | 0 | 0 | | | | 0 |
| 18 | | 0 | | | | 0 | 0 | | | | 0 |
| 19 | | 0 | | | | 0 | 0 | | | | 0 |

# Appendix C

# Electronic Attachments

The zip-folder which follows this master thesis contains folders with the same name as the sections in this appendix. Thus, if the attachment of interest is mentioned in section C.1 Project Thesis, the relevant file is found in the folder with the same name.

## C.1 Project Thesis

- The Project Thesis "Analysis of Wave Damping due to Wave Ship Interaction" : Project Thesis.pdf

- WADAM model used in project thesis: HydroD_Wadam_Model.js

## C.2 Sea State RAOs

The Sea-State RAOs are given in the wamit.out file: Sea_State_RAOs.out

## C.3 Orcaflex

Spreadsheet used to generate Orcaflex data files: Orcaflex1.xlsx

The following Orcaflex Models as been used in the simulations.

- BaseCase_NoShielding_Manifold.bin

- BaseCase_Shielding_Manifold.bin

- BaseCase_NoShielding_ROV.bin

- BaseCase_Shielding_ROV.bin

## C.4 Gumbel Probability Paper

The entire collection of Gumbel probability papers for the Manifold are given in the file: Manifold_Probability_Paper.pdf

and corresponding for the ROV: ROV_Probability_Paper.pdf

## C.5 Poster

The poster made for the exhibition at MTS: Poster.pdf

# Appendix D

# Manifold Probability Papers

## D.1  90° Heading
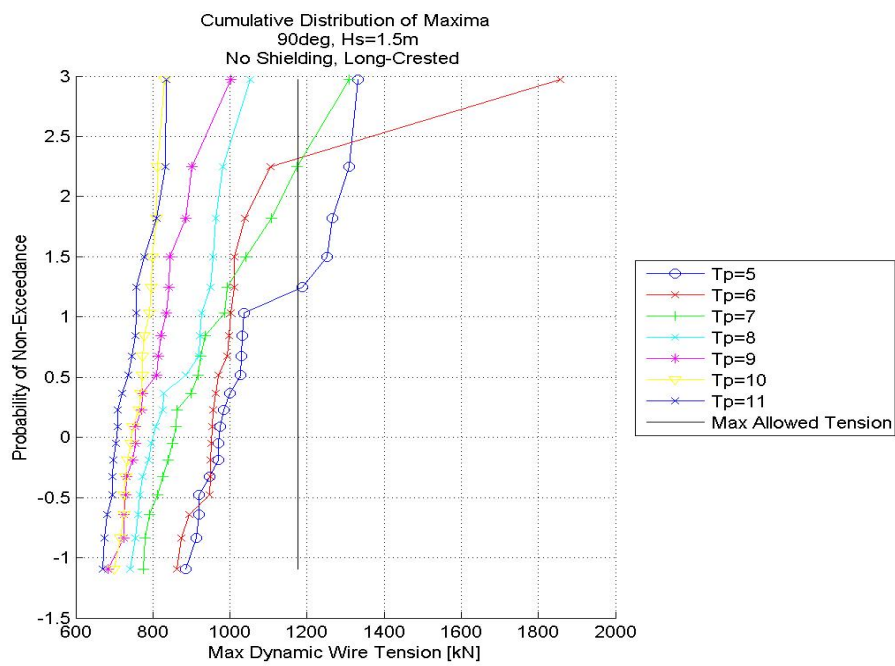


Figure D.1: Distribution of Max Wire Tension Manifold, Hs=1.5, 90deg, Long-crested, No Shielding
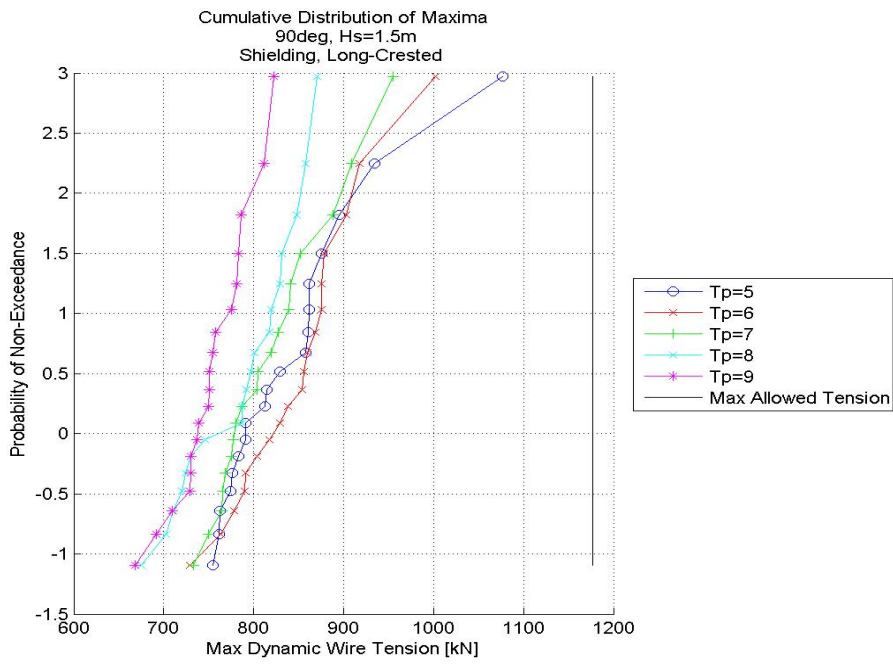
Figure D.2: Distribution of Max Wire Tension Manifold,
Hs=1.5, 90deg, Long-crested, Shielding
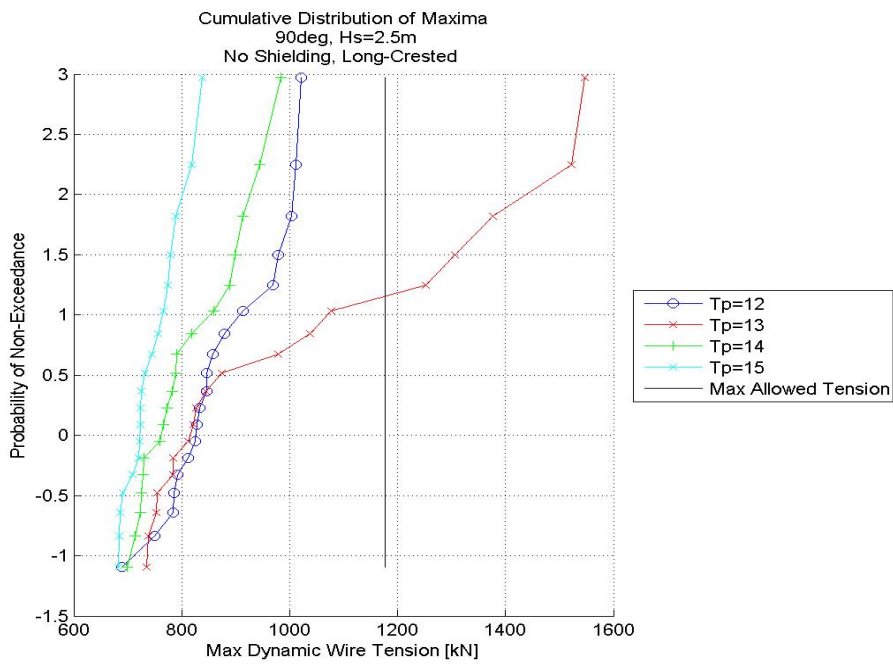


Figure D.3: Distribution of Max Wire Tension Manifold,
Hs=2.5, 90deg, Long-crested, No Shielding

# D.2 120° Heading
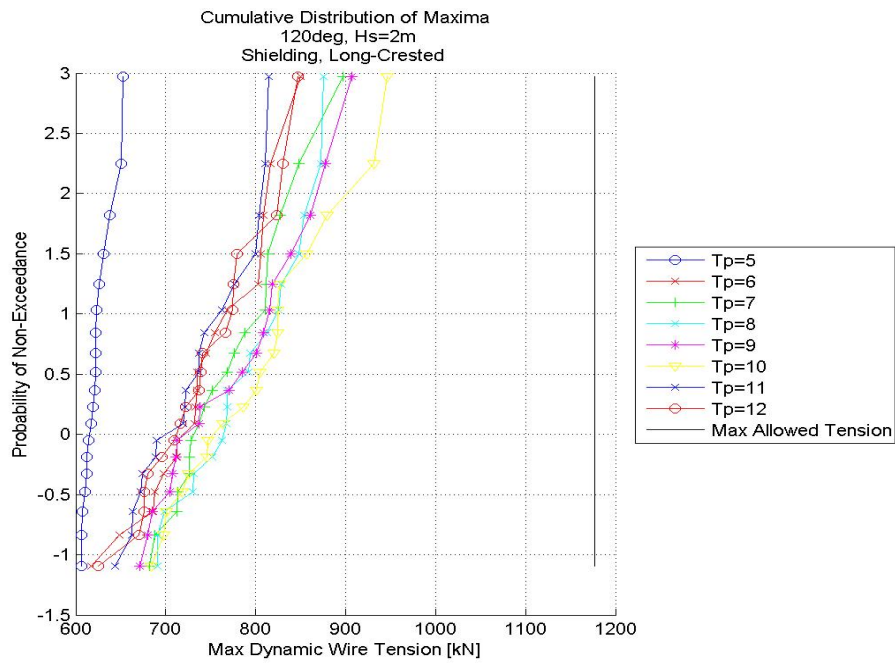


Figure D.4: Distribution of Max Wire Tension Manifold,
Hs=2, 120deg, Long-crested, Shielding
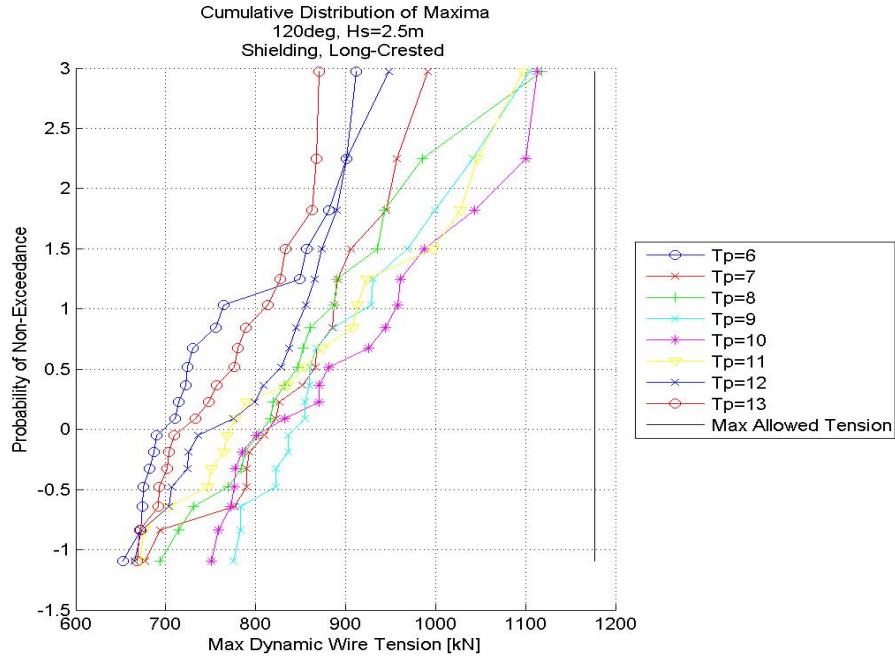


Figure D.5: Distribution of Max Wire Tension Manifold,
Hs=2.5, 120deg, Long-crested, Shielding
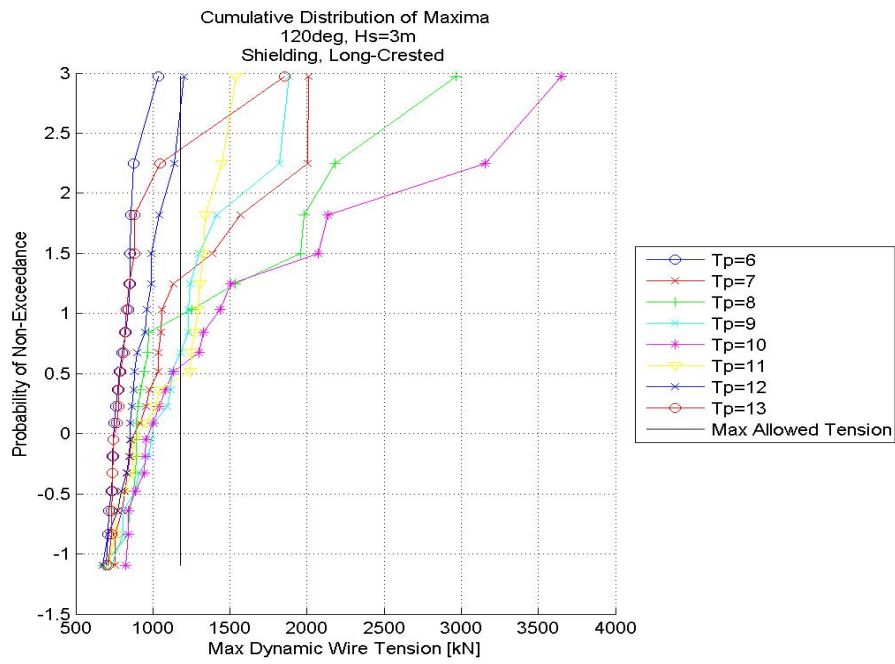
Figure D.6: Distribution of Max Wire Tension Manifold,
Hs=3, 120deg, Long-crested, Shielding

# D.3   180° Heading
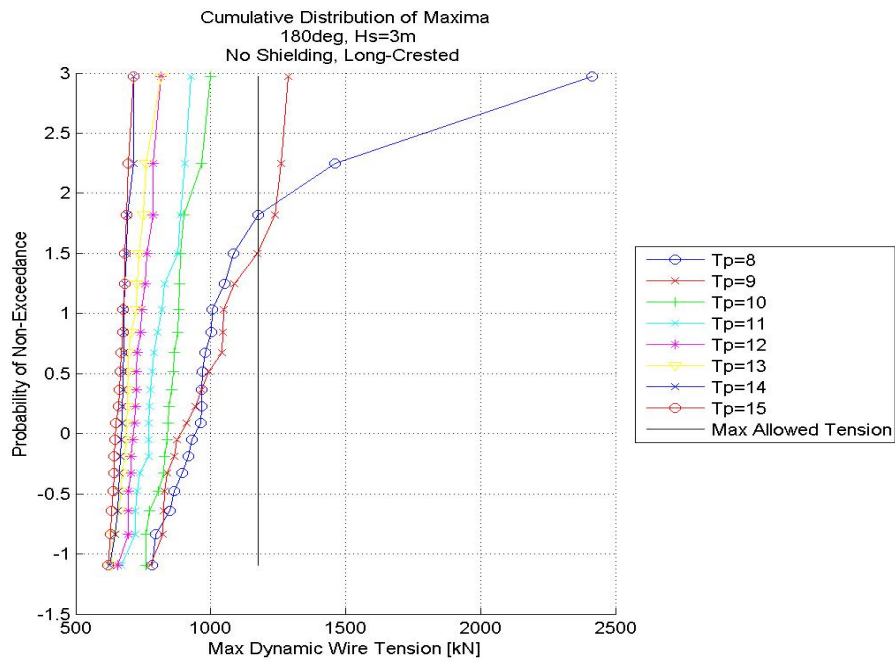


Figure D.7: Distribution of Max Wire Tension Manifold,
Hs=3, 180deg, Long-crested, No Shielding
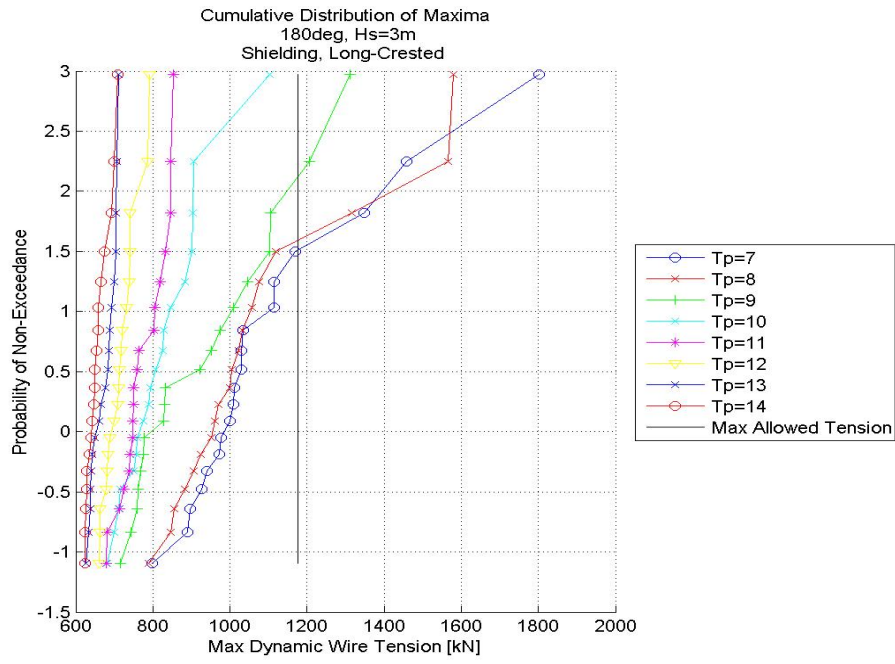
Figure D.8: Distribution of Max Wire Tension Manifold,
Hs=3, 180deg, Long-crested, Shielding

# Appendix E

# Limiting Hs-Tp Values ROV
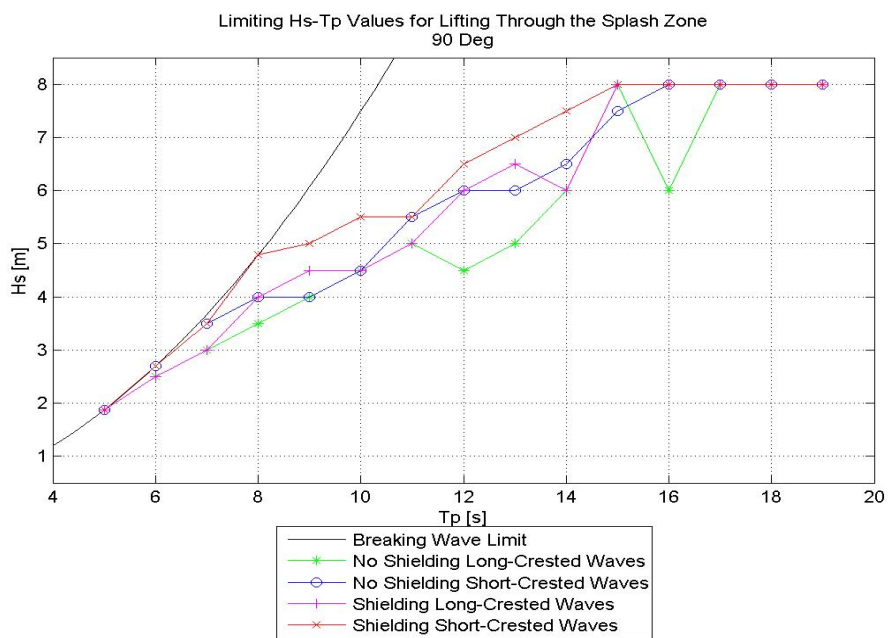
Figure E.1: Limiting Hs-Tp Values ROV, 90deg All Seastates
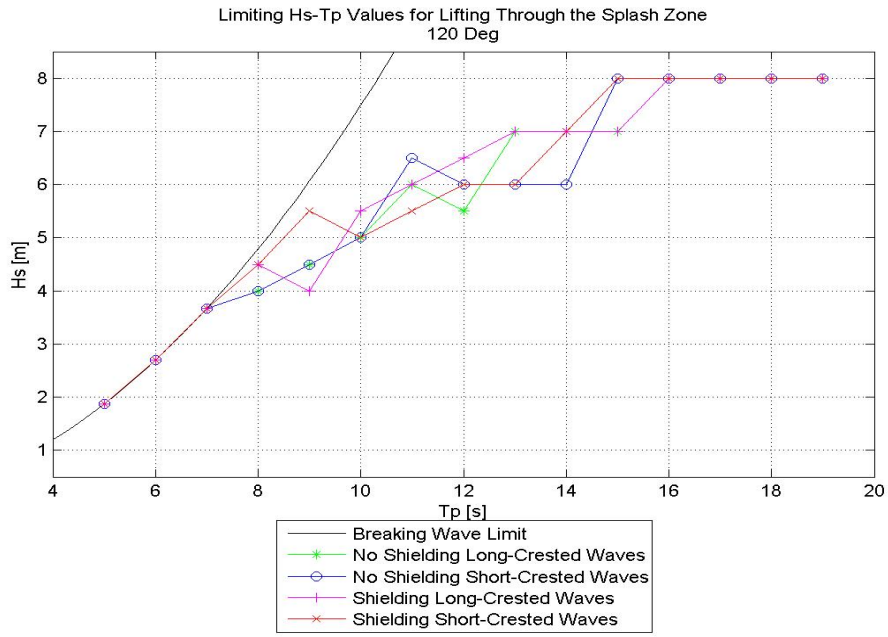
Figure E.2: Limiting Hs-Tp Values ROV, 120deg All Seastates
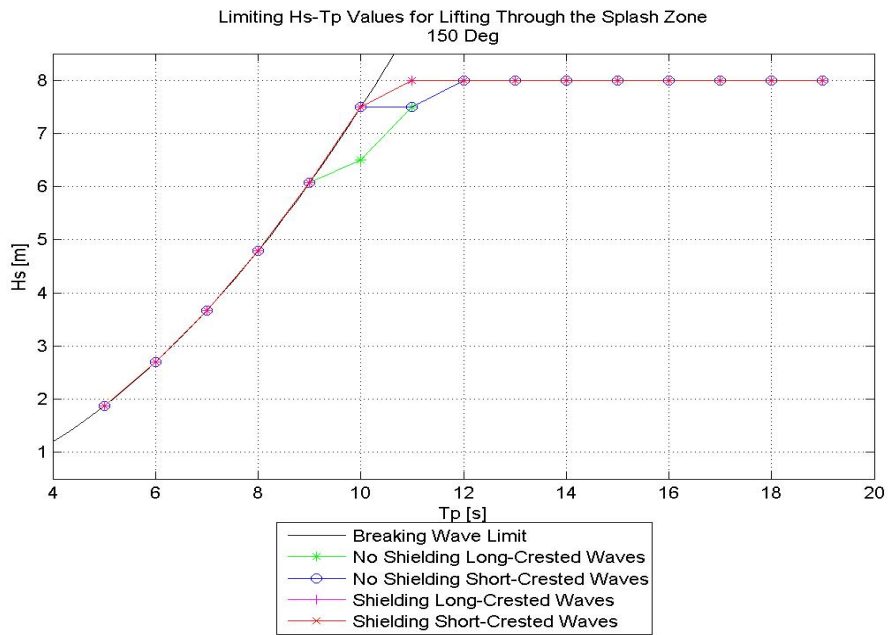


Figure E.3: Limiting Hs-Tp Values ROV, 150deg All Seastates
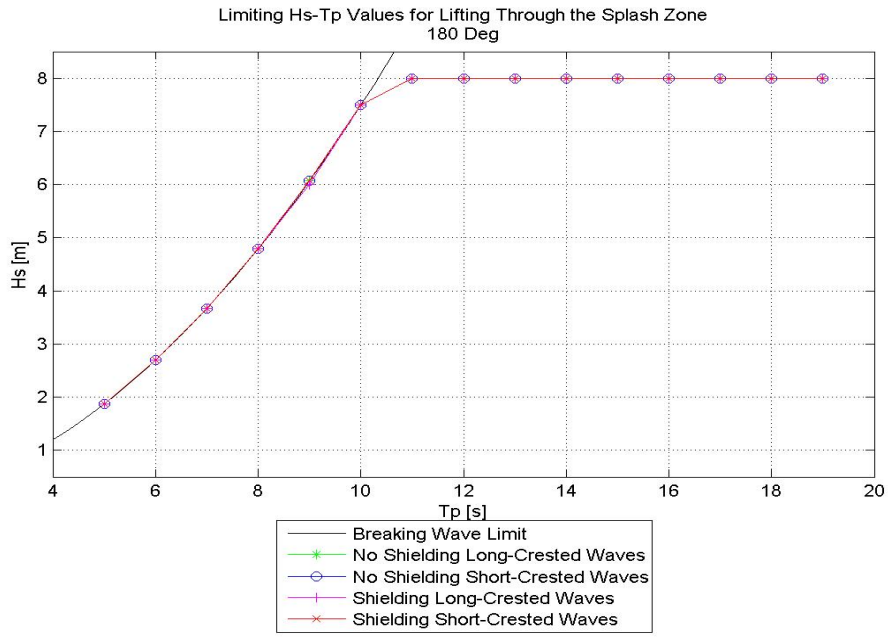
Figure E.4: Limiting Hs-Tp Values ROV, 180deg All Seastates

Table E.1: Limiting Hs-Tp Values ROV

| Tp | 90 No Shielding Long | 90 No Shielding Short | 90 Shielding Long | 90 Shielding Short | 120 No Shielding Long | 120 No Shielding Short | 120 Shielding Long | 120 Shielding Short | 150 No Shielding Long | 150 No Shielding Short | 150 Shielding Long | 150 Shielding Short | 180 No Shielding Long | 180 No Shielding Short | 180 Shielding Long | 180 Shielding Short |
|----|------|------|------|------|------|------|------|------|------|------|------|------|------|------|------|------|
| 5  | 1,9 | 1,9 | 1,9 | 1,9 | 1,9 | 1,9 | 1,9 | 1,9 | 1,9 | 1,9 | 1,9 | 1,9 | 1,9 | 1,9 | 1,9 | 1,9 |
| 6  | 2,5 | 2,7 | 2,5 | 2,7 | 2,7 | 2,7 | 2,7 | 2,7 | 2,7 | 2,7 | 2,7 | 2,7 | 2,7 | 2,7 | 2,7 | 2,7 |
| 7  | 3,0 | 3,5 | 3,0 | 3,5 | 3,7 | 3,7 | 3,7 | 3,7 | 3,7 | 3,7 | 3,7 | 3,7 | 3,7 | 3,7 | 3,7 | 3,7 |
| 8  | 3,5 | 4,0 | 4,0 | 4,8 | 4,0 | 4,0 | 4,5 | 4,5 | 4,8 | 4,8 | 4,8 | 4,8 | 4,8 | 4,8 | 4,8 | 4,8 |
| 9  | 4,0 | 4,0 | 4,5 | 5,0 | 4,5 | 4,5 | 4,0 | 5,5 | 6,1 | 6,1 | 6,1 | 6,1 | 6,1 | 5,5 | 6,0 | 6,1 |
| 10 | 4,5 | 4,5 | 4,5 | 5,5 | 5,0 | 5,0 | 5,5 | 5,0 | 6,5 | 7,5 | 7,5 | 7,5 | 7,5 | 7,5 | 7,5 | 7,5 |
| 11 | 5,0 | 5,5 | 5,0 | 5,5 | 6,0 | 6,5 | 6,0 | 5,5 | 7,5 | 7,5 | 8,0 | 8,0 | 7,0 | 7,0 | 8,0 | 8,0 |
| 12 | 4,5 | 6,0 | 6,0 | 6,5 | 5,5 | 6,0 | 6,5 | 6,0 | 8,0 | 8,0 | 8,0 | 8,0 | 8,0 | 6,5 | 8,0 | 8,0 |
| 13 | 5,0 | 6,0 | 6,5 | 7,0 | 7,0 | 6,0 | 7,0 | 6,0 | 8,0 | 8,0 | 8,0 | 8,0 | 7,0 | 8,0 | 7,0 | 8,0 |
| 14 | 6,0 | 6,5 | 6,0 | 7,5 | 7,0 | 6,0 | 7,0 | 7,0 | 8,0 | 8,0 | 8,0 | 8,0 | 8,0 | 8,0 | 8,0 | 8,0 |
| 15 | 8,0 | 7,5 | 8,0 | 8,0 | 7,0 | 8,0 | 7,0 | 8,0 | 8,0 | 8,0 | 8,0 | 8,0 | 8,0 | 8,0 | 8,0 | 8,0 |
| 16 | 6,0 | 8,0 | 8,0 | 8,0 | 8,0 | 8,0 | 8,0 | 8,0 | 8,0 | 8,0 | 8,0 | 8,0 | 8,0 | 8,0 | 8,0 | 8,0 |
| 17 | 8,0 | 8,0 | 8,0 | 8,0 | 8,0 | 8,0 | 8,0 | 8,0 | 8,0 | 8,0 | 8,0 | 8,0 | 8,0 | 8,0 | 8,0 | 8,0 |
| 18 | 8,0 | 8,0 | 8,0 | 8,0 | 8,0 | 8,0 | 8,0 | 8,0 | 8,0 | 8,0 | 8,0 | 8,0 | 8,0 | 8,0 | 8,0 | 8,0 |
| 19 | 8,0 | 8,0 | 8,0 | 8,0 | 8,0 | 8,0 | 8,0 | 8,0 | 8,0 | 8,0 | 8,0 | 8,0 | 8,0 | 8,0 | 8,0 | 8,0 |

# Appendix F

# Registered Slack for ROV

## F.1 90° Heading

### F.1.1 No Shielding

**Long-Crested Waves**

Table F.1: Occurrence of Slack, No Shielding, Long-Crested Waves, 90° Heading , ROV Launch

| Tp/Hs | 2 | 2.5 | 3 | 3.5 | 4 | 4.5 | 5 | 5.5 | 6 | 6.5 | 7 | 7.5 | 8 |
|---|---|---|---|---|---|---|---|---|---|---|---|---|---|
| 5 | 13 | | | | | | | | | | | | |
| 6 | 11 | 14 | 18 | | | | | | | | | | |
| 7 | 10 | 11 | 19 | 17 | 19 | | | | | | | | |
| 8 | 6 | 16 | 15 | 16 | 16 | 19 | 19 | | | | | | |
| 9 | 6 | 10 | 11 | 15 | 14 | 19 | 18 | 18 | 20 | 20 | | | |
| 10 | 2 | 2 | 8 | 17 | 15 | 17 | 18 | 20 | 19 | 19 | 20 | 19 | 20 |
| 11 | 1 | 4 | 8 | 12 | 13 | 15 | 19 | 18 | 19 | 19 | 20 | 18 | 18 |
| 12 | 1 | 4 | 10 | 6 | 7 | 15 | 16 | 18 | 17 | 20 | 19 | 19 | 18 |
| 13 | | | 4 | 9 | | 11 | 14 | 17 | 18 | 20 | 20 | 19 | 18 |
| 14 | | | | | | | 12 | 12 | 13 | 18 | 18 | 19 | 18 |
| 15 | | | | | | | 6 | 7 | 13 | 15 | 17 | 18 | 16 |
| 16 | | | | | | | 7 | 8 | 13 | 14 | 14 | 12 | 16 |
| 17 | | | | | | | 7 | 7 | 10 | 7 | 14 | 11 | 16 |
| 18 | | | | | | | 7 | 5 | 4 | 7 | 10 | 10 | 14 |
| 19 | | | | | | | 1 | 1 | 6 | 7 | 9 | 14 | 12 |

Table F.2: Occurrence of Slack, No Shielding, Long-Crested Waves, 90° Heading , ROV Recovery

| Tp/Hs | 2 | 2.5 | 3 | 3.5 | 4 | 4.5 | 5 | 5.5 | 6 | 6.5 | 7 | 7.5 | 8 |
|---|---|---|---|---|---|---|---|---|---|---|---|---|---|
| 5 | 0 | | | | | | | | | | | | |
| 6 | 1 | 2 | 7 | | | | | | | | | | |
| 7 | 1 | 1 | 2 | 8 | 6 | | | | | | | | |
| 8 | 0 | 0 | 0 | 2 | 3 | 9 | 8 | | | | | | |
| 9 | 0 | 0 | 0 | 3 | 5 | 7 | 7 | 11 | 9 | 14 | | | |
| 10 | 0 | 0 | 1 | 2 | 0 | 4 | 6 | 7 | 11 | 9 | 12 | 16 | 13 |
| 11 | 0 | 0 | 0 | 2 | 1 | 3 | 6 | 5 | 11 | 6 | 9 | 10 | 13 |
| 12 | 0 | 0 | 0 | 0 | 1 | 2 | 2 | 3 | 7 | 9 | 8 | 8 | 12 |
| 13 | | | 0 | 0 | | 0 | 0 | 3 | 4 | 9 | 7 | 12 | 9 |
| 14 | | | | | | | 0 | 0 | 0 | 5 | 5 | 6 | 9 |
| 15 | | | | | | | 0 | 0 | 1 | 2 | 3 | 5 | 5 |
| 16 | | | | | | | 0 | 0 | 0 | 1 | 1 | 3 | 4 |
| 17 | | | | | | | 0 | 0 | 0 | 1 | 0 | 1 | 3 |
| 18 | | | | | | | 0 | 0 | 0 | 0 | 2 | 0 | 0 |
| 19 | | | | | | | 0 | 0 | 0 | 0 | 1 | 0 | 1 |

**Short-Crested Waves**

Table F.3: Occurrence of Slack, No Shielding, Short-Crested Waves, 90° Heading , ROV Launch

| Tp/Hs | 2 | 2.5 | 3 | 3.5 | 4 | 4.5 | 5 | 5.5 | 6 | 6.5 | 7 | 7.5 | 8 |
|---|---|---|---|---|---|---|---|---|---|---|---|---|---|
| 5 | 7 | | | | | | | | | | | | |
| 6 | 8 | 10 | 12 | | | | | | | | | | |
| 7 | 7 | 12 | 8 | 11 | 18 | | | | | | | | |
| 8 | 5 | 2 | 14 | 14 | 14 | 16 | 17 | | | | | | |
| 9 | 3 | 6 | 8 | 13 | 17 | 16 | 18 | 18 | 19 | 19 | | | |
| 10 | 2 | 5 | 6 | 8 | 14 | 15 | 16 | 18 | 19 | 18 | 19 | 19 | 20 |
| 11 | 0 | 1 | 5 | 6 | 7 | 14 | 15 | 12 | 16 | 17 | 17 | 20 | 20 |
| 12 | 0 | 3 | 1 | 7 | 7 | 13 | 16 | 14 | 14 | 17 | 20 | 15 | 18 |
| 13 | | 0 | 2 | 5 | 0 | 5 | 9 | 11 | 16 | 17 | 17 | 20 | 17 |
| 14 | | | | | 0 | | 9 | 16 | 15 | 15 | 17 | 17 | 18 |
| 15 | | | | | | | 9 | 5 | 11 | 11 | 13 | 14 | 18 |
| 16 | | | | | | | 6 | 10 | 8 | 10 | 15 | 14 | 15 |
| 17 | | | | | | | 7 | 4 | 11 | 12 | 12 | 8 | 11 |
| 18 | | | | | | | 5 | 2 | 3 | 7 | 8 | 10 | 10 |
| 19 | | | | | | | 3 | 1 | 3 | 6 | 8 | 7 | 11 |

Table F.4: Occurrence of Slack, No Shielding, Short-Crested Waves, 90° Heading , ROV Recovery

| Tp/Hs | 2 | 2.5 | 3 | 3.5 | 4 | 4.5 | 5 | 5.5 | 6 | 6.5 | 7 | 7.5 | 8 |
|---|---|---|---|---|---|---|---|---|---|---|---|---|---|
| 5 | 0 | | | | | | | | | | | | |
| 6 | 0 | 0 | 2 | | | | | | | | | | |
| 7 | 0 | 0 | 2 | 2 | 4 | | | | | | | | |
| 8 | 0 | 0 | 1 | 3 | 0 | 4 | 6 | | | | | | |
| 9 | 0 | 0 | 0 | 0 | 1 | 7 | 5 | 2 | 8 | 6 | | | |
| 10 | 0 | 0 | 0 | 0 | 1 | 1 | 4 | 3 | 5 | 4 | 9 | 11 | 13 |
| 11 | 0 | 0 | 0 | 0 | 0 | 0 | 0 | 2 | 3 | 7 | 10 | 10 | 7 |
| 12 | 0 | 0 | 0 | 0 | 0 | 1 | 0 | 0 | 1 | 1 | 3 | 6 | 8 |
| 13 | | 0 | 0 | 0 | | 0 | 1 | 0 | 1 | 3 | 3 | 4 | 4 |
| 14 | | | | | | 0 | 0 | 0 | 0 | 3 | 2 | 6 | 9 |
| 15 | | | | | | 0 | 0 | 0 | 0 | 1 | 2 | 1 | 4 |
| 16 | | | | | | | 0 | 0 | 0 | 0 | 1 | 2 | 0 |
| 17 | | | | | | | 0 | 0 | 0 | 0 | 0 | 3 | 1 |
| 18 | | | | | | | 0 | 0 | 0 | 0 | 0 | 0 | 1 |
| 19 | | | | | | | 0 | 0 | 0 | 0 | 0 | 0 | 0 |

## F.1.2   Shielding

**Long-Crested Waves**

Table F.5: Occurrence of Slack, Shielding, Long-Crested Waves, 90° Heading , ROV Launch

| Tp/Hs | 2 | 2.5 | 3 | 3.5 | 4 | 4.5 | 5 | 5.5 | 6 | 6.5 | 7 | 7.5 | 8 |
|---|---|---|---|---|---|---|---|---|---|---|---|---|---|
| 5 | 4 | | | | | | | | | | | | |
| 6 | 1 | 12 | 13 | | | | | | | | | | |
| 7 | 3 | 9 | 14 | 16 | 17 | | | | | | | | |
| 8 | 4 | 11 | 11 | 15 | 13 | 18 | 18 | | | | | | |
| 9 | 0 | 6 | 7 | 13 | 12 | 20 | 18 | 16 | 18 | 20 | | | |
| 10 | 2 | 5 | 4 | 12 | 14 | 18 | 17 | 19 | 19 | 19 | 20 | 19 | 20 |
| 11 | 0 | 4 | 6 | 14 | 12 | 14 | 16 | 16 | 17 | 19 | 20 | 19 | 19 |
| 12 | 0 | 3 | | 6 | 7 | 14 | 15 | 14 | 18 | 19 | 17 | 17 | 18 |
| 13 | | | | 5 | | 8 | 13 | 16 | 16 | 19 | 18 | 19 | 19 |
| 14 | | | | | | | 8 | 13 | 10 | 16 | 17 | 18 | 18 |
| 15 | | | | | | | 5 | 6 | 10 | 14 | 17 | 17 | 16 |
| 16 | | | | | | | 7 | 11 | 11 | 12 | 17 | 13 | 15 |
| 17 | | | | | | | 4 | 8 | 7 | 7 | 13 | 8 | 13 |
| 18 | | | | | | | 6 | 3 | 4 | 9 | 10 | 8 | 13 |
| 19 | | | | | | | 1 | 1 | 5 | 4 | 9 | 11 | 9 |

Table F.6: Occurrence of Slack, Shielding, Long-Crested Waves, 90° Heading , ROV Recovery

| Tp/Hs | 2 | 2.5 | 3 | 3.5 | 4 | 4.5 | 5 | 5.5 | 6 | 6.5 | 7 | 7.5 | 8 |
|---|---|---|---|---|---|---|---|---|---|---|---|---|---|
| 5 | 0 | | | | | | | | | | | | |
| 6 | 0 | 1 | 8 | | | | | | | | | | |
| 7 | 0 | 1 | 3 | 8 | 7 | | | | | | | | |
| 8 | 0 | 1 | 1 | 4 | 4 | 7 | 10 | | | | | | |
| 9 | 0 | 0 | 0 | 1 | 5 | 8 | 7 | 7 | 8 | 11 | | | |
| 10 | 0 | 0 | 0 | 1 | 1 | 5 | 7 | 4 | 8 | 12 | 11 | 13 | 15 |
| 11 | 0 | 0 | 0 | 2 | 1 | 1 | 2 | 6 | 8 | 5 | 11 | 6 | 9 |
| 12 | 0 | 0 | | 0 | 0 | 2 | 3 | 2 | 5 | 6 | 5 | 8 | 12 |
| 13 | | | | 0 | | 0 | 2 | 3 | 3 | 4 | 9 | 8 | 7 |
| 14 | | | | | | | 0 | 0 | 0 | 3 | 3 | 6 | 7 |
| 15 | | | | | | | 0 | 0 | 0 | 1 | 3 | 4 | 2 |
| 16 | | | | | | | 0 | 0 | 0 | 1 | 1 | 3 | 4 |
| 17 | | | | | | | 0 | 0 | 0 | 0 | 0 | 1 | 1 |
| 18 | | | | | | | 0 | 0 | 0 | 0 | 1 | 0 | 1 |
| 19 | | | | | | | 0 | 0 | 0 | 0 | 0 | 0 | 1 |

**Short-Crested Waves**

Table F.7: Occurrence of Slack, Shielding, Short-Crested Waves, 90° Heading , ROV Launch

| Tp/Hs | 2 | 2.5 | 3 | 3.5 | 4 | 4.5 | 5 | 5.5 | 6 | 6.5 | 7 | 7.5 | 8 |
|---|---|---|---|---|---|---|---|---|---|---|---|---|---|
| 5 | 0 | | | | | | | | | | | | |
| 6 | 0 | 3 | 4 | | | | | | | | | | |
| 7 | 0 | 3 | 2 | 5 | 13 | | | | | | | | |
| 8 | 2 | 1 | 9 | 7 | 12 | 12 | 12 | | | | | | |
| 9 | 2 | 1 | 2 | 6 | 11 | 16 | 13 | 18 | 16 | 19 | | | |
| 10 | 0 | 1 | 5 | 2 | 9 | 9 | 14 | 15 | 19 | 16 | 16 | 15 | 19 |
| 11 | 0 | 1 | 1 | 2 | 2 | 11 | 13 | 8 | 15 | 16 | 16 | 15 | 18 |
| 12 | 0 | 1 | | 5 | 4 | 9 | 11 | 12 | 11 | 14 | 19 | 14 | 17 |
| 13 | | | | 4 | | 7 | 11 | 11 | 11 | 18 | 16 | 20 | 17 |
| 14 | | | | | | | 7 | 13 | 9 | 13 | 14 | 17 | 18 |
| 15 | | | | | | | 4 | 6 | 10 | 12 | 8 | 13 | 13 |
| 16 | | | | | | | 6 | 8 | 4 | 7 | 13 | 13 | 13 |
| 17 | | | | | | | 6 | 4 | 9 | 8 | 8 | 10 | 11 |
| 18 | | | | | | | 2 | 2 | 3 | 6 | 6 | 10 | 9 |
| 19 | | | | | | | 2 | 0 | 2 | 4 | 6 | 7 | 10 |

Table F.8: Occurrence of Slack, Shielding, Short-Crested Waves, 90° Heading , ROV Recovery

| Tp/Hs | 2 | 2.5 | 3 | 3.5 | 4 | 4.5 | 5 | 5.5 | 6 | 6.5 | 7 | 7.5 | 8 |
|---|---|---|---|---|---|---|---|---|---|---|---|---|---|
| 5 | 0 | | | | | | | | | | | | |
| 6 | 0 | 1 | 2 | | | | | | | | | | |
| 7 | 0 | 0 | 0 | 1 | 4 | | | | | | | | |
| 8 | 0 | 0 | 1 | 0 | 1 | 4 | 4 | | | | | | |
| 9 | 0 | 0 | 0 | 0 | 1 | 0 | 0 | 2 | 6 | 6 | | | |
| 10 | 0 | 0 | 0 | 0 | 0 | 0 | 2 | 4 | 10 | 4 | 3 | 9 | 11 |
| 11 | 0 | 0 | 0 | 0 | 0 | 1 | 0 | 0 | 4 | 7 | 7 | 8 | 4 |
| 12 | 0 | 0 | | 0 | 1 | 0 | 1 | 0 | 1 | 3 | 3 | 4 | 4 |
| 13 | | | | 0 | | 0 | 1 | 0 | 1 | 3 | 1 | 2 | 1 |
| 14 | | | | | | | 0 | 0 | 0 | 3 | 3 | 3 | 6 |
| 15 | | | | | | | 0 | 0 | 0 | 1 | 0 | 2 | 2 |
| 16 | | | | | | | 0 | 0 | 0 | 0 | 0 | 1 | 1 |
| 17 | | | | | | | 0 | 0 | 0 | 0 | 0 | 3 | 1 |
| 18 | | | | | | | 0 | 0 | 0 | 0 | 0 | 0 | 1 |
| 19 | | | | | | | 0 | 0 | 0 | 0 | 0 | 0 | 0 |

# F.2    120° Heading

## F.2.1    No Shielding

**Long-Crested Waves**

Table F.9: Occurrence of Slack, No Shielding, Long-Crested Waves, 120° Heading , ROV Launch

| Tp/Hs | 2 | 2.5 | 3 | 3.5 | 4 | 4.5 | 5 | 5.5 | 6 | 6.5 | 7 | 7.5 | 8 |
|---|---|---|---|---|---|---|---|---|---|---|---|---|---|
| 5 | 4 | | | | | | | | | | | | |
| 6 | 6 | 12 | 15 | | | | | | | | | | |
| 7 | 4 | 7 | 11 | 13 | 16 | | | | | | | | |
| 8 | 4 | 9 | 13 | 14 | 14 | 18 | 17 | | | | | | |
| 9 | 3 | 9 | 9 | 10 | 12 | 19 | 16 | 19 | 16 | 19 | | | |
| 10 | 2 | 0 | 8 | 10 | 11 | 13 | 18 | 19 | 19 | 19 | 20 | 19 | 20 |
| 11 | 1 | 2 | 7 | 12 | 8 | 14 | 19 | 13 | 16 | 19 | 20 | 19 | 20 |
| 12 | 1 | 0 | 4 | 6 | 12 | 11 | 15 | 13 | 16 | 15 | 19 | 19 | 17 |
| 13 | | | 2 | 5 | | 12 | 11 | 11 | 14 | 17 | 18 | 18 | 18 |
| 14 | | | | | | | 11 | 12 | 12 | 14 | 16 | 18 | 17 |
| 15 | | | | | | | 9 | 11 | 16 | 11 | 10 | 15 | 17 |
| 16 | | | | | | | 6 | 11 | 12 | 12 | 15 | 15 | 19 |
| 17 | | | | | | | 1 | 4 | 5 | 10 | 8 | 12 | 14 |
| 18 | | | | | | | 5 | 2 | 6 | 6 | 6 | 13 | 12 |
| 19 | | | | | | | 4 | 1 | 7 | 6 | 8 | 8 | 9 |

Table F.10: Occurrence of Slack, No Shielding, Long-Crested Waves, 120° Heading , ROV Recovery

| Tp/Hs | 2 | 2.5 | 3 | 3.5 | 4 | 4.5 | 5 | 5.5 | 6 | 6.5 | 7 | 7.5 | 8 |
|---|---|---|---|---|---|---|---|---|---|---|---|---|---|
| 5 | 0 | | | | | | | | | | | | |
| 6 | 0 | 0 | 1 | | | | | | | | | | |
| 7 | 0 | 0 | 0 | 0 | 3 | | | | | | | | |
| 8 | 1 | 0 | 1 | 0 | 2 | 7 | 6 | | | | | | |
| 9 | 0 | 0 | 1 | 0 | 1 | 1 | 3 | 8 | 9 | 6 | | | |
| 10 | 0 | 0 | 0 | 0 | 1 | 2 | 2 | 5 | 5 | 4 | 10 | 8 | 10 |
| 11 | 0 | 0 | 0 | 0 | 1 | 0 | 3 | 2 | 2 | 6 | 10 | 7 | 11 |
| 12 | 0 | 0 | 0 | 0 | 0 | 1 | 0 | 2 | 2 | 4 | 3 | 7 | 10 |
| 13 | | | 0 | 0 | | 0 | 1 | 1 | 3 | 6 | 4 | 5 | 7 |
| 14 | | | | | | | 1 | 0 | 1 | 0 | 2 | 4 | 6 |
| 15 | | | | | | | 0 | 0 | 1 | 0 | 1 | 2 | 2 |
| 16 | | | | | | | 0 | 1 | 0 | 0 | 0 | 3 | 1 |
| 17 | | | | | | | 0 | 0 | 0 | 0 | 0 | 2 | 1 |
| 18 | | | | | | | 0 | 0 | 0 | 0 | 0 | 0 | 0 |
| 19 | | | | | | | 0 | 0 | 0 | 0 | 1 | 0 | 1 |

**Short-Crested Waves**

Table F.11: Occurrence of Slack, No Shielding, Short-Crested Waves, 120° Heading , ROV Launch

| Tp/Hs | 2 | 2.5 | 3 | 3.5 | 4 | 4.5 | 5 | 5.5 | 6 | 6.5 | 7 | 7.5 | 8 |
|---|---|---|---|---|---|---|---|---|---|---|---|---|---|
| 5 | 8 | | | | | | | | | | | | |
| 6 | 5 | 8 | | | | | | | | | | | |
| 7 | 3 | 12 | 0 | 13 | | | | | | | | | |
| 8 | 1 | 10 | 10 | 13 | 17 | 17 | 16 | | | | | | |
| 9 | 0 | 2 | 12 | 16 | 12 | 16 | 18 | 19 | 18 | 18 | | | |
| 10 | 2 | 4 | 14 | 7 | 14 | 16 | 14 | 18 | 17 | 16 | 19 | 18 | 18 |
| 11 | 0 | 0 | 9 | 9 | 16 | 9 | 12 | 14 | 19 | 18 | 17 | 18 | 18 |
| 12 | 0 | 1 | 7 | 4 | 12 | 13 | 14 | 14 | 15 | 17 | 18 | 18 | 20 |
| 13 | | 0 | 3 | 4 | 10 | 11 | 8 | 15 | 14 | 17 | 18 | 18 | 18 |
| 14 | | | 2 | 0 | | 0 | 10 | 13 | 15 | 14 | 16 | 18 | 17 |
| 15 | | | | | | | 8 | 14 | 15 | 15 | 16 | 14 | 15 |
| 16 | | | | | | | 3 | 7 | 12 | 10 | 15 | 16 | 17 |
| 17 | | | | | | | 3 | 6 | 5 | 4 | 8 | 14 | 14 |
| 18 | | | | | | | 3 | 4 | 9 | 8 | 11 | 9 | 9 |
| 19 | | | | | | | 3 | 2 | 5 | 9 | 5 | 9 | 10 |

Table F.12: Occurrence of Slack, No Shielding, Short-Crested Waves, 120° Heading , ROV Recovery

| Tp/Hs | 2 | 2.5 | 3 | 3.5 | 4 | 4.5 | 5 | 5.5 | 6 | 6.5 | 7 | 7.5 | 8 |
|---|---|---|---|---|---|---|---|---|---|---|---|---|---|
| 5 | 0 | | | | | | | | | | | | |
| 6 | 0 | 0 | 1 | | | | | | | | | | |
| 7 | 0 | 0 | 0 | 2 | 3 | | | | | | | | |
| 8 | 0 | 0 | 1 | 1 | 2 | 3 | 6 | | | | | | |
| 9 | 0 | 0 | 0 | 0 | 0 | 3 | 4 | 2 | 7 | 11 | | | |
| 10 | 0 | 0 | 0 | 0 | 1 | 2 | 1 | 3 | 3 | 6 | 3 | 11 | 11 |
| 11 | 0 | 0 | 0 | 0 | 0 | 2 | 2 | 2 | 4 | 2 | 8 | 6 | 7 |
| 12 | 0 | 0 | 0 | 0 | 1 | 0 | 0 | 4 | 1 | 3 | 5 | 6 | 5 |
| 13 | | 0 | | 0 | 0 | 0 | 0 | 1 | 0 | 2 | 2 | 2 | 3 |
| 14 | | | | 0 | | 0 | 0 | 0 | 1 | 0 | 0 | 4 | 2 |
| 15 | | | | | | | 0 | 0 | 0 | 2 | 0 | 0 | 1 |
| 16 | | | | | | | 0 | 0 | 0 | 0 | 0 | 1 | 1 |
| 17 | | | | | | | 0 | 0 | 0 | 0 | 0 | 1 | 1 |
| 18 | | | | | | | 0 | 0 | 0 | 0 | 0 | 0 | 0 |
| 19 | | | | | | | 0 | 0 | 0 | 0 | 0 | 0 | 0 |

## F.2.2   Shielding

**Long-Crested Waves**

Table F.13: Occurrence of Slack, Shielding, Long-Crested Waves, 120° Heading , ROV Launch

| Tp/Hs | 2 | 2.5 | 3 | 3.5 | 4 | 4.5 | 5 | 5.5 | 6 | 6.5 | 7 | 7.5 | 8 |
|---|---|---|---|---|---|---|---|---|---|---|---|---|---|
| 5 | 0 | | | | | | | | | | | | |
| 6 | 0 | 5 | 3 | | | | | | | | | | |
| 7 | 0 | 0 | 5 | 11 | 12 | | | | | | | | |
| 8 | 0 | 5 | 4 | 9 | 10 | 13 | 17 | | | | | | |
| 9 | 0 | 5 | 5 | 12 | 9 | 15 | 15 | 18 | 16 | 18 | | | |
| 10 | 2 | 0 | 5 | 7 | 10 | 11 | 16 | 14 | 15 | 16 | 17 | 16 | 18 |
| 11 | 2 | 0 | 5 | 5 | 5 | 12 | 15 | 9 | 14 | 19 | 20 | 17 | 19 |
| 12 | 0 | 0 | 2 | 4 | 7 | 10 | 13 | 13 | 14 | 12 | 18 | 20 | 17 |
| 13 | | | 1 | 2 | | 9 | 10 | 10 | 13 | 16 | 18 | 16 | 19 |
| 14 | | | | | | | 8 | 11 | 10 | 13 | 14 | 15 | 16 |
| 15 | | | | | | | 8 | 10 | 15 | 13 | 10 | 14 | 15 |
| 16 | | | | | | | 8 | 8 | 11 | 12 | 13 | 14 | 16 |
| 17 | | | | | | | 1 | 4 | 7 | 7 | 9 | 11 | 14 |
| 18 | | | | | | | 2 | 2 | 8 | 6 | 7 | 11 | 11 |
| 19 | | | | | | | 3 | 3 | 8 | 7 | 8 | 9 | 9 |

Table F.14: Occurrence of Slack, Shielding, Long-Crested Waves, 120° Heading , ROV Recovery

| Tp/Hs | 2 | 2.5 | 3 | 3.5 | 4 | 4.5 | 5 | 5.5 | 6 | 6.5 | 7 | 7.5 | 8 |
|---|---|---|---|---|---|---|---|---|---|---|---|---|---|
| 5 | 0 | | | | | | | | | | | | |
| 6 | 0 | 0 | 0 | | | | | | | | | | |
| 7 | 0 | 0 | 0 | 0 | 2 | | | | | | | | |
| 8 | 0 | 0 | 0 | 0 | 3 | 6 | 6 | | | | | | |
| 9 | 0 | 0 | 0 | 0 | 1 | 0 | 4 | 3 | 7 | 7 | | | |
| 10 | 0 | 0 | 0 | 0 | 1 | 0 | 1 | 2 | 4 | 3 | 10 | 8 | 8 |
| 11 | 0 | 0 | 0 | 0 | 0 | 0 | 1 | 1 | 2 | 6 | 6 | 7 | 11 |
| 12 | 0 | 0 | 0 | 0 | 0 | 0 | 0 | 0 | 4 | 2 | 4 | 6 | 7 |
| 13 | | | 0 | 0 | | 0 | 1 | 0 | 0 | 2 | 4 | 5 | 5 |
| 14 | | | | | | | 1 | 0 | 1 | 1 | 1 | 5 | 4 |
| 15 | | | | | | | 0 | 0 | 0 | 0 | 0 | 1 | 0 |
| 16 | | | | | | | 0 | 0 | 0 | 0 | 1 | 1 | 1 |
| 17 | | | | | | | 0 | 0 | 0 | 0 | 0 | 1 | 1 |
| 18 | | | | | | | 0 | 0 | 0 | 0 | 0 | 0 | 0 |
| 19 | | | | | | | 0 | 0 | 0 | 0 | 0 | 0 | 1 |

**Short-Crested Waves**

Table F.15: Occurrence of Slack, Shielding, Short-Crested Waves, 120° Heading , ROV Launch

| Tp/Hs | 2 | 2.5 | 3 | 3.5 | 4 | 4.5 | 5 | 5.5 | 6 | 6.5 | 7 | 7.5 | 8 |
|---|---|---|---|---|---|---|---|---|---|---|---|---|---|
| 5 | 1 | | | | | | | | | | | | |
| 6 | 1 | 2 | 4 | | | | | | | | | | |
| 7 | 1 | 2 | 7 | 8 | 13 | | | | | | | | |
| 8 | 0 | 3 | 6 | 9 | 7 | 14 | 13 | | | | | | |
| 9 | 0 | 1 | 1 | 10 | 13 | 16 | 14 | 15 | 16 | 16 | | | |
| 10 | 0 | 1 | 1 | 5 | 10 | 11 | 13 | 12 | 14 | 16 | 16 | 19 | 18 |
| 11 | 0 | 1 | 4 | 7 | 11 | 10 | 11 | 12 | 16 | 15 | 18 | 16 | 19 |
| 12 | 0 | 0 | 2 | 5 | 6 | 12 | 9 | 8 | 11 | 15 | 15 | 17 | 19 |
| 13 | | | 1 | 1 | | 9 | 3 | 8 | 12 | 16 | 15 | 15 | 17 |
| 14 | | | | | | | 6 | 10 | 13 | 15 | 14 | 16 | 17 |
| 15 | | | | | | | 3 | 9 | 15 | 11 | 11 | 13 | 13 |
| 16 | | | | | | | 4 | 3 | 9 | 11 | 12 | 14 | 16 |
| 17 | | | | | | | 1 | 3 | 5 | 3 | 10 | 14 | 10 |
| 18 | | | | | | | 2 | 1 | 8 | 5 | 5 | 7 | 7 |
| 19 | | | | | | | 1 | 3 | 3 | 5 | 1 | 7 | 11 |

Table F.16: Occurrence of Slack, Shielding, Short-Crested Waves, 120° Heading , ROV Recovery

| Tp/Hs | 2 | 2.5 | 3 | 3.5 | 4 | 4.5 | 5 | 5.5 | 6 | 6.5 | 7 | 7.5 | 8 |
|---|---|---|---|---|---|---|---|---|---|---|---|---|---|
| 5 | 0 | | | | | | | | | | | | |
| 6 | 0 | 0 | 0 | | | | | | | | | | |
| 7 | 0 | 0 | 0 | 1 | 1 | | | | | | | | |
| 8 | 0 | 0 | 0 | 0 | 2 | 2 | 3 | | | | | | |
| 9 | 0 | 0 | 0 | 0 | 0 | 3 | 2 | 3 | 4 | 4 | | | |
| 10 | 0 | 0 | 0 | 0 | 0 | 2 | 0 | 1 | 0 | 6 | 1 | 7 | 11 |
| 11 | 0 | 0 | 0 | 0 | 0 | 0 | 1 | 3 | 3 | 2 | 5 | 7 | 7 |
| 12 | 0 | 0 | 0 | 0 | 0 | 0 | 0 | 4 | 0 | 3 | 3 | 7 | 2 |
| 13 | | | 0 | 0 | | 0 | 0 | 0 | 0 | 0 | 2 | 3 | 6 |
| 14 | | | | | | | 0 | 0 | 1 | 0 | 0 | 6 | 1 |
| 15 | | | | | | | 0 | 0 | 0 | 2 | 0 | 0 | 1 |
| 16 | | | | | | | 0 | 0 | 0 | 0 | 0 | 1 | 0 |
| 17 | | | | | | | 0 | 0 | 0 | 0 | 0 | 0 | 0 |
| 18 | | | | | | | 0 | 0 | 0 | 0 | 0 | 0 | 0 |
| 19 | | | | | | | 0 | 0 | 0 | 0 | 0 | 0 | 0 |

# F.3   150° Heading

## F.3.1   No Shielding

**Long-Crested Waves**

Table F.17: Occurrence of Slack, No Shielding, Long-Crested Waves, 150° Heading , ROV Launch

| Tp/Hs | 2 | 2.5 | 3 | 3.5 | 4 | 4.5 | 5 | 5.5 | 6 | 6.5 | 7 | 7.5 | 8 |
|---|---|---|---|---|---|---|---|---|---|---|---|---|---|
| 5 | 7 | | | | | | | | | | | | |
| 6 | 4 | 8 | 12 | | | | | | | | | | |
| 7 | 4 | 11 | 7 | 12 | 16 | | | | | | | | |
| 8 | 4 | 6 | 4 | 10 | 11 | 14 | 12 | | | | | | |
| 9 | 0 | 4 | 7 | 5 | 10 | 8 | 13 | 11 | 16 | 17 | | | |
| 10 | 0 | 2 | 5 | 5 | 5 | 6 | 13 | 12 | 16 | 15 | 14 | 17 | 18 |
| 11 | 0 | 2 | 1 | 3 | 8 | 8 | 13 | 14 | 10 | 16 | 19 | 14 | 16 |
| 12 | 0 | 0 | 1 | 2 | 8 | 6 | 10 | 16 | 11 | 8 | 16 | 17 | 18 |
| 13 | | | 1 | 0 | 0 | 4 | 6 | 8 | 10 | 11 | 15 | 18 | 13 |
| 14 | | | | 0 | 0 | | 1 | 10 | 10 | 9 | 8 | 10 | 12 |
| 15 | | | | | | | 3 | 3 | 6 | 6 | 11 | 10 | 12 |
| 16 | | | | | | | 3 | 2 | 9 | 4 | 7 | 8 | 12 |
| 17 | | | | | | | 0 | 3 | 2 | 6 | 5 | 9 | 6 |
| 18 | | | | | | | 0 | 2 | 3 | 2 | 7 | 3 | 5 |
| 19 | | | | | | | 0 | 0 | 0 | 2 | 1 | 3 | 5 |

Table F.18: Occurrence of Slack, No Shielding, Long-Crested Waves, 150° Heading , ROV Recovery

| Tp/Hs | 2 | 2.5 | 3 | 3.5 | 4 | 4.5 | 5 | 5.5 | 6 | 6.5 | 7 | 7.5 | 8 |
|---|---|---|---|---|---|---|---|---|---|---|---|---|---|
| 5 | 0 | | | | | | | | | | | | |
| 6 | 0 | 2 | 2 | | | | | | | | | | |
| 7 | 0 | 0 | 0 | 0 | 2 | | | | | | | | |
| 8 | 0 | 0 | 0 | 0 | 0 | 2 | 2 | | | | | | |
| 9 | 0 | 0 | 0 | 1 | 0 | 0 | 0 | 1 | 3 | 5 | | | |
| 10 | 0 | 0 | 0 | 0 | 0 | 1 | 1 | 2 | 1 | 2 | 4 | 1 | 2 |
| 11 | 0 | 0 | 0 | 0 | 0 | 0 | 1 | 0 | 1 | 2 | 3 | 4 | 6 |
| 12 | 0 | 0 | 0 | 0 | 0 | 0 | 0 | 0 | 0 | 0 | 1 | 1 | 2 |
| 13 | | | 0 | 0 | | 0 | 0 | 0 | 1 | 0 | 1 | 1 | 0 |
| 14 | | | | | | | 0 | 0 | 0 | 3 | 0 | 1 | 0 |
| 15 | | | | | | | 0 | 0 | 0 | 0 | 0 | 0 | 0 |
| 16 | | | | | | | 0 | 0 | 0 | 1 | 0 | 0 | 0 |
| 17 | | | | | | | 0 | 0 | 0 | 0 | 0 | 1 | 0 |
| 18 | | | | | | | 0 | 0 | 0 | 0 | 0 | 0 | 0 |
| 19 | | | | | | | 0 | 0 | 0 | 0 | 0 | 0 | 0 |

**Short-Crested Waves**

Table F.19: Occurrence of Slack, No Shielding, Short-Crested Waves, 150° Heading , ROV Launch

| Tp/Hs | 2 | 2.5 | 3 | 3.5 | 4 | 4.5 | 5 | 5.5 | 6 | 6.5 | 7 | 7.5 | 8 |
|---|---|---|---|---|---|---|---|---|---|---|---|---|---|
| 5 | 6 | | | | | | | | | | | | |
| 6 | 4 | 6 | 11 | | | | | | | | | | |
| 7 | 4 | 10 | 9 | 10 | 12 | | | | | | | | |
| 8 | 4 | 2 | 8 | 15 | 12 | 12 | 15 | | | | | | |
| 9 | 0 | 4 | 6 | 6 | 14 | 10 | 13 | 13 | 14 | 19 | | | |
| 10 | 1 | 3 | 3 | 6 | 6 | 8 | 13 | 14 | 16 | 17 | 16 | 17 | 17 |
| 11 | 0 | 2 | 1 | 4 | 3 | 10 | 16 | 13 | 13 | 20 | 13 | 17 | 19 |
| 12 | 0 | 0 | 3 | 5 | 8 | 8 | 9 | 11 | 12 | 15 | 17 | 16 | 17 |
| 13 | | | 1 | 2 | | 8 | 5 | 7 | 10 | 12 | 12 | 15 | 13 |
| 14 | | | | | | | 6 | 5 | 9 | 10 | 12 | 14 | 13 |
| 15 | | | | | | | 4 | 3 | 7 | 7 | 9 | 7 | 17 |
| 16 | | | | | | | 2 | 5 | 4 | 2 | 5 | 10 | 12 |
| 17 | | | | | | | 1 | 3 | 6 | 5 | 6 | 7 | 9 |
| 18 | | | | | | | 3 | 2 | 0 | 5 | 3 | 5 | 3 |
| 19 | | | | | | | 0 | 1 | 3 | 4 | 3 | 5 | 3 |

Table F.20: Occurrence of Slack, No Shielding, Short-Crested Waves, 150° Heading , ROV Recovery

| Tp/Hs | 2 | 2.5 | 3 | 3.5 | 4 | 4.5 | 5 | 5.5 | 6 | 6.5 | 7 | 7.5 | 8 |
|---|---|---|---|---|---|---|---|---|---|---|---|---|---|
| 5 | 0 | | | | | | | | | | | | |
| 6 | 0 | 0 | 1 | | | | | | | | | | |
| 7 | 0 | 0 | 1 | 2 | 2 | | | | | | | | |
| 8 | 0 | 0 | 1 | 0 | 0 | 1 | 0 | | | | | | |
| 9 | 0 | 0 | 0 | 0 | 0 | 0 | 2 | 0 | 1 | 3 | | | |
| 10 | 0 | 0 | 0 | 0 | 0 | 0 | 1 | 0 | 2 | 2 | 0 | 1 | 2 |
| 11 | 0 | 0 | 0 | 0 | 0 | 1 | 0 | 1 | 0 | 0 | 2 | 2 | 2 |
| 12 | 0 | 0 | 0 | 0 | 0 | 0 | 0 | 1 | 0 | 0 | 1 | 1 | 1 |
| 13 | | | 0 | 0 | | 0 | 0 | 0 | 1 | 1 | 0 | 0 | 3 |
| 14 | | | | | | | 0 | 0 | 0 | 0 | 0 | 0 | 0 |
| 15 | | | | | | | 0 | 0 | 0 | 0 | 0 | 1 | 1 |
| 16 | | | | | | | 0 | 0 | 0 | 0 | 0 | 0 | 0 |
| 17 | | | | | | | 0 | 0 | 0 | 0 | 0 | 0 | 0 |
| 18 | | | | | | | 0 | 0 | 0 | 0 | 0 | 0 | 0 |
| 19 | | | | | | | 0 | 0 | 0 | 0 | 0 | 0 | 0 |

## F.3.2   Shielding

**Long-Crested Waves**

Table F.21: Occurrence of Slack, Shielding, Long-Crested Waves, 150° Heading , ROV Launch

| Tp/Hs | 2 | 2.5 | 3 | 3.5 | 4 | 4.5 | 5 | 5.5 | 6 | 6.5 | 7 | 7.5 | 8 |
|---|---|---|---|---|---|---|---|---|---|---|---|---|---|
| 5 | 0 | | | | | | | | | | | | |
| 6 | 0 | 1 | 2 | | | | | | | | | | |
| 7 | 0 | 1 | 0 | 3 | 2 | | | | | | | | |
| 8 | 0 | 0 | 0 | 1 | 1 | 3 | 3 | | | | | | |
| 9 | 0 | 0 | 2 | 1 | 1 | 2 | 15 | 3 | 1 | 9 | | | |
| 10 | 0 | 0 | 0 | 1 | 1 | 3 | 9 | 5 | 5 | 2 | 7 | 9 | 9 |
| 11 | 0 | 0 | 0 | 0 | 1 | 3 | 7 | 3 | 4 | 9 | 12 | 8 | 11 |
| 12 | 0 | 0 | 0 | 0 | 2 | 1 | 4 | 6 | 4 | 4 | 9 | 10 | 12 |
| 13 | | | 0 | 0 | | 1 | 4 | 3 | 4 | 7 | 8 | 10 | 9 |
| 14 | | | | | | | 0 | 5 | 4 | 5 | 4 | 7 | 8 |
| 15 | | | | | | | 1 | 2 | 3 | 2 | 5 | 5 | 6 |
| 16 | | | | | | | 0 | 0 | 6 | 2 | 1 | 6 | 3 |
| 17 | | | | | | | 0 | 2 | 3 | 1 | 1 | 0 | 2 |
| 18 | | | | | | | 0 | 1 | 1 | 1 | 2 | 2 | 3 |
| 19 | | | | | | | 0 | 0 | 0 | 2 | 0 | 0 | 2 |

Table F.22: Occurrence of Slack, Shielding, Long-Crested Waves, 150° Heading , ROV Recovery

| Tp/Hs | 2 | 2.5 | 3 | 3.5 | 4 | 4.5 | 5 | 5.5 | 6 | 6.5 | 7 | 7.5 | 8 |
|---|---|---|---|---|---|---|---|---|---|---|---|---|---|
| 5 | 0 | | | | | | | | | | | | |
| 6 | 0 | 0 | 0 | | | | | | | | | | |
| 7 | 0 | 0 | 0 | 0 | 0 | | | | | | | | |
| 8 | 0 | 0 | 0 | 0 | 0 | 0 | 0 | | | | | | |
| 9 | 0 | 0 | 0 | 0 | 0 | 0 | 1 | 0 | 0 | 0 | | | |
| 10 | 0 | 0 | 0 | 0 | 0 | 0 | 0 | 0 | 0 | 0 | 0 | 0 | 0 |
| 11 | 0 | 0 | 0 | 0 | 0 | 0 | 0 | 0 | 0 | 0 | 0 | 0 | 1 |
| 12 | 0 | 0 | 0 | 0 | 0 | 0 | 0 | 0 | 0 | 0 | 0 | 0 | 0 |
| 13 | | | 0 | 0 | | 0 | 0 | 0 | 0 | 0 | 0 | 0 | 0 |
| 14 | | | | | | | 0 | 0 | 0 | 0 | 0 | 0 | 0 |
| 15 | | | | | | | 0 | 0 | 0 | 0 | 0 | 0 | 0 |
| 16 | | | | | | | 0 | 0 | 0 | 0 | 0 | 0 | 0 |
| 17 | | | | | | | 0 | 0 | 0 | 0 | 0 | 0 | 0 |
| 18 | | | | | | | 0 | 0 | 0 | 0 | 0 | 0 | 0 |
| 19 | | | | | | | 0 | 0 | 0 | 0 | 0 | 0 | 0 |

**Short-Crested Waves**

Table F.23: Occurrence of Slack, Shielding, Short-Crested Waves, 150° Heading , ROV Launch

| Tp/Hs | 2 | 2.5 | 3 | 3.5 | 4 | 4.5 | 5 | 5.5 | 6 | 6.5 | 7 | 7.5 | 8 |
|---|---|---|---|---|---|---|---|---|---|---|---|---|---|
| 5 | 1 | | | | | | | | | | | | |
| 6 | 1 | 3 | 8 | | | | | | | | | | |
| 7 | 1 | 1 | 3 | 6 | 5 | | | | | | | | |
| 8 | 0 | 0 | 2 | 2 | 9 | 6 | 10 | 8 | | | | | |
| 9 | 0 | 0 | 4 | 2 | 5 | 14 | 7 | 11 | 10 | 11 | | | |
| 10 | 0 | 0 | 2 | 4 | 5 | 5 | 8 | 6 | 9 | 11 | 15 | 13 | 16 |
| 11 | 0 | 1 | 1 | 4 | 2 | 4 | 10 | 10 | 9 | 16 | 11 | 13 | 14 |
| 12 | 0 | 0 | 1 | 1 | 3 | 2 | 6 | 2 | 8 | 8 | 10 | 13 | 14 |
| 13 | | | 0 | 1 | | 3 | 3 | 5 | 8 | 7 | 9 | 11 | 9 |
| 14 | | | | | | | 5 | 2 | 5 | 3 | 5 | 10 | 8 |
| 15 | | | | | | | 1 | 3 | 6 | 6 | 7 | 3 | 10 |
| 16 | | | | | | | 1 | 3 | 2 | 1 | 4 | 10 | 5 |
| 17 | | | | | | | 1 | 3 | 2 | 1 | 4 | 6 | 5 |
| 18 | | | | | | | 1 | 2 | 1 | 3 | 1 | 3 | 3 |
| 19 | | | | | | | 0 | | 1 | 2 | 1 | 3 | 1 |

Table F.24: Occurrence of Slack, Shielding, Short-Crested Waves, 150° Heading , ROV Recovery

| Tp/Hs | 2 | 2.5 | 3 | 3.5 | 4 | 4.5 | 5 | 5.5 | 6 | 6.5 | 7 | 7.5 | 8 |
|-------|---|-----|---|-----|---|-----|---|-----|---|-----|---|-----|---|
| 5 | 0 | | | | | | | | | | | | |
| 6 | 0 | 0 | 0 | | | | | | | | | | |
| 7 | 0 | 0 | 0 | 0 | 0 | | | | | | | | |
| 8 | 0 | 0 | 0 | 0 | 0 | 0 | 0 | | | | | | |
| 9 | 0 | 0 | 0 | 0 | 0 | 0 | 0 | 0 | 0 | 0 | | | |
| 10 | 0 | 0 | 0 | 0 | 0 | 0 | 0 | 0 | 0 | 0 | 0 | 1 | 1 |
| 11 | 0 | 0 | 0 | 0 | 0 | 0 | 0 | 0 | 0 | 0 | 0 | 0 | 0 |
| 12 | 0 | 0 | 0 | 0 | 0 | 0 | 0 | 0 | 0 | 0 | 0 | 0 | 0 |
| 13 | | | 0 | 0 | | 0 | 0 | 0 | 0 | 0 | 0 | 0 | 1 |
| 14 | | | | | | | 0 | 0 | 0 | 0 | 0 | 0 | 0 |
| 15 | | | | | | | 0 | 0 | 0 | 0 | 0 | 0 | 0 |
| 16 | | | | | | | 0 | 0 | 0 | 0 | 0 | 0 | 0 |
| 17 | | | | | | | 0 | 0 | 0 | 0 | 0 | 0 | 0 |
| 18 | | | | | | | 0 | 0 | 0 | 0 | 0 | 0 | 0 |
| 19 | | | | | | | 0 | 0 | 0 | 0 | 0 | 0 | 0 |

# F.4  180° Heading

## F.4.1  No Shielding

**Long-Crested Waves**

Table F.25: Occurrence of Slack, No Shielding, Long-Crested Waves, 180° Heading , ROV Launch

| Tp/Hs | 2 | 2.5 | 3 | 3.5 | 4 | 4.5 | 5 | 5.5 | 6 | 6.5 | 7 | 7.5 | 8 |
|-------|---|-----|---|-----|---|-----|---|-----|---|-----|---|-----|---|
| 5 | 5 | | | | | | | | | | | | |
| 6 | 3 | 6 | 8 | | | | | | | | | | |
| 7 | 1 | 3 | 8 | 7 | 12 | | | | | | | | |
| 8 | 1 | 5 | 6 | 3 | 9 | 13 | 12 | | | | | | |
| 9 | 0 | 0 | 3 | 6 | 8 | 6 | 12 | 12 | 14 | 15 | | | |
| 10 | 0 | 0 | 4 | 3 | 2 | 9 | 6 | 8 | 9 | 10 | 11 | 12 | 10 |
| 11 | 0 | 1 | 0 | 2 | 3 | 3 | 6 | 8 | 4 | 11 | 8 | 13 | 12 |
| 12 | 0 | 0 | 0 | 2 | 1 | 0 | 5 | 8 | 5 | 8 | 3 | 11 | 9 |
| 13 | | | 0 | 0 | | 0 | 0 | 3 | 2 | 7 | 9 | 6 | 8 |
| 14 | | | | | | | 1 | 1 | 7 | 2 | 2 | 2 | 11 |
| 15 | | | | | | | 0 | 1 | 1 | 1 | 2 | 4 | 4 |
| 16 | | | | | | | 0 | 0 | 1 | 1 | 1 | 3 | 0 |
| 17 | | | | | | | 0 | 0 | 0 | 0 | 0 | 0 | 3 |
| 18 | | | | | | | 0 | 0 | 0 | 0 | 0 | 1 | 0 |
| 19 | | | | | | | 0 | 0 | 0 | 0 | 0 | 0 | 1 |

Table F.26: Occurrence of Slack, No Shielding, Long-Crested Waves, 180° Heading , ROV Recovery

| Tp/Hs | 2 | 2.5 | 3 | 3.5 | 4 | 4.5 | 5 | 5.5 | 6 | 6.5 | 7 | 7.5 | 8 |
|---|---|---|---|---|---|---|---|---|---|---|---|---|---|
| 5 | 0 | | | | | | | | | | | | |
| 6 | 0 | 0 | 0 | | | | | | | | | | |
| 7 | 0 | 0 | 2 | 0 | 0 | | | | | | | | |
| 8 | 0 | 0 | 0 | 0 | 0 | 0 | 1 | | | | | | |
| 9 | 0 | 1 | 0 | 0 | 0 | 1 | 1 | 2 | 3 | 2 | | | |
| 10 | 0 | 0 | 1 | 0 | 0 | 1 | 0 | 2 | 3 | 3 | 2 | 0 | 5 |
| 11 | 0 | 0 | 0 | 0 | 0 | 0 | 0 | 0 | 1 | 2 | 1 | 3 | 1 |
| 12 | 0 | 0 | 0 | 0 | 0 | 0 | 0 | 1 | 2 | 1 | 1 | 1 | 2 |
| 13 | | | 0 | 0 | | 0 | 0 | 0 | 2 | 0 | 2 | 3 | 0 |
| 14 | | | | | | | 1 | 0 | 1 | 1 | 2 | 1 | 0 |
| 15 | | | | | | | 0 | 0 | 0 | 0 | 0 | 1 | 1 |
| 16 | | | | | | | 0 | 0 | 0 | 0 | 0 | 0 | 0 |
| 17 | | | | | | | 0 | 0 | 0 | 0 | 0 | 0 | 0 |
| 18 | | | | | | | 0 | 0 | 0 | 0 | 0 | 0 | 0 |
| 19 | | | | | | | 0 | 0 | 0 | 0 | 0 | 1 | 0 |

**Short-Crested Waves**

Table F.27: Occurrence of Slack, No Shielding, Short-Crested Waves, 180° Heading , ROV Launch

| Tp/Hs | 2 | 2.5 | 3 | 3.5 | 4 | 4.5 | 5 | 5.5 | 6 | 6.5 | 7 | 7.5 | 8 |
|---|---|---|---|---|---|---|---|---|---|---|---|---|---|
| 5 | 7 | | | | | | | | | | | | |
| 6 | 3 | 5 | 12 | | | | | | | | | | |
| 7 | 0 | 4 | 7 | 9 | 10 | | | | | | | | |
| 8 | 1 | 2 | 5 | 5 | 10 | 9 | 14 | | | | | | |
| 9 | 1 | 2 | 3 | 5 | 7 | 9 | 10 | 11 | 14 | 13 | | | |
| 10 | 0 | 3 | 3 | 3 | 6 | 6 | 10 | 8 | 9 | 9 | 12 | 16 | 14 |
| 11 | 0 | 0 | 1 | 5 | 5 | 6 | 7 | 7 | 11 | 11 | 14 | 16 | 14 |
| 12 | 0 | 2 | 0 | 2 | 6 | 2 | 7 | 5 | 4 | 10 | 9 | 11 | 11 |
| 13 | | | 0 | 1 | | 4 | 8 | 6 | 7 | 8 | 11 | 13 | 8 |
| 14 | | | | | | | 4 | 3 | 4 | 7 | 12 | 8 | 8 |
| 15 | | | | | | | 1 | 2 | 5 | 4 | 7 | 8 | 6 |
| 16 | | | | | | | 2 | 3 | 5 | 4 | 4 | 4 | 7 |
| 17 | | | | | | | 0 | 0 | 1 | 1 | 4 | 2 | 1 |
| 18 | | | | | | | 0 | 0 | 0 | 1 | 2 | 2 | 5 |
| 19 | | | | | | | 0 | 0 | 1 | 1 | 2 | 2 | 2 |

Table F.28: Occurrence of Slack, No Shielding, Short-Crested Waves, 180° Heading , ROV Recovery

| Tp/Hs | 2 | 2.5 | 3 | 3.5 | 4 | 4.5 | 5 | 5.5 | 6 | 6.5 | 7 | 7.5 | 8 |
|---|---|---|---|---|---|---|---|---|---|---|---|---|---|
| 5 | 0 | | | | | | | | | | | | |
| 6 | 0 | 0 | 0 | | | | | | | | | | |
| 7 | 0 | 0 | 1 | 1 | 2 | | | | | | | | |
| 8 | 0 | 0 | 0 | 0 | 2 | 2 | 1 | | | | | | |
| 9 | 0 | 0 | 0 | 0 | 0 | 2 | 2 | 2 | 3 | 1 | | | |
| 10 | 0 | 0 | 0 | 0 | 1 | 0 | 1 | 2 | 1 | 1 | 2 | 0 | 6 |
| 11 | 0 | 0 | 0 | 0 | 0 | 0 | 0 | 1 | 1 | 0 | 2 | 4 | 2 |
| 12 | 0 | 0 | 0 | 0 | 0 | 0 | 0 | 0 | 0 | 0 | 3 | 1 | 0 |
| 13 | | | 0 | 0 | | 0 | 0 | 1 | 0 | 0 | 0 | 1 | 3 |
| 14 | | | | | | | 0 | 0 | 0 | 0 | 0 | 1 | 0 |
| 15 | | | | | | | 0 | 0 | 0 | 0 | 0 | 2 | 2 |
| 16 | | | | | | | 0 | 0 | 0 | 0 | 0 | 1 | 0 |
| 17 | | | | | | | 0 | 0 | 0 | 0 | 0 | 0 | 0 |
| 18 | | | | | | | 0 | 0 | 0 | 0 | 0 | 0 | 0 |
| 19 | | | | | | | 0 | 0 | 0 | 0 | 0 | 0 | 0 |

## F.4.2　Shielding

**Long-Crested Waves**

Table F.29: Occurrence of Slack, Shielding, Long-Crested Waves, 180° Heading , ROV Launch

| Tp/Hs | 2 | 2.5 | 3 | 3.5 | 4 | 4.5 | 5 | 5.5 | 6 | 6.5 | 7 | 7.5 | 8 |
|---|---|---|---|---|---|---|---|---|---|---|---|---|---|
| 5 | 4 | | | | | | | | | | | | |
| 6 | 2 | 7 | 9 | | | | | | | | | | |
| 7 | 1 | 3 | 12 | 6 | 7 | | | | | | | | |
| 8 | 1 | 5 | 5 | 6 | 10 | 11 | 10 | | | | | | |
| 9 | 0 | 1 | 5 | 5 | 9 | 9 | 15 | 11 | 12 | 17 | | | |
| 10 | 0 | 0 | 5 | 3 | 4 | 7 | 9 | 9 | 10 | 13 | 9 | 12 | 12 |
| 11 | 0 | 0 | 0 | 4 | 3 | 8 | 7 | 9 | 5 | 13 | 10 | 11 | 12 |
| 12 | 0 | 0 | 1 | 2 | 2 | 0 | 4 | 7 | 6 | 10 | 5 | 11 | 10 |
| 13 | | | 0 | 0 | | 0 | 4 | 4 | 1 | 6 | 9 | 4 | 10 |
| 14 | | | | | | | 0 | 1 | 7 | 4 | 2 | 3 | 11 |
| 15 | | | | | | | 1 | 1 | 1 | 2 | 1 | 3 | 3 |
| 16 | | | | | | | 0 | 0 | 1 | 2 | 0 | 4 | 0 |
| 17 | | | | | | | 0 | 0 | 0 | 0 | 0 | 2 | 4 |
| 18 | | | | | | | 0 | 0 | 0 | 0 | 0 | 1 | 0 |
| 19 | | | | | | | 0 | 0 | 0 | 0 | 0 | 0 | 2 |

Table F.30: Occurrence of Slack, Shielding, Long-Crested Waves, 180° Heading , ROV Recovery

| Tp/Hs | 2 | 2.5 | 3 | 3.5 | 4 | 4.5 | 5 | 5.5 | 6 | 6.5 | 7 | 7.5 | 8 |
|---|---|---|---|---|---|---|---|---|---|---|---|---|---|
| 5 | 0 | | | | | | | | | | | | |
| 6 | 0 | 0 | 0 | | | | | | | | | | |
| 7 | 0 | 0 | 1 | 0 | 0 | | | | | | | | |
| 8 | 0 | 0 | 0 | 0 | 2 | 0 | 1 | | | | | | |
| 9 | 0 | 1 | 0 | 0 | 0 | 0 | 1 | 1 | 3 | 4 | | | |
| 10 | 0 | 0 | 0 | 0 | 0 | 0 | 0 | 2 | 2 | 2 | 1 | 1 | 5 |
| 11 | 0 | 0 | 0 | 0 | 0 | 0 | 0 | 0 | 1 | 2 | 1 | 1 | 2 |
| 12 | 0 | 0 | 0 | 0 | 0 | 0 | 0 | 1 | 2 | 2 | 1 | 0 | 2 |
| 13 | | | 0 | 0 | | 0 | 0 | 0 | 2 | 0 | 2 | 3 | 0 |
| 14 | | | | | | | 0 | 0 | 1 | 0 | 2 | 1 | 0 |
| 15 | | | | | | | 0 | 0 | 0 | 0 | 0 | 2 | 1 |
| 16 | | | | | | | 0 | 0 | 0 | 0 | 0 | 0 | 0 |
| 17 | | | | | | | 0 | 0 | 0 | 0 | 0 | 0 | 0 |
| 18 | | | | | | | 0 | 0 | 0 | 0 | 0 | 0 | 0 |
| 19 | | | | | | | 0 | 0 | 0 | 0 | 0 | 0 | 0 |

**Short-Crested Waves**

Table F.31: Occurrence of Slack, Shielding, Short-Crested Waves, 180° Heading , ROV Launch

| Tp/Hs | 2 | 2.5 | 3 | 3.5 | 4 | 4.5 | 5 | 5.5 | 6 | 6.5 | 7 | 7.5 | 8 |
|---|---|---|---|---|---|---|---|---|---|---|---|---|---|
| 5 | 2 | | | | | | | | | | | | |
| 6 | 0 | 4 | 5 | | | | | | | | | | |
| 7 | 1 | 5 | 5 | 9 | 9 | | | | | | | | |
| 8 | 1 | 2 | 5 | 5 | 10 | 4 | 10 | | | | | | |
| 9 | 1 | 3 | 5 | 6 | 5 | 8 | 9 | 7 | 10 | 11 | | | |
| 10 | 0 | 1 | 3 | 0 | 3 | 7 | 8 | 7 | 5 | 8 | 11 | 16 | 11 |
| 11 | 0 | 0 | 1 | 3 | 2 | 5 | 5 | 7 | 9 | 9 | 13 | 15 | 12 |
| 12 | 0 | 1 | 0 | 0 | 3 | 3 | 5 | 4 | 4 | 9 | 10 | 13 | 12 |
| 13 | | | 0 | 1 | | 3 | 4 | 6 | 5 | 10 | 10 | 9 | 6 |
| 14 | | | | | | | 4 | 3 | 4 | 6 | 8 | 8 | 9 |
| 15 | | | | | | | 1 | 1 | 6 | 5 | 6 | 9 | 5 |
| 16 | | | | | | | 2 | 2 | 5 | 4 | 3 | 2 | 7 |
| 17 | | | | | | | 0 | 0 | 0 | 0 | 1 | 1 | 1 |
| 18 | | | | | | | 0 | 0 | 0 | 1 | 1 | 2 | 2 |
| 19 | | | | | | | 0 | 0 | 2 | 0 | 2 | 1 | 2 |

Table F.32: Occurrence of Slack, Shielding, Short-Crested Waves, 180° Heading , ROV Recovery

| Tp/Hs | 2 | 2.5 | 3 | 3.5 | 4 | 4.5 | 5 | 5.5 | 6 | 6.5 | 7 | 7.5 | 8 |
|-------|---|-----|---|-----|---|-----|---|-----|---|-----|---|-----|---|
| 5 | 0 | | | | | | | | | | | | |
| 6 | 0 | 0 | 1 | | | | | | | | | | |
| 7 | 0 | 0 | 0 | 0 | 0 | | | | | | | | |
| 8 | 0 | 0 | 0 | 0 | 0 | 0 | 0 | | | | | | |
| 9 | 0 | 0 | 0 | 0 | 0 | 0 | 1 | 1 | 1 | 1 | | | |
| 10 | 0 | 0 | 0 | 0 | 0 | 0 | 0 | 0 | 0 | 1 | 0 | 0 | 3 |
| 11 | 0 | 0 | 0 | 0 | 0 | 0 | 0 | 1 | 1 | 0 | 1 | 1 | 1 |
| 12 | 0 | 0 | 0 | 0 | 0 | 0 | 0 | 0 | 0 | 0 | 2 | 1 | 1 |
| 13 | | | 0 | 0 | | 0 | 0 | 1 | 0 | 0 | 0 | 0 | 1 |
| 14 | | | | | | | 0 | 0 | 0 | 0 | 0 | 0 | 0 |
| 15 | | | | | | | 0 | 0 | 0 | 0 | 0 | 1 | 2 |
| 16 | | | | | | | 0 | 0 | 0 | 0 | 0 | 0 | 0 |
| 17 | | | | | | | 0 | 0 | 0 | 0 | 0 | 0 | 0 |
| 18 | | | | | | | 0 | 0 | 0 | 0 | 0 | 0 | 0 |
| 19 | | | | | | | 0 | 0 | 0 | 0 | 0 | 0 | 0 |